Localization and interaction of circadian clock and TOR pathway components in *Neurospora crassa*

ROSA ESKANDARI

A THESIS SUBMITTED TO THE FACULTY OF GRADUATE STUDIES IN PARTIAL FULFILLMENT OF THE REQUIREMENTS FOR THE DEGREE OF

DOCTOR OF PHILOSOPHY

GRADUATE PROGRAM IN BIOLOGY
YORK UNIVERSITY
TORONTO, ONTARIO

August 2022

Abstract

Circadian (daily) rhythmicity is an attribute of almost all eukaryotic cells and some prokaryotes. Our lab utilizes the filamentous fungus *Neurospora crassa* as a model organism to study the molecular basis of rhythmicity. Models for the endogenous oscillators that regulate circadian rhythms in eukaryotes are primarily based on a small number of ‘‘clock genes’’ operating as transcription/translation feedback loops (TTFL). Still, rhythms can be observed, when TTFLs are nonoperating. Understanding the mechanism of rhythmicity operating outside of TTFLs is the key unresolved problem in circadian biology.

Our lab has identified two genes in *Neurospora crassa* required for this TTFL-less rhythmicity, *vta*, and *gtr2*. Both are components of the TOR (Target of Rapamycin) nutrient-sensing pathway preserved in eukaryotes. Coimmunoprecipitation and mass spectrometry found TOR pathway components, including GTR2 (homologous to yeast Gtr2 and RAG C/D in mammals) as binding partners of VTA (homologous to yeast EGO1 and mammalian LAMTOR 1).

In this thesis I report reciprocal co-IP with GTR2 confirming VTA as a binding partner. I also report that the expression of GTR2 protein is rhythmic, and VTA is required for GTR2 rhythmicity. FRQ protein, central to the clock TTFL, is rhythmic in the presence of GTR2 but dampened in the absence of GTR2.

I also report my research regarding the subcellular localization of VTA and GTR2 in different nutritional states and the presence and absence of TOR pathway inhibitors. Kog1/Raptor is a regulator for TOR1 activity in yeast and mammals, and I report the localization of KOG1 in *Neurospora crassa*. My data indicate that GTR2-RFP localizes in filamentous structures identified as vacuolar membranes but is cytoplasmic in the absence of VTA. KOG1-GFP looks similar to GTR2-RFP. In the presence of arginine, KOG-1 is localized around the vacuole. Starvation using no glucose media looks similar to the *vta* ^{ko} condition in the GTR2 strain. In KOG-1GFP, there is the presence of KOG1 P bodies around the edges of the vacuole. The latter effect is similar to the yeast homolog kog-1 protein behavior in the absence of glucose. In the presence of TOR pathway inhibitors, Torin I and Torin II, there is an abnormal structural morphology in both cases. It is indicated that there is a destruction of the vacuolar structure and internal hyphal network in inhibitors that moves the fluorescence signal to the outer plasma membrane.

These results support the connection between the mutual components of the clock and TOR pathway and the essential interaction to maintain the proper function of the signaling pathway and the circadian clock. As we have previously reported, the TTFL cannot explain the whole circadian clock mechanism. An independent oscillator may be linked to the TTFL to help maintain its function. This link is identified as the TOR pathway, a significant and nutrient-sensitive pathway conserved in eukaryotes. The circadian clock is also conserved in almost all organisms. Our results established a network between the control of metabolism through the TOR pathway and the circadian clock.

Acknowledgments

I would like to express my deepest gratitude to my advisor, Dr. Patricia Lakin-Thomas, whose sincerity, and encouragement I will never forget. Dr. Pat has been an inspiration as I hurdled through the path of this Ph.D. degree. She is the true definition of a leader and the ultimate role model.

This thesis would not have been possible without my committee members, Dr. Kubiseski and Dr. Scheid, whose guidance from the initial step of this research enabled me to develop an understanding of the subject. I am thankful for the extraordinary experiences all these great scientists arranged for me and for providing opportunities to grow professionally.

I am grateful for my parents and sister, whose constant love and support kept me motivated and confident. My accomplishments and success are because they believed in me. My Deepest thanks to our undergraduate student associates who keep me grounded, remind me of what is essential in life, and are always supportive of my adventures. Finally, I owe my deepest gratitude to my husband, Mosa, who is my love. I am forever thankful for the unconditional love and support he gave me throughout the entire thesis process and every day.

Table of Contents

List of figures

List of tables

Abbreviations

AU: Airy Unit

AOMF: Advanced Optical Microscopy Facility

ATG13: Autophagy related 13

ATG 101: Autophagy-related protein 101

ATF4: Activating transcription factor 4

AMPKB: AMPK regulatory subunit B

AMPK: AMP kinase

AKT (PKB): Protein kinase B

AGC: Kinase group AGC which includes protein kinase A (PKA), G (PKG) and C (PKC) families

ADP: Adenosine diphosphate

4EBP: EIF4E binding protein

BSA: Bovine Serum Albumin

BMAL1: Brain and muscle Arnt-like protein-1

BLAST: Basic Local Alignment Search Tool

CYC: CYCLE

csp-1: Conidial separation mutant

CRY2: Cryptochrome2

CRY1: Cryptochrome1

CRY: CRYPTOCHROME

CLS: Chronological life span

CLK: CLOCK

chol-1: Choline-requiring mutant

CHE: CCA1 HIKING EXPEDITION

CCA1: CIRCADIAN CLOCK ASSOCIATED1

CASTOR: Arginine sensor in mammals, that blocks GATOR2 complex

CAPS: Cleaved Amplified Polymorphic Sequences

CAD: Carbamoyl-phosphate synthetase

C7ORF59: Chromosome 7 open reading frame 59

DTT: Dithiothreitol

DNA: Deoxyribonucleic acid

DEPTOR: DEP domain-containing mTOR interacting protein

DD: Constant darkness

ESR: Environmental stress response

ERK: Exteracellular signal-regulator kinase

EIF4E: Eukaryotic translation initiation factor 4E

eIF2a: Eukaryotic translation initiation factor 2A

EGO: Exit from rapamycin induced growth arrest

EGFR: Epidermal growth factor receptor

EGF: Epidermal growth factor

EE: Evening element

EDTA: Ethylenediaminetetraacetic acid

FungiDB: Fungi data base

Frq10: Frequency null mutation

FRQ: Frequency

FRB domain: FKBP-rapamycin-binding domain

FoXO1/3: Forkhead box O transcription factor family 1,3

FLO: FRQ-less oscillator

FKBP: FK506 binding proteins

FIP2000: Focal adhesion kinase family interacting protein of 200 kD

FGSC: Fungal Genetics Stock Center

FATC: C-terminal FAT/kinase domain

GTR2: GTP binding protein resemblance 2

GTR1: GTP binding protein resemblance 1

GTPase: Guanosine triphosphatase

GTP: Guanosine triphosphate

GMP: Guanosine monophosphate

GI: GIGANTEA

GFP: Green fluorescent protein

GEF: Guanine nucleotide exchange factor

GDP: Guanosine diphosphate

GCN4: General control non-derepressible 4

GCN2: General control non-derepressible 2

GATOR2: GAP activity towards Rags 2

GATOR1: GAP activity towards Rags 1

GAP: GTPase activating protein

GAAC: General amino acid control

gDNA: Genomic DNA

HygBR: Hygromycin B resistance

his-3: Histidine requiring mutant

HIF1a: Hypoxia inducible factor 1 subunit alpha

HEAT repeats: Protein tandem repeat structural motif

HRP: Horseradish peroxidase

IRS: Insulin receptor substrate

IP-MS: Immunoprecipitation – Mass spectrometry

kog1: Kontroller of growth

LSM: Laser Scanning Microscope

LiOAc: Lithium acetate

LL: Constant light

LKB1: Liver kinase B1

LHY: Late elongated hypocotyl

LeuRS: Leucyl-tRNA synthetases

LD: Light-dark

LB: Luria-Bertani

LATS: Large tumor suppressor

LAMTOR: Late endosomal / lysosomal adapter and MAPK and mTOR activator

LAMTOR1: Late endosomal / lysosomal adapter and MAPK and mTOR activator 1

mTORC1: Mammalian target of rapamycin complex 1

mTORC2: Mammalian target of rapamycin complex 2

mTOR: Mechanistic / Mammalian target of rapamycin

MTHFD2: Methylenetetrahydrofolate Dehydrogenase (NADP+ Dependent) 2

Msn2/4: Zn-finger transcription factors

mSIN1: mammalian stress-activated protein kinase interacting protein 1

mRNA: Messenger RNA

MP1: Mitogen activated protein kinase scaffold protein 1

mLST8: mammalian lethal with sec 13 protein 8

Mios: WD repeat-containing protein MIO

Meh1: Multicopy suppressor of Ers1 Hygromycin B sensitivity

MA: Maltose-arginine

NR: Nitrate reductase

NCR: Nitrogen catabolite repression

NADs: Nicotamide adenine dinucleotide

NADPH: Nicotinamide adenine dinucleotide phosphate

NEB: New England BioLabs

OD: Optical Density

PTO: Post-translational Oscillator

PTEN: Phosphatase and tensin homolog

PRR1: PSEUDO-RESPONSE REGULATOR

PRE: ROR response element

prd-1: Period mutation

PRAS40: Proline rich AKT substrate

PRARY: Peroxisome proliferator-activated receptor Y

PRAR: Peroxisome proliferator-activated receptor

PPP: Pentose phosphate pathway

PP2A: Protein phosphatase 2 A

PP1: Protein phosphatase 1

PP: Protein phosphatase

PKG: Cyclic GMP dependent kinase

PKC: Protein kinase C

PKA: Cyclic AMP dependent kinase

PIP3: Phosphatidylinositol (3,4,5)-trisphosphate (PtdIns(3,4,5)P_3)

PIKK: Phosphatidylinositol 3-kinase-related kinase

PI3K: Phosphoinositide 3-kinase

PFK: Phospho- fructokinase

PER2: Period2

PER1: Period1

Per: Period

PDK1: Pyruvate dehydrogenase kinase 1

PDCD4: Programmed Cell Death 4

PCR: Polymerase chain reaction

p70 S6K1: p70S6 kinase

p18: Lipid raft adapter protein p18

p14: Endosomal adapter protein p14

PVDF membrane: Polyvinylidene difluoride membrane

PMSF: Phenylmethylsulfonyl fluoride

PEG: Polyethylene glycol

PEB: Protein extraction buffer

PBS: Phosphate Buffered Saline

PAS: Pre-autophagosomal structure

RagD: Ras related GTP binding protein D

RagC: Ras related GTP binding protein C

RagB: Ras related GTP binding protein B

RagA: Ras related GTP binding protein A

Raptor: Regulatory-associated protein of mTOR

REDD1: Regulated in DNA damage and development

Rheb: Ras homolog enriched in brain

RiBi: Ribosome biogenesis factors

Rictor: Rapamycin-insensitive component of mTORC2

rRNA: Ribosomal ribonucleic acid

RNAi: RNA interference

RNA: Ribonucleic acid

RLS: Replicative life span

STP1: Sugar Transporter Protein 1

STF4: Transcription factor 4

SREBP: Sterol responsive element binding protein

SPS: Stress-polarity signaling

Snf1: Sucrose non-fermenting 1

SLC38A9: Lysosomal amino acid transporter

sit4: Suppressor of initiation of transcription 4

SIRT1: Silent mating type information regulation 2 homolog 1

SGK: Serum and glucocorticoid-regulated kinase

SG: Silica gel

sfp1: Split-finger protein 1

Ser: Serine

Sec13: SEC13 Homolog, Nuclear Pore and COPII Coat Complex Component

SEACIT: She-1 associated sub-complex that inhibits TORC1

SEACAT: She 1- associated subcomplex activating TORC1

SCN: The suprachiasmatic nuclei

SCM: Synthetic crossing medium

SCH9: Serine/threonine protein kinase SCH9

SOC media: Super Optimal broth with Catabolite repression

SDS PAGE: Sodium dodecyl sulfate–polyacrylamide gel electrophoresis

SC URA: Yeast Nitrogen base, glucose only and no Uracil

S6K: S6 kinase

TTFL: Transcription/Translation Feedback Loops

TSC2: Tuberous sclerosis complex 2

TSC1: Tuberous sclerosis complex 1

TOS: TOR-signaling motif

TOR2: Target of Rapamycin 2

TOR1: Target of Rapamycin 1

TOR: Target of Rapamycin

TOC1: TIMING OF CAB EXPRESSION 1

Tim: Timeless

Thr: Threonine

TFEB: Transcription factor EB

TE: Tris-EDTA

TBC1D7: TBC1 domain family member 7

Tap42: Two A phosphatase associated protein 42

UV: Ultraviolet

UPS: Ubiquitin-proteasome system

uORF: upstream open reading frames

Ypk2: Yeast protein kinase 2

Ypk1: Yeast protein kinase 1

YPD: Yeast Extract–Peptone–Dextrose

WT: Wild type

WDR59: WD Repeat Domain 59

WDR24: WD Repeat Domain 24

WCC: White-Collar Complex

WC: white collar

WC-2: White Collar 2

WC-1: White Collar 1

VTA: Vacuolar TOR-associated protein

VAM6: Vacuolar morphogenesis 6

ULK1: Unc-51 like autophagy activating kinase 1

Tm: Melting temperature

TAE: Tris-acetate-EDTA

Chapter 1. INTRODUCTION

1.1. *Circadian Rhythms*

An endogenous timekeeping process named as the circadian clock assists organisms to adapt to the environmental changes including variations in light, temperature, and food availability during a daily cycle of 24-hours. Because of the importance of circadian clocks in different fields of biology and their enormous impact on all aspects of life, they are of great interest and there are growing efforts to uncover the mechanisms behind their regulation and output pathways. Three functional characteristics of the circadian clock include: a self-sustained rhythm, stable period length in a wide range of temperatures (temperature compensation) and its ability to synchronize with environmental cues (Kumar Jha et al., 2015). It is important to note that while the individual components of the clock are not always homologous, their molecular attributes and mechanisms as well as their assembly are very similar across kingdoms (Loros and Dunlap, 2001; Pittendrigh, 1960).

1.1.1. Circadian Clock in Mammals

The suprachiasmatic nuclei (SCN), the anterior hypothalamus area above the optic chiasm, is the center of the mammalian clock and regulates the behavioural and physiological day/night rhythms. Regulation of the circadian clock in the SCN is primarily conducted by light. Light enables it to adapt to environment changes. A study that successfully hypothesized that even mice without the classic rod and cone visual photoreceptors can still synchronize their internal clocks to light led to significant advances in developing further understanding of how entrainment of oscillators occurs in animals. The light photoreceptors are a small number of retinal ganglion cells that express the photo pigment melanopsin. Mice without the functional form of these cells can still have normal vision, though they experience disruption in their synchronization to light. Linkages to the hypothalamic pacemaker neurons in the suprachiasmatic nucleus pass through some of these melanopsin cells (Bass, 2012a). The process of generation of circadian rhythms in mammals is rather complex. In mammals, ganglion cells located in retina can recognize the presence of light and transduce it to the retinohypothalamic tract. Then through the retinohypothalamic tract, circadian rhythms that are produced by SCN neurons are entrained to overt 24 hours rhythmic cycles. These coordinated outputs are then

transferred to the other parts of the body via autonomic, behavioural, and neuroendocrine pathways (Bass, 2012a).

1.1.1.1. Molecular Machinery in Mammals

The endogenous molecular mechanism that is responsible for the circadian clock in mammals is comprised of transcription-translation feedback loops (Figure 1). As part of the primary feedback loop, the heterodimeric transcription factors CLOCK and BMAL1 stimulate the transcription of the genes that encode four proteins, PER1 (period1), PER2 (period2), CRY1(cryptochrome1) and CRY2 (cryptochrome2) by the attaching E-box motifs and the recruitment of various coactivators, including CBP/P300. The mRNA levels of CRY and PER then increase, and proteins get translated. Thereafter, these corepressors assemble into large protein complexes which bind to CLOCK- BMAL1 heterodimers and inactivate the CLOCK-BMAL1 complex promoters which represses the *cry* and *per* transcription. The concentration of CRY1/2 and PER1/2 drops until the inhibition of the expression is relieved and a new daily accumulation of CRY-PER complex restarts. The secondary feedback loop is comprised of the nuclear orphan receptors REV-ERB a, REV-ERB b, and RORa-c. REV-ERB *a* binds to the ROR response element (PRE) of BMAL1 and CLOCK promoters and represses their transcription, and in contrast to REV-ERBs inhibition, ROR also binds with the PRE of BMAL1 and induces its transcription (Bass, 2012b) (Figure 1).

Protein phosphorylation/dephosphorylation, sumoylation, ubiquitination, acetylation/deacetylation, and poly ADP ribosylation are examples of post translational modifications. They help the activation of the primary and secondary loops. Some of these mechanisms create a connection between metabolic and circadian cycles. (Dibner and Schibler, 2015).

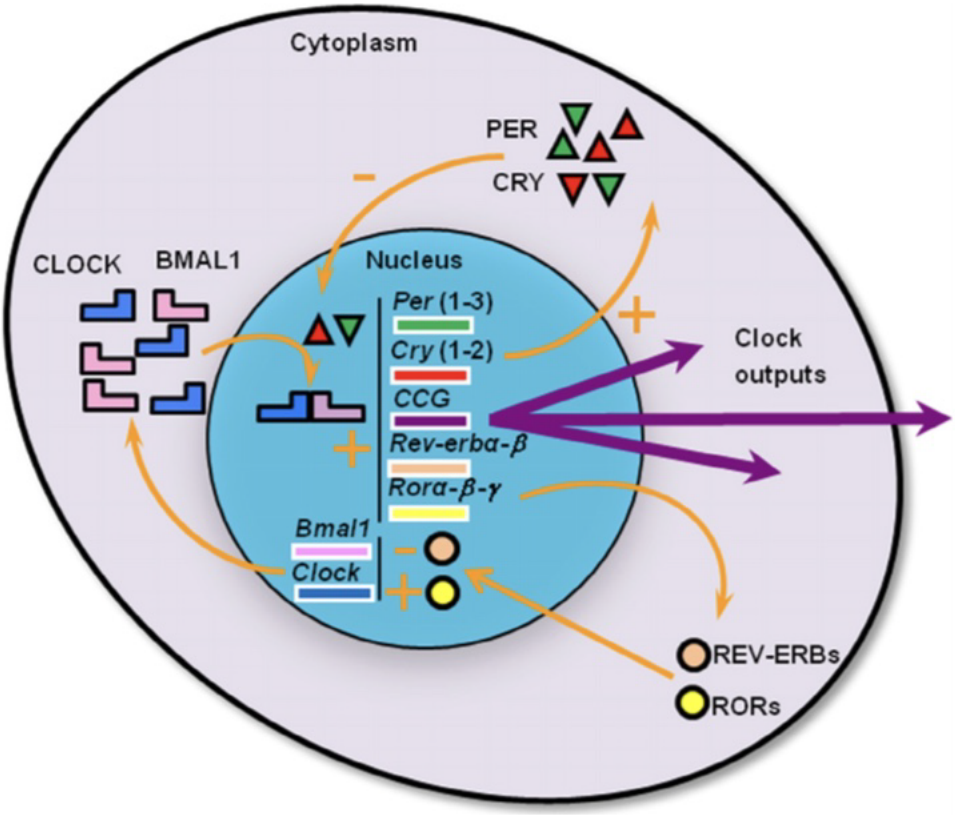

Figure 1: Molecular mechanism of circadian clock in the SCN and peripheral clocks
(Adapted from Kumar Jha, et al, 2015)

1.1.1.2. Interactions between metabolism and circadian clocks in mammals

Living organisms extract energy from their environment and consume the energy for their metabolic processes. The circadian system is instrumental in the coordination of both anabolic and catabolic metabolic pathways. The major components of energy homeostasis in mammals including water and food intake, metabolism and thermoregulation are controlled by the hypothalamus. Three factors regulate energy intake and consumption in animals: their sleep/wake cycle, their feeding/fasting period and whether an animal is diurnal or nocturnal. (Foster & Kreitzman, 2017). Regulation by the circadian clock in the SCN is associated with glucose metabolism, energy homeostasis, and insulin secretion. (Kumar Jha et al., 2015).

1.1.1.3. Connections between metabolites and circadian genes

Environmental signals adjust the circadian rhythm that is generated by the molecular machinery. Extensive metabolomics and lipidomic studies in laboratory rodents and humans

exhibit the oscillation of a large number of metabolites in saliva, tissues, and plasma. NADs (Nicotamide adenine dinucleotide) exhibit a strong connection between metabolites and circadian core clock components. NADs function as the indicators of energy metabolism and can impact the activity of clock transcription factors through an NAD-dependent enzyme. Various experiments demonstrated that DNA binding of CLOCK/BNPAS2 BMAL1 heterodimers is dependent on the ratio of reduced to oxidized NAD [NAD (P) H/ NAD (P)+]. (Dibner and Schibler, 2015). In peripheral organs, cellular metabolism is connected to the expression of clock genes through cellular energy sensors like SIRT1. These cellular energy sensors regulate the expression of clock genes by promoting deacetylation of clock proteins and AMPK. AMPK primarily modulates the molecular clock by destabilizing PER2-CRY1 proteins (Kumar Jha et al., 2015).

1.1.1.4. Circadian clock impairments and metabolism

Impairment in the function of CLOCK and BMAL1 causes metabolic abnormalities (Scott, Carter, and Grant 2008; Sookoian et al. 2007; Woon et al. 2007). For example, the homozygous clock mutant mice exhibit metabolic disruptions such as hepatic steatosis dyslipidemia and decreased gluconeogenesis. They also demonstrate disruption in the daily rhythm of food intake, hyperphagia and increase adiposity. Clock mutation in melatonin proficient mice leads to impaired glucose tolerance. Clock gene mutations dampen the oscillation of hepatic glycogen and glycogen synthase 2 and thereby limit the rate of gluconeogenesis (Doi, Oishi, and Ishida 2010).

Mice that lack BMAL1 demonstrate impaired glucose tolerance in all tissues and usually also suffer abnormal energy balance. In such mice, global BMAL1 KO is generally unable to trigger liver gluconeogenesis (Rudic et al. 2004). Mice lacking BMAL1 especially in beta pancreas cells are likely to have diabetes mellitus and a higher levels of plasma glucose, glucose intolerance and relatively diminished glucose-stimulated insulin secretion in *B* cells (Lee et al. 2013; Marcheva et al. 2010; Sadacca et al. 2011). PER2 disruption leads to enhanced glucose-induced insulin secretion, decreased level of fasting glycemia, altered glycogen accumulation in liver, and impaired gluconeogenesis. PER2 disruption also dampens the corticosterone rhythms (Schmutz et al. 2010; Zani et al. 2013; Zhao et al. 2012). Cry mutation (loss of CRY1/2) causes elevated blood glucose levels in response to acute feeding after an overnight fast and delayed disposal of glucose in a glucose tolerance test (Kumar Jha et al., 2015).

REV-ERB *a* (NR1D1), was primarily discovered as a nuclear receptor that has been considered the key to regulate lipid metabolism and adipocyte differentiation (Fontaine et al. 2003). The modulatory function of REV-ERB in the molecular clock mechanism and its interactions with metabolic transcription elements such as peroxisome proliferator-activated receptor (PRAR) lead to the significance of its functional position at the interface between a metabolic process and the circadian clock (Preitner et al. 2002; Teboul et al. 2008). It has been hypothesized that REV-ERB might also be responsible for regulating glucose homeostasis (through its transcriptional control of glucogenic enzymes in cultured hepatocytes, including glucose 6- phosphate and PEPCL). Glucose-induced insulin secretion is impaired by in vitro down-regulation of *reverb* by RNA interference in pancreatic beta cells or insulinoma cells. REV-ERB is highly expressed in oxidative skeletal muscle cells. REV-ERB also controls muscle mitochondria content and oxidative functions. When REV-ERB expression is deficient in muscles, then such deficiency might cause disruption in glucose homeostasis (Kumar Jha et al., 2015).

1.1.1.5. Circadian clock misalignments and metabolism

During daytime, humans are engaged in feeding, working and exercise. Due to modern lifestyle and busy schedules, during recent times, our society has altered this circadian rhythm by enhancing night activity, shift work and numerous similar activities. Such activities have the potential to disrupt the circadian clock in the long term. Numerous studies indicate that such abnormal disruptions disturb metabolic rhythms and thus lead to metabolic anomalies such as obesity, type 2 diabetes and cardiovascular diseases (Salgado-Delgado et al., 2013). In addition to these, circadian misalignment of glucose metabolism can cause cardiovascular disease. When animals such as rodents are forced to feed and remain active during the sleep phase, then that causes increased body weight gains. Such misalignments in humans lead to more serious health problems in the long run. Human activities such as eating at night leads to sleep-related eating disorders, eventually causing obesity and hormonal and neurochemical disturbances. Disruptions in the circadian clock in adipose tissue and/or disrupted mealtimes cause abnormal expression in the pattern of enzymes engaged in lipid metabolism and perturbs fatty acid homeostasis (Kumar Jha et al., 2015).

1.1.2. Circadian clock in Drosophila

Drosophila was the pioneer model organism which enhanced the understanding of the

transcription translation feedback loop in which the transcription of a gene will lead to translation of a protein product which will eventually increase and repress its own transcription in a negative feedback loop. Protein will then be degraded and the inhibition of transcription relieved and the cycle repeats (Hardin, 2011)

Studying the circadian clock in *Drosophila* enhanced the understanding of the circadian rhythm initiation and entrainment by environmental cycles. *Drosophila* is an amazing model organism to study molecular and neural mechanism underlying circadian rhythms. The molecular machinery of *Drosophila* includes circadian transcription factors CLOCK (CLK) and CYCLE (CYC) that form a heterodimeric complex and stimulate period (*per*) and timeless (*tim*) transcription (Allada et al., 1998; Darlington et al., 1998; Rutila et al., 1998), which leads to the accumulation and heterodimer formation of PER and TIM during the night. (Zeng et al., 1996). The PER/TIM complex flows into the nucleus and stimulates the phosphorylation of CLK/CYC, which restricts its activity, and moderates its affinity for DNA (Yu et al., 2009). However, PER and TIM are also slowly altered by phosphorylation during the day. This finally causes their degradation and discharges CLK/CYC from repression to start a new cycle. *Drosophila*'s molecular clock's strongest input is light, which is received through the activation of CRYPTOCHROME (CRY). Upon the assimilation of photon, this blue-light photoreceptor goes through a conformational transformation that facilitates it to attach TIM (Vaidya et al., 2013). This stimulates TIM ubiquitination and proteasomal degradation, therefore thereby resets the clock (Tataroglu and Emery, 2014)

1.1.3. Circadian rhythms in plants

A ship captain named Androsthenes was the first to find objective evidence of the presence of a circadian clock in plants. He made the observation of the folding and unfolding of leaves in a sensitive plant called *Mimosa pudica*, which continued even in darkness. He subsequently proposed that this rhythmicity could be an internal rhythm. Circadian rhythms help plants survive and increase fitness by anticipating the environmental and seasonal changes by adapting with their physiology (Resco et al., 2009; Yakir et al., 2007). Leaf movement, flowering, and photosynthesis are some examples of the presence of a circadian clock in plants (Altenburger and Matile, 1988).

A transcription/translation feedback model that drives circadian rhythms in plants consists of a single negative feedback loop in which clock genes called CIRCADIAN CLOCK ASSOCIATED1 (CCA1), LATE ELONGATED HYPOCOTYL (LHY) act as a repressor of TIMING OF CAB EXPRESSION 1/ PSEUDO-RESPONSE REGULATOR (TOC1/PRR1). This process directly binds to the evening element (EE) in the TOC1 promoter. (Harmer and Kay, 2005). TOC1 stimulates the expression of CCA1 and LHY via a CCA-1 binding transcription factor, CCA1 HIKING EXPEDITION (CHE) mechanism (Alabadí et al., 2001)

Further research on the concept of the TTFL indicates that there seem to be multiple interlocked TTFLs, which create a synchronized process. Until now, two additional models have been found that explain plants' circadian clock. The second model is the presence of an early morning TTFL. As per the model, CCA1 and LHY directly bind to the promoters and generate the expression of PRR7 and PRR9, which encode repressors of CCA1 and LHY (Salomé and McClung, 2005; Zeilinger et al., 2006). Upon discovery of this model, a further study also anticipated the existence of a third loop, called the "evening loop," which is composed of TOC1 and GIGANTEA (GI) (Locke et al., 2006; Zeilinger et al., 2006). The unidentified clock components should be studied to gain deeper insights into the circadian clock (Srivastava et al., 2019).

1.1.4. Circadian clock in Cyanobacteria

Nitrogen fixation is a mechanism that is regulated by the circadian clock. This is the primary indication of the circadian clock in *Cyanobacterium* at its highest-level during nighttime. (Grobbelaar et al., 1986). The circadian clock has an essential impact on synchronizing a separation of two important metabolic events, which results in the presence of photosynthesis during the day while nitrogen fixation occurs at nighttime. Oxygen is produced by photosynthesis during the day, while nitrogen fixation, an oxygen-sensitive process, occurs at night. In order to get a better understanding of the mechanism, a study was conducted on *S.elongatus* PCC 7942. This organism does not fix nitrogen. Results indicate that all promoters in *S. elongatus* are regulated by the circadian clock and are activated during the day except the purF promoter, which has a nocturnal phase, and the protein product has a role in an oxygen-sensitive pathway (Liu et al., 1996, 1995). DNA topology and transcriptional factor activities are some of the main elements that help synchronize the circadian gene expression in *cyanobacteria*. *Kai A, Kai B, and Kai C* were identified as three essential clock genes in *S. elongatus*. (Ishiura et

al., 2016). The primary belief was that the expression pattern of *KaiABC* is similar to the traditional transcription/ translation feedback model in eukaryotes (Hardin et al., 1990). The presence of evidence such as the abundance of the KaiB and KaiC proteins and oscillation of transcripts (Ishiura et al., 2016; Tomita et al., 2005; Xu et al., 2000), inhibition of KaiC expression in response to overexpression of KaiC protein (Ishiura et al., 2016; Xu et al., 2000), and rhythmic phosphorylation of KaiC protein in vivo (Iwasaki et al., 2002) are similar to the eukaryote clock system. Due to these findings, it was believed that the KAaiABC model is similar to the transcriptional/ translational feedback loop TTFL in which rhythmic transcription of clock genes leads to the rise in mRNA levels and subsequently to the translation of clock proteins. In an important study in Dr. Takao Kondo's group, they purified KaiA KaiB and Kai C proteins, combined them with ATP in a test tube, and rebuilt the KaiC phosphorylation. This rhythm was temperature compensated. Mutations in KaiC, which would alter circadian period in vivo during the rhythm, had the same effects while altering the periods of a post-translational oscillator (PTO) in vitro. Crystallization of Kai A, Kai B, and Kai C proteins, and the in vitro PTO model made the cyanobacteria the primary circadian system in which biophysical methods were first found to be useful.

1.2. *Circadian clock in Neurospora*

1.2.1. Neurospora crassa as a model organism

Neurospora crassa has served as a unique model organism over the years and it was the model organism for the one gene – one enzyme hypothesis introduced by Beadle and Tatum in 1941 (Beadle and Tatum, 1941) . It is from the *Sordariaceae* family and is a filamentous ascomycete. As a eukaryotic multicellular organism, it has numerous advantages as a model organism for research such as genetics, developmental biology, and molecular biology. Biological regulations based on circadian rhythm (Loros and Dunlap, 2001), RNA interference (RNAi) post-transcriptional gene silencing (Cogoni and Macino, 1999), and DNA methylation-mediated epigenetic control have been pioneered by researchers leveraging the properties of *Neurospora crassa* as a model organism. There are many advantages over other model organism such as the availability of molecular techniques, fast growth, and sexual mating. A wide number of single gene knock out collections are available from the Fungal Genetics Stock Center (FGSC) (Honda et al., 2020). *Neurospora crassa's* entire genome has been sequenced and all the

information is available on FungiDB (https://fungidb.org/fungidb/app). Neurospora has 10,000 genes, which is almost two times the number of those in budding yeast, and its haploid life cycle is quite simple.

1.2.2. Neurospora crassa life cycle

Neurospora crassa is a multinucleated organism that grows in hyphae (Ramos-García et al., 2009) and its filaments contain incomplete septa with bifurcating branches (Ziv et al., 2009).It is a haploid organism, and the life cycle can be divided into two different cycles: one is the asexual, and the other one is sexual cycle. During the asexual process, haploid nuclei go through mitosis, leading to hypha formation. Then the multinucleated hyphae grow and produce multinucleate asexual spores (conidia), germinating to form new mycelia. Near dawn, *Neurospora crassa* undertakes developmental modifications to shape aerial hyphae that segment into conidia (Adamovich et al., 2014; Bell-Pedersen, 2000). The circadian clock in *Neurospora crassa* regulates conidiation, and rhythmic spore formation can easily be monitored during growth as a pattern of thick conidiation ‘‘bands’’ alternating with thin growth in ‘‘interbands’’with a period of about 22 hours between bands as the fungal mycelium advances across a solid agar surface. Clock phenotypes are assayed using the bands of conidiospores that form rhythmically when cultures are grown on agar medium in long glass growth tubes known as “race tubes”. Cultures in constant temperature and constant darkness produce a “free-running” rhythm of conidiation.

The second life cycle of *Neurospora crassa* includes a sexual cycle in which inoculating *Neurospora crassa* on SC media (Appendix I) starved for nitrogen leads to the formation of protoperithecia. When exposed to conidia of the opposite mating type it will be fertilized. Their cell walls and nuclei fuse, resulting in many transient diploid nuclei inside fruiting bodies called perithecia. Each diploid nucleus undergoes meiosis. The four haploid products of one meiosis stay together in an ascus sac. Then each of the four products of meiosis ensures an additional mitotic division. Each ascus contains eight haploid ascospores (sexual spores) containing a single nucleus.

1.2.3. Transcription/Translation Feedback Loops (TTFL) in *Neurospora crassa*

The current model for the *Neurospora crassa* circadian oscillator (called the FRQ/WCC TTFL) comprises interlocked negative and positive feedback loops that include the clock genes *frq, wc-1* and *wc-2* (Li et al., 2011). WC-1 and WC-2 proteins heterodimerize to form the White-

Collar Complex (WCC). When WCC is active the levels of *frq* mRNA will increase and FRQ protein is translated. The FRQ protein then will negatively regulate its own transcription by obstructing the activity of WCC and lead to a decrease in *frq* mRNA levels. FRQ protein is degraded, and disruption of transcription is relieved and once the *frq* mRNA builds up again, the cycle repeats. In a positive feedback loop, FRQ protein also causes acceleration in the levels of WCC at posttranscriptional or post translational levels. The rhythmic activity of the WCC regulates the observed rhythms by controlling transcription of downstream genes (Lakin-Thomas et al., 2011) (Figure 2).

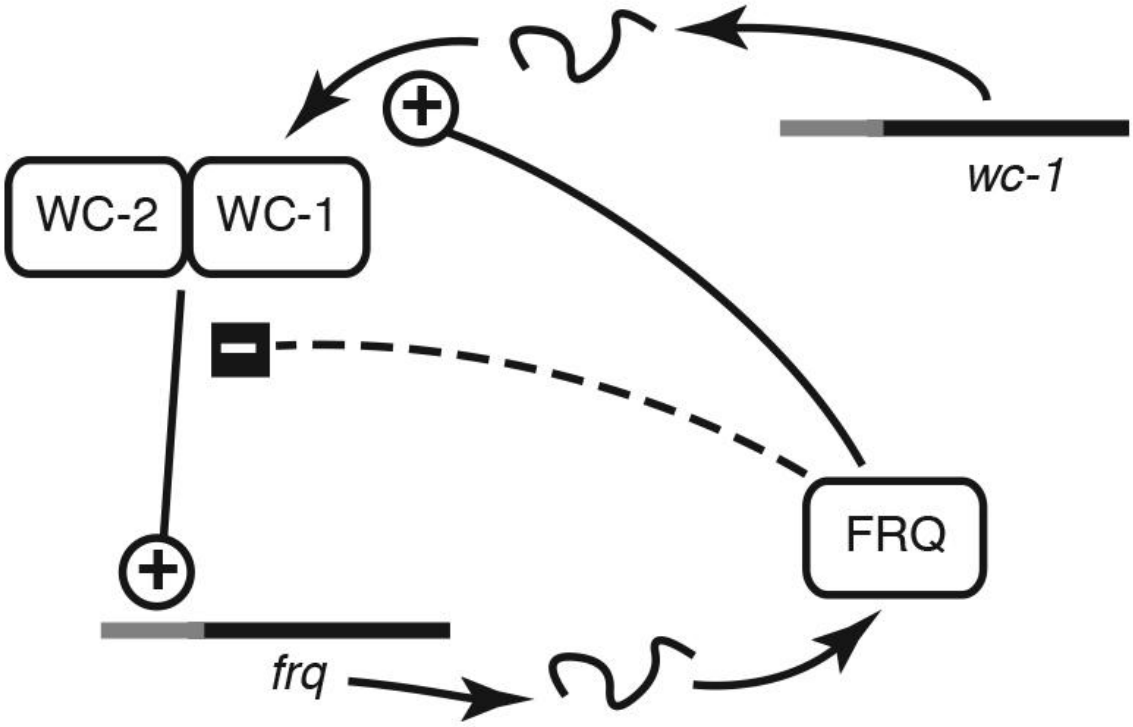

Figure 2: The current model for the Neurospora circadian oscillator (called the FRQ/WCC TTFL). It comprises interlocked negative and positive feedback loops involving the clock genes frq, wc-1 and wc-2. (Adapted from Lakin-Thomas, 2006)

1.2.4. Existence of non-TTFL rhythmicity in different organisms and FRQ-LESS rhythmicity in *Neurospora crassa*

Numerous examples of rhythmicity exist in the absence of rhythmic expression of clock

genes and functional clock proteins. Some prominent examples are *Drosophila*, isolated mammalian fibroblasts (O'Neill et al., 2011), and rhythmic protein phosphorylation in a test tube with a limited number of components in *cyanobacteria* (Tseng et al., 2017). To better understand the circadian oscillators in eukaryotes, we need to identify clock components that operate outside the TTFL. This is a critical yet unexplained problem in circadian biology. Although most of the investigation on the *Neurospora crassa* circadian system is dedicated to the FRQ/WCC feedback loop, it has been known for many years that rhythmic conidiation can be seen in the absence of a functional *frq* gene. Over the years, numerous examples to indicate the presence of FRQ-less rhythms in different conditions and genetic backgrounds have been reported. (Lakin-Thomas et al., 2011). An oscillator must regulate rhythmicity in the absence of FRQ/WCC function. Our lab is dedicated to study the association between the FRQ/WCC and the FRQ-less oscillator(s) (FLOs).

In choline-requiring *chol-1* mutant strains, the duration of the free-running rhythm in constant conditions is governed by the choline concentration in the medium; this rhythm continues in FRQ-less strains (Lakin-Thomas PL and Brody S, 2000). In a second assay, race tubes are entrained (synchronized) by repeated short (2h) pulses of high temperature (22°C>32°C) at various intervals (T-cycles). The timing and shape of the entrained bands change with the T-cycle if a competent oscillator is present. This assay also demonstrates the presence of an oscillator in FRQ-less strains (Lakin-Thomas, 2006).

1.3. *TOR Pathway*

TOR (Target of Rapamycin) is a nutrient sensitive, central controller of cell growth and aging and is the target of the drug rapamycin, which is a lipophilic macrolide and a natural secondary metabolite, generated by *Stereptomyces hygroscopius*. It restricts the growth of tumor cells directly and has the indirect effect of impeding the growth of fresh blood vessels. In the early 1970s it was also used as an antifungal agent. Such conditions are due to abnormal and unfavorable cell growth, suggesting that the molecular target of rapamycin is a central controller of cell growth. FKBP (FK506) binding protein has been identified in mammalian cells as a rapamycin binding protein (Heitman et al., 1991; Koltin et al., 1991; Wiederrecht et al., 1991). The encoding gene *fpr1* in yeast is identical to the *fkbp12* gene in humans, providing evidence that the mode of action of rapamycin was conserved from human to yeast (Loewith and Hall, 2011)

1.3.1. TOR (Target of Rapamycin) in Mammals

The mammalian target of rapamycin integrates both extracellular and intracellular signals to promote cell growth, proliferation, and cellular metabolism. Various studies have demonstrated a fundamental role of mTOR in regulating important cell processes such as protein synthesis, and its impact in cancer and diabetes progression. mTOR also regulates the process of aging. During the process of tumor formation, aging, adipogenesis, and insulin resistance, mTOR is activated. Whereas, during diabetes type 2 and cancer, mTOR is inhibited (Laplante and Sabatini, 2009).

mTOR is a 289 kD protein and is a Serine / Threonine kinase that is part of a super-family of PI3K family kinases and is composed of two functionally and structurally distinct complexes: mTORC1 and mTORC2. Throughout the process of evolution, mTOR is conserved (González and Hall, 2017).

1.3.1.1. mTORC1 Components

mTORC1 has 3 core subunits: 1. mTOR, the catalytic subunit, 2.Raptor, the regulatory subunit that is responsible to facilitate the substrate binding of TOR by attaching to signaling TOR (TOS) motif on some of the substrates and is primarily important for the correct localization of TOR, 3. mLST8 (mammalian lethal with sec 13 protein 8) (Hara et al. 2002) that combines with the catalytic subunit of TOR and stabilizes the kinase activation loop. mTORC1 also has 2 inhibitory subunits: DEP domain-containing mTOR interacting protein or DEPTOR and PRAS40, which is the proline-rich AKT substrate (Sancak et al. 2007; Haar et al. 2007). Both subunits function as negative regulators of mTORC1 as they increase inhibition when the activity of mTORC1 is reduced; while when mTORC1 is active, DEPTOR and PRAS40 reduce their physical interaction with mTOR, thus increasing its function (Saxton and Sabatini, 2017).

1.3.1.2. mTORC2 components

mTORC2 consists of four subunits: mTOR, Rictor (a rapamycin-insensitive component of mTORC2) (Jacinto et al. 2004), mammalian stress-activated protein kinase interacting protein (mSIN1) and protein noticed with Rictor 1 (protor-1/2). Although various studies have proven that Rapamycin- FKBP12 (rapamycin binding protein) directly inhibits mTORC1, it does not inhibit the functions of mTORC2.

1.3.1.3. Upstream effectors of mTORC1

Upstream effectors of mTOR pathway comprise growth factors, insulin, oxygen levels, and

energy levels. These pathways impact TOR through the inhibition or activation of the TSC complex. TSC is a heterotrimeric complex that contains TSC1, TSC2 and TBC1D7. TSC acts as a GAP for small GTPase Rheb, which is localized on the lysosomal membrane and is active when it is in its GTP bound form. The activation of TSC initiates its GTPase activity. The activity hydrolyzes the bound GTP and inactivates Rheb, that in turn activates or inhibits mTORC1. Insulin binds to its receptor IRS which phosphorylates AKT through the PI3K pathways; after this process, AKT inhibits TSC, that in-turn activates mTORC1. EGF functions by binding to its receptor EGFR. EGFR activation activates a cascade of components downstream including ERK that eventually inhibits TSC complex. During the condition of hypoxia, REDD1 (regulated in DNA damage and development) mediates mTORC1 inhibition by regulating the TSC complex. Under the conditions of energy stress, the tumor suppressor LKB1 is activated. The activation of LKB1 phosphorylates and activates the AMPK pathways. The TSC complex inhibition by these factors eventually inhibits the activities of mTORC1. mTORC1 also responds to and is inhibited through the DNA damage-response pathways by induction of p53 target genes including the AMPK regulatory subunit (AMPKB), PTEN, and TSC2. All of these sub-units enhance the activities of TSC and reduce the activities of mTORC1 (Boutouja et al., 2019).

By different strategies, mTORC1 responds to glucose deprivation. These strategies include: 1. mTORC1 is inhibited by the regulator AMPK, a conserved signaling pathway that is activated by metabolic stress. AMPK directly inhibits the activities of mTORC1 through the process of phosphorylation of RAPTOR Ser 792 and Ser 722, and indirectly by phosphorylating and activating TSC2 and inhibiting Rheb. 2. Through the inhibition of RAG GTPases, glucose deprivation also restricts mTORC1 in the cells that lack AMPK (Inoki et al., 2003) (Figure 3).

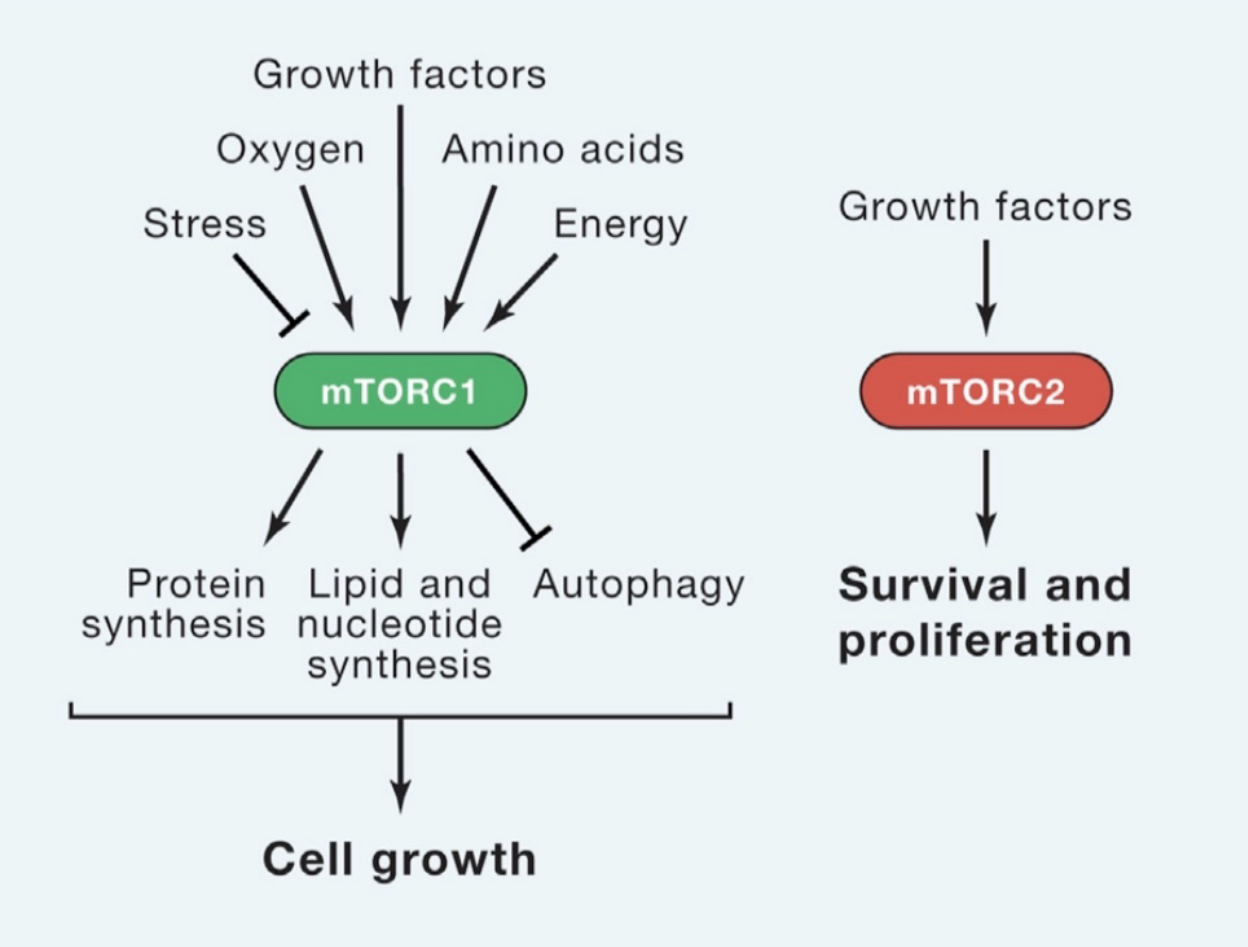

Figure 3: Upstream and downstream factors of the TOR pathway in Mammals. (Adapted from Saxton, Robert A, Sabatini, David M, 2017)

1.3.1.4. Amino acid activation of mTORC1

The activation of mTORC1 by amino acids is independent of TSC1/2, as the mTORC1 pathway remains sensitive to amino acid deficiency in cells that doesn't contain TSC1 or TSC2. Various studies have demonstrated that TOR is activated in a different manner by amino acids. Under this activation process, amino acids sufficiency is sensed via small RAG family of GTPases. RAGS form heterodimers of RAGA/ B and RAG C/D and are tethered to the lysosomal membrane by their interaction with the Ragulator complex (Sancak et al., 2008). The Ragulator complex is usually a pentameric complex that consists of MP1, P14, P18, HPC1D, and C7ORF59. Amino acids adequately promote the active conformation of RAGS. Under this complex process, RAGA/B becomes loaded with GTP (Durán and Hall, 2012). As part of the same process, RAG C/D gets loaded with GDP, and it allows them to associate with RAPTOR,

which recruits mTORC1 to the lysosomal surface, where the growth factor stimulated Rheb is located. mTORC1 perceives both intra-lysosomal and cytosolic amino acids by different mechanisms. Amino acids inside the lysosomal lumen change the RAG nucleotide state by a process dependent on the lysosomal v-ATPase, which interacts with the RAGULATOR-RAGS complex to stimulate the nucleotide exchange factor GEF activity of RAGULATOR through RAGA/B (Saxton and Sabatini, 2017). Through the interaction of the lysosomal amino acid transporter SLC38A9 with the RAG- RAGULATOR-v-ATPase complex, arginine activates mTORC1. In addition to these, through separate pathways including the GATOR1 and GATOR2 complexes, cytosolic leucine and arginine signal to mTORC1. GATOR 1 consists of DEPDC5, Npr12, and Npr13 and acts as a GAP for Rag A/B that inhibits mTORC1. GATOR2 is a pentameric complex that comprises of Mios, WDR24, WDR59, I1L, and Sec13 and acts as a positive regulator of mTORC1, which tethers GATOR1 on the lysosomal membrane. Under amino acid deprivation conditions, Sestrine 2, which is identified as a GATOR2 interacting protein and is also a direct Leucine sensor upstream of mTORC1 combines and restricts GATOR2 function in the absence of leucine. GATOR 1 is associated with the lysosomal membrane through the kicstor complex (Boutouja et al., 2019).

1.3.1.5. Downstream of mTORC1

mTORC1 phosphorylates important substrates such as p70 S6K1, and EIF4E binding protein (4EBP). Phosphorylation of S6K1 by mTORC1 directly occurs on the hydrophobic motif Thr389 and that enables its subsequent phosphorylation by PDK1. As a result of phosphorylation of S6K1, it phosphorylates several subunits that promote mRNA translation. For example, the phosphorylation of EIF4B, which is a positive regulator of 5’ cap-dependent translation(Holz et al. 2005) and also stimulates the degradation of PDCD4 that restricts EIF4B, increases translation efficiency of spliced mRNA. mTORC1 also phosphorylates 4EBP to inhibit its assembly of EIF4F complex (Gingras et al. 1999) that enables the 5’ cap-dependent mRNA translation (Saxton and Sabatini, 2017).

mTORC1 leads to the promotion of denovo lipid synthesis via the sterol responsive element binding protein (SREBP) transcription factors and also via the peroxisome proliferator-activated receptor Y (PRARY). PRARY controls the expression of genes engaged in biosynthesis of cholesterol and fatty acids. mTORC1 activates SREBP through both an S6K-dependent mechanism (Düvel et al. 2010) and phosphorylation of lipin1, which restricts SREBP in the

absence of mTORC1 signaling (Peterson et al. 2011). As a reaction to the low sterol levels, SREBP also activates. The process of blocking of mTORC1 with Rapamycin restricts the expression and activities of PRARY (Laplante and Sabatini, 2009).

By stimulating the expression of STF4 (transcription factor 4)-dependent of MTHFD2 (one of the components of mitochondrial tetrahydrofolate cycle), mTORC1 stimulates the synthesis of nucleotides for DNA replication and ribosomal biogenesis in proliferating cells. The process facilitates one carbon unit for purine synthesis. S6K also activates the carbamoyl-phosphate synthetase (CAD) (Robitaille et al. 2013), which is an important part of the denovo pyrimidine synthesis pathway (Saxton and Sabatini, 2017).

By stimulating an alteration in glucose metabolism from oxidative phosphorylation to glycolysis, mTORC1 enables growth. mTORC1 enhances the translation of the transcription factor HIF1a, which leads to the expression of several glycolytic enzymes such as phospho-fructokinase (PFK). Furthermore, via the oxidative pentose phosphate pathway (PPP), mTORC1-dependent activation of SREBP results in increased flux. The process uses carbons from glucose to generate NADPH and other intermediary metabolites required for proliferation and growth (Saxton and Sabatini, 2017).

During the process of autophagy, separation of the intracellular material into autophagosomes occurs, and the resultant material is then degraded in the lysosome. This process is important for the organelle degradation and also for protein turnover. Autophagy is induced by mTORC1 inhibition. The activation of ULK1 with ATG13, FIP2000 and ATG 101 further promotes the autophagosome formation. mTORC1 causes phosphorylation of ULK1 and prevents its activation by AMPK, which is an important factor for autophagy. mTORC1 also inhibits the complex formation of ULK1 with FIP2000 and ATG13 that eventually inhibits autophagy.

An additional role of mTORC1 is to regulate autophagy by phosphorylating and inhibiting transcription factor EB (TFEB), which is responsible for the expression of genes for lysosomal biogenesis and autophagy(Martina et al. 2012; Settembre et al. 2012).

Ubiquitin-proteasome system (UPS) is another essential pathway responsible for the protein turnover in humans. In UPS, proteins are selectively targeted for degradation by the 20S proteasome and covalent modification with ubiquitin. UPS is inhibited upon TORC1 activation (Saxton and Sabatini, 2017).

1.3.1.6. Upstream of mTORC2

The insulin/ PI3K signaling pathway is known as an upstream effector of mTORC2. mTORC2 subunit mSin1 has a phosphoinositide-binding PH domain which is vital for the insulin-dependent regulation of mTORC2 activity. In the absence of insulin, the PH domain restricts mTORC2 catalytic activity and upon binding to PI3K-generated PIP3 at the plasma membrane this inhibition gets relieved. (P. Liu et al. 2015) As an additional function, AKT is responsible for phosphorylating mSin1, which demonstrates a positive feedback loop. Under this process, partial activation of AKT stimulates the activation of mTORC2, which as a result phosphorylates and activates AKT (Yang et al. 2015).

1.3.1.7. Downstream of mTORC2

mTORC2 regulates proliferation and survival via a complex process of phosphorylation of many members of the AGC family of protein kinases such as PKA, PKG and PKC. The first substrate that was identified for the mTORC2 was PKCa, which is a regulator of the actin cytoskeleton, and up-regulates the level of B integrin, which regulates cytoskeletal remodelling, and cell migration. As an additional function, mTORC2 phosphorylates and activates AKT. AKT is considered an important effector of insulin/ PI3K signaling pathway. Activated AKT stimulates cell growth and survival by phosphorylating many substrates including FoXO1/3 (Guertin et al. 2006) transcription factors and TCS2, which is an inhibitor of mTORC2 (Saxton and Sabatini, 2017) In addition to these, another important AGC family kinase that gets phosphorylated by mTORC2 is SGK. SGK regulates ion transport and cell survival as part of a complex mechanism (Boutouja et al., 2019).

1.3.2. TOR Pathway in Yeast

1.3.2.1. TOR protein Structure

An important aspect of the TOR signaling pathway is that it is conserved as a major regulator of growth among all eukaryotes. The domain structure of all TORs is similar. The domain from N to C terminus is composed of HEAT repeats, the FAT domain, the FRB domain, and the kinase domain (Schmelzle, Helliwell, and Hall 2002). The Heat repeats are at the N-terminal half of TOR and are the primary site for associating with the sub-units of TOR complexes. The primary FRB domain is considered the FKBP-rapamycin binding region. The kinase domain

phosphorylates Ser /Thr residues in protein substrates. The FATC domain is always located at the C terminal and is vital for the kinase activity.

In yeast TOR 1 and TOR 2 proteins are 282 kDa in size and 67% identical. Yeast is unusual from other organisms because it has two TOR genes and most other organisms have a single TOR. These are considered the founding members of kinase- related protein kinase (PIKK) family of atypical Ser/Thr specific kinases.

1.3.2.2. TOR complexes in Yeast and their interaction with Rapamycin

Based on various experiments in yeast, two multi-protein complexes termed TORC1 and TORC2 have been identified. These complexes have been extracted from yeast cells and are assigned to the two genetically defined TOR-signaling branches. These branches are believed to control a broad range of readouts such as mRNA synthesis and degradation, protein synthesis and degradation, Ribosome biogenesis, nutrient transport, and autophagy. TORC1 is primarily rapamycin sensitive, and it mediates the TOR-shared pathway. In contrary to it, TORC2 is rapamycin insensitive and mediates the TOR2-unique pathway, that eventually regulates the actin cytoskeleton organization, endocytosis, and sphingolipid synthesis (Loewith and Hall, 2011).

1.3.2.3. TORC1 and its localization in Yeast

TORC1 comprises kog1, Lst 8, Tco89 and either TOR1 or TOR2. GFP tagging of yeast kog1, TCO89, Lst8, and TOR1 consistently exhibits that yeast TORC1 is primarily accumulated on the vacuolar membrane and since the vacuole is a major nutrient reservoir, TORC1 signaling is responsive to nutrient signals (Urban et al. 2007; Sturgill et al. 2008; Binda et al. 2009).

1.3.2.4. EGO complex and Amino acid activation in yeast

In yeast, EGO complex comprises EGO1, EGO3, Gtr1, and Gtr2. Gtr1 and Gtr2 are a part of Ras-family GTPases. Similar to TORC1, the EGO complex localizes to the vacuolar membrane and reacts to intra vacuolar amino acid levels. The $Gtr1^{GTP}$ $Gtr2^{GDP}$ combination leads to the activation of TORC1. In yeast $GTR1^{GTP}$ / $GTR2^{GDP}$ binds kog 1 and activates TORC1. TORC1 is located on the vacuolar membrane despite being active or inactive, and irrespective of the presence of nitrogen source or amino acids. The nucleotide binding status of yeast Gtr1/2 is controlled by conserved GAP and GEFs. The vacuolar protein Vam6 acts as a GEF for GTR

(Binda et al., 2009) . The heterotrimeric protein complex SEACIT (She-1 associated sub-complex that inhibits TORC1), which is homologous to GATOR1 in mammals, functions as GAP for Gtr1 in yeast. SEACIT comprises Npr2, Npr3, and catalytic sub-unit Iml1. Another complex known as SEACAT (She 1- associated subcomplex activating TORC1) in yeast is homologous to GATOR2 in mammals and consists of Sec13, I1, Sea2, Sea3 and Sea4, which eventually binds and negatively regulates SEACIT. Yeast proteins Lst4 and Lst7 also function as a GAP for GTR2 (González and Hall, 2017).

The process of amino acid sensing in budding yeast is rather complex. In budding yeast, leucine activates TORC1 via Gtr1 although it is not yet known whether leucine signals to Gtr1 through SEACAT. Yeast doesn't have SESTRIN orthologs, and this suggests that functional counterparts of SESTRINS exist or that yeast and mammalian cells sense leucine differently. Two studies exhibited that yeast and mammalian leucyl-tRNA synthetases (LeuRS) function as cytoplasmic leucine sensors to activate TORC1/mTORC1, although via different mechanisms. These studies further showed that in yeast leucine-bound LeuRS binds Gtr1, and indicated that this interaction is necessary and is sufficient to mediate leucine signaling to TORC1 (González and Hall, 2017). (Figure 4).

Arginine sensing in yeast is different from the process in mammals. It is interesting to note that CASTOR (arginine sensor in mammals, that blocks GATOR2 complex) homologs are present in vertebrates, but are absent in worms, flies, and yeast. However, how arginine is sensed in non-vertebrates is yet to be known (González and Hall, 2017).

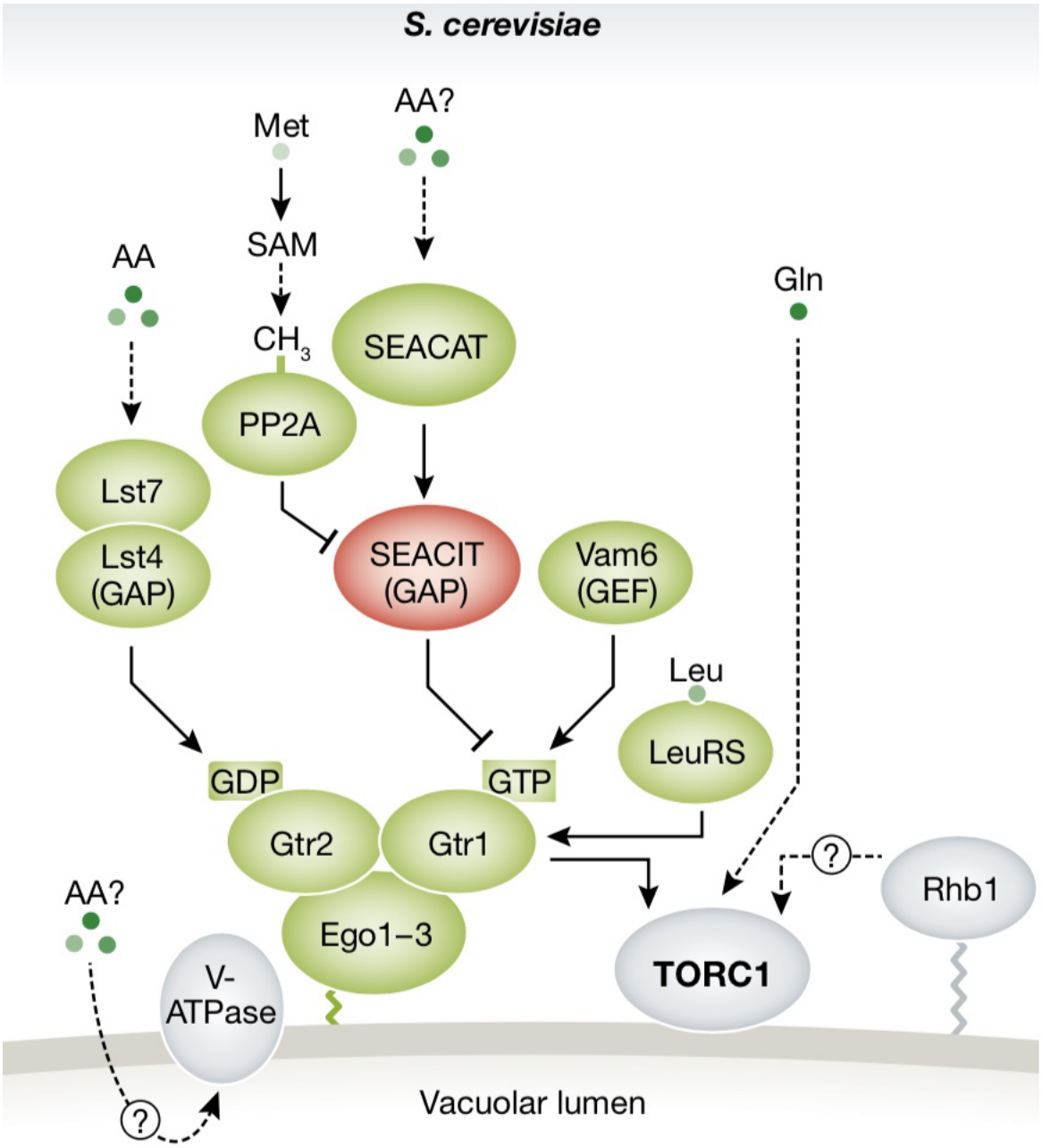

Figure 4: TORC1 regulation by amino acids in yeast. Adapted from (González and Hall, 2017)

1.3.2.5. Downstream of TORC1 in yeast

In response to intracellular amino acid levels through the EGO complex, the activities of TORC1 stimulate the initiation of translation. Restriction of translation by cycloheximide leads

to an increase in TORC1 activity by prompting a build-up in amino acid levels. TORC1 regulates ribosome biogenesis by SCH9 (homologous to S6K), which is considered one of the best-characterized substrates of TORC1, and transcription factor sfp1. Deletion of sfp1 and SCH9 eventually reduces ribosome biogenesis and increases TORC1 activity by increasing amino acid levels. Activated TORC1 phosphorylates Sch9 and regulates phosphatases through regulatory protein Tap42. Tap42 is phosphorylated and is associated with the phosphatase Rrd complex when TORC1 is active. Inactivation of TORC1 causes Tap42 dephosphorylation and a weak association with phosphatases that results in their activation or change in substrate preference (Loewith and Hall, 2011).

1.3.2.6. Ribosome Biogenesis

Yeast cells have the ability to rapidly grow and divide. The prerequisite of a faster growth is a strong ability to synthesize protein, which needs ribosomes. A developing yeast cell contains around 200,000 ribosomes, and it implies that every cell produces 2000 ribosome per minute. Each ribosome is comprised of 78 unique proteins, four rRNA molecules out of which three are extracted from RNA POL I transcribed 35 S pre-rRNA and the remaining one is transcribed by RNA pol III. 50% of RNA pol II transcription is usually directed for ribosomal proteins. Additionally, many protein and ribosome biogenesis factors (RiBi) are needed for the correct processing, folding, assembly, and nuclear export of pre-ribosomal particles to the cytoplasm, and final maturation into the 40S and 60S particles. TORC1 mediates the major production of all these molecules at the level of transcription. In addition, TORC1 also controls the accumulation of RNA pol I at multiple levels and rapamycin exposure leads to a quick drop in RNA Pol I transcript. The decline is usually due to a decreased translation. A drop in translation also reduces free ribosomal proteins. TORC1 controls RNA pol III through SCH9 and Maf1, which is a suppressor for RNA pol III. SCH9 directly phosphorylates 7 sites in Maf1 that prevents its inhibition on Pol III (Loewith and Hall, 2011).

Cell growth and cell division are inter-linked. Ribosome biogenesis plays an important role in determining the size of a cell. The condition of adverse growth decreases the activity level of TORC1 and eventually the activity levels of sfp1 and sch9. As a result, it also reduces ribosome biogenesis, that eventually lowers the threshold for cell size that is required for cell division. TORC1 also controls the G1 cycle and stimulates S phase by maintaining deoxynucleoside triphosphate pools. Further, TORC1 influences the G2/M transition by the TAP42-Ppase branch

(Loewith and Hall, 2011).

1.3.2.7. Responses to Environmental Stressors

A transcriptional response known as the environmental stress response (ESR) is stimulated by environmental stressors such as nutrient starvation (Gasch and Werner-Washburne 2002). The process includes around 300 genes that encode processes including protein chaperones and oxygen radical scavengers to assist cells to bear the stressful environment. ESR pathway includes Zn-finger transcription factors Msn2/4 and Gis1, LATS family kinase Rim 15 and a-endo sulfine family Igo1 and Igo2 (de Virgilio 2012). TORC1 promotes the cytoplasmic anchoring of Rim 15 to 14-3-3 proteins by phosphorylating Rim 15 on Ser 1061 and TAP42Ppase (Wanke et al. 2008). Restriction of TORC1 causes nuclear localization of Rim 15, which prompts the expression of Msn 2/4, Gis1 dependent ESR genes (Loewith and Hall, 2011).

In various experiments, yeast has demonstrated its ability to compete with other microbes in the environment for using available nutrients to promote fast growth. Yeast cells absorb preferred sources of nutrition before utilizing non-preferred ones. In response to the nutritional stress conditions, yeast cells control the expression and sorting of membrane transporters. This process enables yeast cells to selectively import nutrients. When the conditions are nutrient-rich, then yeast cells express many high-affinity substrate selective permeases and sort them to the plasma membrane to actively pump in nutrients that are utilized for the ATP production and anabolism of nitrogenous compounds. In contrast to this, when nutrients are absent, then these high affinity permeases get replaced with few low-affinity specificity permeases that allows the uptake of a wide range of carbon and nitrogenous compounds. TORC1 controls this permease sorting program by TAP 42 Ppase and its effector Npr1. Npr1 is a fungal- specific Ser / Thr kinase which is phosphorylated under normal conditions and upon TORC1 inactivation is rapidly dephosphorylated and activated. In addition to the permease localization, TORC1 is also responsible to regulating the expression of a large number of permeases that are necessary for the alternative nitrogenous sources. TORC1 is responsible for controlling the expression of nitrogen catabolite repression (NCR)-sensitive genes via TAP42, and proteins encoded by these genes enable cells to transport and metabolize poor nitrogen sources such as proline and alatonin (Loewith and Hall, 2011)

In addition to the NCR pathway, TORC1 regulates many processes in organisms. For example, TORC1 controls the expression of amino acid permeases by modulating the activity of

the SPS-sensing pathway. The sensing of amino acids activates SPS pathway in yeast and that happens only in fungi (Martı, 2005) It is comprised of a cytoplasmic localized complex that consists of Ssys1, which is a transmembrane sensor related to amino acid permease though lacks the capacity to transport. Ssys 5, which is a zymogen and also has a catalytic domain, an inhibitory domain and a ptr2, which is a scaffold protein. Binding of extracellular amino acids to Ssy1 induces a conformational change that stimulates the phosphorylation of the catalytic subunit of Ssys5. Active Ssys 5 cleaves the N-terminal cytoplasmic motifs of transcription factors STP1-3 and translocates them to the nucleus, which eventually induces expression of genes encoding amino acids. TORC1 and SPS are connected. TORC1 uses pp2A phosphatases sit4 to promote the stability of STP1 in the nucleus and increase amino acid uptake (González and Hall, 2017).

The conserved GAAC (general amino acid control) signaling pathway coordinates amino acid availability with translation initiation to permit cells to adapt to amino acid deficiency. The GAAC signaling pathway perceives the deficiency of amino acids via uncharged tRNAs that build up, when free amino acid levels are less. In amino acid-deficient cells, uncharged tRNAs associate with and stimulate the protein kinase GCN2 (general control non-derepressible 2) (Wek, Jackson, and Hinnebusch 1989; Diallinas and Thireos 1994; Dong et al. 2000). Active GCN2 phosphorylates the alpha sub-unit of eIF2 (eukaryotic initiation factor 2a). As a result, it inhibits eIF2 and eventually leads to general repression of mRNA translation. Interestingly, this supports choosy translation of mRNA with a unique 5'UTR structure containing short uORFs (upstream open reading frames). The uORF containing mRNA encodes a basic leucine zipper transcription factor termed as ATF4 (activating transcription factor 4) in mammals and Gcn4 in yeast (Hinnebusch 1984). ATF4/Gcn4 induces the expression of amino acid transporters, enzymes involved in amino acid metabolism and factors engaged in autophagy thereby allowing adaptation to amino acid starvation. A link between TORC1 and GAAC has been demonstrated in *S. cerevisiae*. In yeast TORC1 signals to eIF2a via both the Sch9 and Tap42-Ppase branches. TORC1 prevents the dephosphorylation of Ser577 in Gcn2 by inhibiting one or more phosphatases. Phosphorylation of Gcn2 at Ser577 inhibits Gcn2 by decreasing its uncharged tRNA binding ability. Thus, in budding yeast, Gcn2 activation upon amino acid starvation is a consequence of an increase in uncharged tRNAs and the release of an inhibitory effect of TORC1. Despite the conserved role of Gcn2 in translation, it is unknown if mTORC1 regulates

GCN2 as well or not (González and Hall, 2017)

Yeast cells do not express TSC2, but the AMPK Snf1 is essential for the TORC1 inactivation in glucose-starved cells. AMPK snf1 phosphorylates kog1 at two different sites, Ser 491 and Ser 494. Phosphorylation of kog1 leads to dissociation from TORC1 to pre vacuolar sites (Hughes Hallett, Luo, & Capaldi, 2015). The process eventually leads to a reduction in TORC1 activation. The deprivation in glucose inhibits TORC1 in yeast cells expressing active $GTR1^{GTP}/GTR2^{GDP}$ thus TORC1 inhibition upon glucose deprivation does not require GTR1/2 (González and Hall, 2017).

1.3.2.8. TORC1 inhibition of Autophagy in Yeast

In yeast, two different autophagy mechanisms operate: 1. Microautophagy, under which the cytoplasm gets transferred to the vacuole by invaginations of the vacuolar membrane. 2. Macroautophagy, which involves the de novo formation of double-membrane structures called autophagosomes. Both mechanisms of autophagy are regulated by TORC1. In yeast cells, the regulation of the macroautophagy by TORC1 activity includes signaling of the TORC1 to the Atg1 kinase complex, which is necessary for the induction of macroautophagy. When TORC1 is active Atg13 is hyperphosphorylated and it inhibits the interaction of Atg13 with Atg1, Atg17, Atg31, and Atg29 (Yorimitsu et al. 2009; Kamada et al. 2010). Inhibition of TORC1 results in dephosphorylation of Atg13, assembly of the Atg1 protein kinase complex, phosphorylation and activation of Atg1 and, consequently, macroautophagy mediated by as-yet-unidentified Atg1 substrates (Loewith and Hall, 2011).

1.3.2.9. TORC2 and its localization in yeast

TORC2 comprises TOR2, Avo1, Avo2, Avo3, Bit61 and Lst8, and is located at or near the plasma membrane. TORC2 is localized to plasma membrane structures called MCT (membrane compartment containing TORC2). Plasma membrane localization is important for TORC2 activity, and its localization is mediated by the PH domain in Avo1. A plasma membrane location is also coherent with the role of TORC2 in controlling the actin cytoskeleton and endocytosis. TORC2 directly phosphorylates the AGC kinase family member Ypk (Ypk1 and 2) which is an essential pair of homologous kinases and members of the AGC kinase family and the PH domain containing protein Slm (Slm1 and 2). Downstream effectors include the phosphatase calcineurin, the transcription factor Crz1, and Pkc1. TORC2 regulates the actin cytoskeleton,

endocytosis, sphingolipid biosynthesis, and stress-related transcription (Loewith and Hall, 2011)

1.3.3. Health-related effects of TOR pathway

Hyperactivated TORC1 is the cause of many diseases. For example, mutations in TSC1 or TSC2 eventually cause autosomal-dominant hamartomas and lymphangioleiomyomatosis (Napolioni and Curatolo 2008). Activation of a network that enhances glycolysis by the up regulated expression of the pyruvate kinase is also one of the examples of the downstream effects of mTORC in carcinogenesis. Pyruvate kinase (isoenzyme M2) is a mediator of the Warburg effect, which is a metabolic characteristic of cancer cells that relies on cytosolic substrate-level phosphorylation during anaerobic glycolysis and less on oxidative phosphorylation, which is the preference of most other cells (Burns and Manda 2017). Survival of cancer cells under hypoxic conditions requires the up regulation of glycolytic gene expression. The process is largely dependent on transcription factor HIF1a and this leads to energy production under anaerobic conditions (G. Liu et al. 2014). Another example is the hexokinase isoform II that is a glycolytic enzyme and is up regulated in malignant tumors. TORC1 stimulates the synthesis of HKII by HIFIa in the presence of glucose and insulin. This stimulation supports the anaerobic glycolysis in cancer cells (Boutouja et al., 2019).

Another important health-related impact of TORC1 is the inhibition control of autophagy (Boutouja et al. 2017). Autophagy protects healthy cells by removing damaged ROS-producing organelles like mitochondria and peroxisomes (Janji et al. 2016). Recent evidence indicates the important role of controlled inhibition of TORC1, that eventually reduces numerous types of cancers (Boutouja et al., 2019)

Reduction in the activity of mTOR is demonstrated to have a primary role in extending the life span in several experimental organisms such as *Caenorhabditis elegans* (Vellai et al. 2003), *Drosophila melanogaster* and yeast (Boutouja, Stiehm, and Platta 2019). In yeast, life span can be measured under 2 conditions: 1. Replicative life span (RLS), which is the number of progeny that is produced from a single mother, 2. Chronological life span (CLS), which is a measure of the length of time that a population of yeast cells can remain in stationary phase before they lose the ability to restart growth when they are reinoculated into a fresh media. Experimental evidence demonstrates that GCN4, which is a TORC1-dependent transcription factor that regulates the expression of amino acid biosynthetic genes, can mediate the TORC1 inhibition and 60S depletion in RLS state which causes the extension of RLS. The candidate target for

GCN4 is assumed to be macroautophagy. Induction of macroautophagy such as TORC1 and SCH9 inhibition extends to both RLS and CLS and GCN4 is required for amino acid starvation-induced macroautophagy (Loewith and Hall, 2011).

1.4. *Hypotheses and Objectives*

Our lab's long-term goal is to completely describe a circadian system's molecular network by using *Neurospora crassa* as a model organism and to answer the following question: What is the FRQ-less oscillator and how does it interact with the FRQ/WCC TTFL to build a complete circadian system?

During previous experiments to find components of the FRQ less oscillator, our lab found that a gene that affects the FRQ-less oscillator named *prd-1* (NCU07839) is homologous to the dbp-2 DEAD-box RNA helicases in yeast. This gene binds to S6, which is a member of the small subunit of the ribosome and a substrate of the TOR pathway. Using a mutagenesis screen in an FRQ-less strain, our lab identified a mutation named *vta* that impacts FRQ-less rhythmicity of the conidiation (spore-formation) and the amplitude of the FRQ protein rhythm. The *vta* mutation, therefore, identifies a gene necessary for the robust FRQ-less rhythmicity and for maintaining the amplitude of the entire circadian system, when FRQ is present. Our lab mapped the *vta* mutation and identified the gene as NCU05950. Sequence homology analysis identified the gene as a member of the LAMTOR family, similar to p18/LAMTOR1 in mammals and EGO1/Meh1p/Gse2p in yeast, a component of the TOR nutrient-sensing pathway conserved in eukaryotes. Our lab named the gene product VTA for vacuolar TOR-associated protein.

Further analysis by a former Ph.D. student indicated that VTA is localized on the outer vacuolar membrane, similar to its homologs in mammals and yeast. The mutant does not respond to different amino acid, nitrogen, and glucose levels added to the media compared to the wild-type strain. Coimmunoprecipitation and mass spectrometry analysis identified another TOR pathway component named GTR2, similar to Gtr2 in yeast and RAG C/D in mammals. GTR2 is a component of the TOR pathway, which has shown identical behavior to VTA, and has affected FRQ-less rhythmicity and TTFL.

Our medium-term goal is to answer the question: What is the role of TOR pathway in the circadian system?

I focused on studying connections between the mutual components of the circadian clock and the TOR pathway. I constructed different epitope-tagged proteins to create the tools to conduct

experiments and test my hypotheses.

My hypotheses for my Ph.D. research were as follows:

VTA is essential for maintaining regular GTR2 expression and rhythmicity at different times of the day. To test this, I looked at the protein expression level and rhythmicity of GTR2-FLAG in the presence and absence of VTA across two circadian cycles and from 24 to 72 hours.

As a mutual component of the CLOCK and TOR pathway, the presence of GTR2 is essential for maintaining normal clock function and expression. To test this, I looked at the FRQ expression pattern (as an indicator of clock function) in the presence and absence of GTR2 to indicate if GTR2 is critical to maintaining normal rhythmicity and expression of the clock protein.

The presence of VTA is essential to maintain regular protein interactions and binding partners of GTR2. Since VTA and GTR2 have a strong association, GTR2 will co-precipitate with VTA. To test this, I used coimmunoprecipitation and mass spectrometry to confirm the association of VTA and GTR2.

VTA changes its localization in the starvation and presence of TOR pathway inhibitors. To test this, I examined VTA-GFP (previously constructed by a former Ph.D. student) localization in the presence of TOR pathway inhibitors and the absence of glucose as starvation.

VTA is essential to maintain regular protein-protein interactions of other TOR pathway components. Since GTR2 and VTA are both components of the EGO complex and FLO, to test this I explored the connection between the TOR pathway key components and the EGO complex. I used KOG1- protein similar to Raptor in mammals and Kog-1 in yeast. I did coimmunoprecipitation with KOG1-FLAG and GTR2-FLAG in the presence and absence of VTA.

VTA impacts the TORC regulator protein KOG1 expression pattern. To test this, I looked at the KOG1-FLAG protein expression pattern across two circadian cycles and in the presence and absence of VTA.

As a membrane protein, the presence of VTA is essential for the TOR pathway component's localization. To test this, I looked at the subcellular localizations of GTR2-RFP and KOG1-GFP in the presence and absence of VTA and TOR pathway inhibitors and starvation.

As a component of the TOR pathway, the absence of VTA might induce autophagy. To test this, I investigated the autophagy induction using an Atg8-RFP marker in the presence and

absence of VTA and TOR pathway inhibitors.

My experimental approaches and findings help us better understand the relationship between the TOR pathway components and the circadian clock and the role of VTA in this system.

Chapter 2. MATERIALS AND METHODS

2.1. *Neurospora* methods

2.1.1. Race tubes

For assaying rhythmicity of conidiation, cultures were inoculated from conidiospores. These cultures were grown in the presence or absence of choline (100 μM) on solid agar medium in long glass growth tubes (race tubes) on media containing 1X Vogel's salts (Appendix I), 0.5% maltose, 0.01% arginine, and 2% agar. One week before the race tube experiment, agar slants of appropriate strains were inoculated and incubated at a 30°C incubator.

Race tubes were inoculated either from starter plates or directly from slants. To start the experiment using starter plates, Petri plates containing solid MA medium with or without choline (Appendix I) were inoculated and were left to incubate for three days at room temperature or two days in a 30°C incubator. Before the race tube inoculation, plugs of agar containing mycelium were punched from the growth front, and plugs were transferred from Petri plates to race tubes. To inoculate the race tubes from slants, a small number of spores was placed at the end of the race tubes.

Race tubes were incubated under constant light at 30°C for 24 hours. Then the race tubes were transferred into constant dark at 22°C until the mycelial front reached the end of the tube. The growth front was marked under safe red light every day, noting the date and time. The linear

growth rate and period were then calculated by using a Microsoft Excel spreadsheet, "MacTau", developed by Dr. Patricia Lakin-Thomas (Adhvaryu et al., 2016). Mean periods were compared by unpaired two-tailed Student's t-tests using Prism GraphPad.

2.1.2. *Neurospora crassa* crosses

Neurospora crassa genetic cross preparation methods were followed according to the protocols originating from the *Neurospora crassa* Methods Guide (https://www.fgsc.net). Strains with opposite mating types were selected as parents for the cross. Since there are no male or female strains in *Neurospora crassa*, the strain inoculated on synthetic crossing medium (SCM) (Appendix I) and forming a female structure is named a female parent.

To start a cross, female parents were inoculated on slants of synthetic crossing medium (SCM) with appropriate growth supplements at room temperature for ten days. A male strain was inoculated on a slant of 1xVogel's salts with 2% glucose and any other required nutritional supplements in a 30°C incubator for seven days. Sexual reproduction was started by inoculating spores from the male into the SC slant containing the female parent. Fertilized slants were left for another four weeks until ejected ascospores were seen on the opposite wall of the tube. After four weeks, ascospores were collected using inoculation loops and were added to 1 mL of distilled water and were then counted using a hemocytometer. Microfuge tubes containing the ascospores in distilled water were heat-shocked for 30 minutes in a 60°C water bath to activate the ascospores. Ascospores were then plated at a density of 15-20 spores per plate on sorbose plating media with appropriate supplements and colonies appeared after two days of incubation in constant light at 30°C incubators. Colonies were punched out of the sorbose agar using microcapillary tubes and the plugs were transferred to agar slants for further growth.

Various criteria were used to identify genotypes of the germinated progeny from the cross. *csp-1* (Conidial separation-1) was determined by tapping the tubes (Tap test) to look for the failure of spore separation and/or CAPS assay. Cleaved Amplified Polymorphic Sequence (CAPS) is a method in which specific primers are used to amplify DNA fragments with locus-specific regions to digest with one or more restriction enzymes. The resulting DNA would then separate on an agarose gel. (https://www.ncbi.nlm.nih.gov/probe/docs/techcaps/). Dr. Lakin Thomas designed this assay, and we used specific primer and restriction enzymes (listed in Table 1) to distinguish between wild-type and mutant strains.

Table 1: CAPS assays specific primers and restriction enzymes as well as the final expected fragment sizes.

Forward and Reverse primer	Restriction enzyme	Post digestion final fragment sizes
bd Forward TGCCTTACCATCCAGCTAATC *bd* Reverse CCGAGCTTCTTGTCCTCTTT	Bsr I	PCR product is 621bp After cutting with Bsr I: Wild type is 358/263 and Mutant is 621
csp-1 Forward CGACTCCTATGACTCCCAAATG *csp-1* Reverse GGCTCAGAAGAGGAAGGTTAAG	CviQI	PCR product is 599 After cutting with CviQI: Wild type is 94/504 Mutant is 94/135/369

Race tube experiments were carried out to identify ras^{bd} by slower growth and banding phenotype, or it was identified by CAPS assay. *chol-1* was identified by slow growth without choline supplementation in minimal liquid media. frq^{null} was identified by arrhythmic conidiation on high choline media and the presence of banding rhythms in *chol-1* strains in zero choline media, and by PCR using *frq* forward and reverse specific primers. *vta* mutation was identified by damped or arrhythmic conidiation phenotype or by PCR using vta^{ko} specific primers.

2.1.3. Preparation of conidiospores

Recipient strains were inoculated into 4 to 5 fresh slants on VM agar containing required supplements. They were grown at 30°C for 4-7 days. Mycelium from the slants was inoculated onto 100 mL agar in a 1000 mL flask. VM agar in 100 mL Erlenmeyer flasks was incubated at 30°C in constant darkness for three days and then at 25°C in LL for 7-10 additional days. Conidia were then harvested from the flasks in sterile water, filtered through sterile muslin into fresh tubes and centrifuged at 2620 g for 5 minutes at 25°C. Conidial pellets were pooled, washed in 50 mL sterile water, and centrifuged at 2620 x g for 5 minutes. The previous step was repeated three times. The pellets were washed twice in 30 mL cold sterile 1M sorbitol and the final pellet was resuspended in 1 mL cold sorbitol. Dilutions of 1:10, 1:100, and 1:1000 of the

conidia and cold Sorbitol were prepared and were left on ice to be used immediately. For future use, these were stored at -80°C.

Immediately before the use, the spore suspension was centrifuged at 2620 x g for 5 minutes at 4°C, the supernatant was removed, and 1 mL of cold Sorbitol was added to the pellets. The pellets were vortexed and centrifuged again. Finally, 40µl of 1M sorbitol was added to the tube and was mixed by flicking the tube a few times and leaving it in ice until the transformation started.

2.1.4. *Neurospora crassa* transformation using electroporation

The electroporator (BioRAD Gene Pulser) was adjusted to 1.5 kV (7.5 kV/cm), 25 µF capacitance, and 600 ohms resistance for *Neurospora crassa* transformation. DNA (15 µl) was added to the 40 µl conidia suspension and was transferred to the electroporation cuvette. It was then mixed gently by pipetting up and down a few times and was placed back on ice for another 5 minutes before pulsing in the electroporator.

Immediately after electroporation, 1 mL of recovery medium (Appendix I) was immediately added to the electroporated sample cuvette using a sterile Pasteur pipette and was gently mixed by pipetting up and down. The mixture was then transferred to a 1.5 ml screw-capped tube and was incubated at room temperature for one hour with gentle shaking (around 9 rpm) on a rotator. After the recovery, spores were diluted to make 1 mL of a 1/10, 1/100, and of further dilutions. 60 mL of plating media containing top agar and FIGS (Appendix I) were prepared for each dilution. Transformed spore mixtures were transferred to 100 mL flasks containing 60 mL of plating media at about 40°C. Flasks were swirled to mix well and were immediately poured into three labeled 10 cm Petri plates (15–20 mL per plate). Plates were taped using micropore tape and were incubated at 30°C incubators under LL conditions for 2-3 days and until colonies developed. Transformed colonies were picked using microcapillary tubes and grown on slants containing Vogel's minimal media, including required supplements and selection agent. Slants were left at 30°C for seven days. Spores were then checked for the presence of different mutations and finally genotyped using specified primers. The same procedure was performed during a *his-3* targeting transformation and 25 mg/ml histidine was added to the plating media.

2.1.5. Liquid media cultures

To extract protein from *Neurospora crassa* strains, 24 well plates were used. 1 mL of

minimal media (1xVogel's salts, 2% glucose) and any other required nutritional supplements were added to each well. Spores of specific strains and controls were inoculated in each well, and plates were sealed with micropore tapes and incubated at room temperature for three days or in the 30°C incubator for two days. Fungal mats were harvested and washed with distilled water on system vacuum filtration system with Whatman P8, 3.5 cm filter papers, and were frozen in liquid nitrogen.

2.1.6. Time course experiments on agar cultures

Spores were inoculated on starter plates containing 1x Vogel's salts, 0.5% maltose, 0.01% arginine, 2% agar, and 100µM choline, and were incubated in LL at 30°C. After several days of growth, mycelium plugs were removed from the growth front by punching with sterile glass pipettes. Plugs were inoculated on the top of cellophane layered over plates containing the same medium. Plates were incubated at 30°C in LL, then transferred to 22°C in DD at various times and harvested after 48-76 hours of the total growth. The times of transfer to DD were varied, so that total hours in DD varied from 24 to 72 hours. Samples were harvested from one centimeter of the growth front, were then immediately frozen in liquid nitrogen and were stored at -80°C until protein extraction. Three independent time courses were carried out for each strain.

2.2. DNA methods

2.2.1. *Neurospora crassa* genomic DNA extraction

Conidia were inoculated in either 24 well plates with two replicates or 12 well plates with one replicate and in 1 or in 2 mL of minimal liquid media containing 1xVogel's salts, 2% glucose along with any other required nutritional supplements at room temperature for three days or at 30°C for two days under LL conditions. The fungal disc was removed from the plate and was placed on a vacuum filtration system over Whatman P8, 3.5 cm filter papers. Samples were then rinsed three times with distilled water and were dried using a vacuum. Samples were transferred into 1.5 mL microcentrifuge tubes and were immediately frozen in liquid nitrogen. Frozen fungus was ground in liquid nitrogen in a pre-cooled mortar and pestle and was immediately transferred into 600 µL of DNA extraction buffer (100 mM Tris- HCl pH 8.0, 50 mM EDTA, 1% SDS) and 3 µL Proteinase K (20 mg/mL in 20 mM Tris-HCl, 1 mM CaCl2, 50% glycerol, pH 7.5) (Appendix I). Samples were vortexed and were incubated at 65°C for 1 hour. Samples were vortexed again and 200 µL of 7.5 M ammonium acetate was added. The mixtures were vortexed

again and incubated on ice for 5 minutes. Samples were centrifuged for 3 minutes at 16,000 x *g,* 4°C, and supernatants were transferred into fresh 1.5 mL screw-capped tubes. 6 µL of Rnase A (5 mg/mL in 10mM Tris-HCl, pH 8.0, 50% glycerol) was added, and tubes were incubated again for another 1 hour at 37°C. Tubes were vortexed and were placed on ice. 500 µL of chloroform was added, and samples were vortexed and centrifuged for 5 minutes at 14000 x *g*, 4°C. At this point, three layers formed in the mixture. The top layer containing the supernatant was removed and transferred into a new tube and was mixed with 650 µL of isopropanol, followed by centrifugation for 15 minutes at 14000 x *g*, 4°C. DNA pellets were washed with 1 mL of 70% ethanol and centrifuged for 5 minutes at 7500 x *g* at 4°C. The final DNA pellet was air-dried for 20 minutes, and 70-100 µL of TE buffer (10 mM Tris, one mM EDTA, pH 8.0) (Appendix I) was added to dissolve the pellet.

2.2.2. Bacterial transformation using NEB 10-beta Competent *E. coli* (High Efficiency) (C3019)

A tube of NEB 10-beta competent *E. coli* cells was thawed and was placed on ice. 1-5 µl (1pg-100 ng) of DNA was added to the cell mixture, flicked gently for 4-5 times, and was then placed on ice for 30 minutes. Then tubes were heat-shocked in a water bath at 42°C for 30 minutes and put back on the ice for 5 minutes. 950 µl of room temperature SOC media was added to the mixture. Tubes were incubated at 37°C for 60 minutes with shaking at 250 rpm. Cells were mixed by flicking the tubes and inverting, and then several ten-fold serial dilutions were made in SOC. 50-100 µl of each dilution was spread onto pre-warmed LB plates (Appendix I) containing appropriate antibiotic as a selectable marker, using sterile glass beads. Plates were then inverted and placed in the 37°C incubator overnight. The next day, single colonies were picked and streaked on LB plates containing Ampicillin/Kanamycin as a selectable marker and were incubated for another 24 hours. Single colonies from the second plate were inoculated into LB liquid media containing antibiotic and were incubated overnight at 37°C with shaking at 150 rpm. Plasmid extraction was performed the day after using a Qiagen midi plasmid extraction kit protocol. The final DNA pellet was redissolved in an appropriate volume of TE buffer.

2.2.3. Plasmid DNA extraction

Plasmid mini preparations were used to obtain small amounts of plasmid DNA. Plasmids were extracted from overnight grown cultures using the QIAprep Spin Miniprep kit from QIAGEN. Plasmids were transformed into E-coli, and plasmid Midi-preparations were

performed using QIAGEN kit to obtain a large amount of plasmid DNA.

2.2.4. Snap-Freezing bacterial cultures

To freeze the bacterial cultures, 50% Glycerol was prepared, and an equal amount of glycerol and bacterial cultures were added to 1.5 microfuge tubes and were vortexed vigorously. Samples were then snap-frozen by immersing the tubes in liquid nitrogen (150°C) for 30 seconds and transferred and stored in a -80°C freezer.

2.2.5. Primers

All primers in this project were designed using ApE software. The annealing temperature was calculated using the NEB Tm calculator application, and temperature gradient PCR reactions were performed for each primer pair with Tm ± 5 °C to optimize the primer annealing temperature. Primers were received from Invitrogen or Integrated DNA Technologies (IDT). Both 1 mM primer stocks and 10 µM working primer tubes were stored at –20°C.

2.2.5.1. Primers used for Gene construction and Genotyping

Table 2: Primers used

Primer Name	**Sequence** **5’ -> 3’**
KOG-1 5’ Flank Forward	GTAACGCCAGGGTTTTCCCAGTCACGACGTACAACGAACGCCTCTGG
KOG-1 5’ Flank Reverse	CCTCCGCCTCCGCCTCCGCCGCCTCCGCC GAAGGGGCCAACCTTCTC
KOG-13’ Flank Forward	TGCTATACGAAGTTATGGATCCGAGCTCG ATTACGAGAGGGGTGGCATC
KOG-1 3’ Flank Reverse	GCGGATAACAATTTCACACAGGAAACAGC ATTCACCCTCCTTCCCTCC
Gtr25’ Flank	GTAACGCCAGGGTTTTCCCAGTCACGACGCCTTCATTCTACCCTCATAC

Forward	
Gtr2 5’ Flank Reverse	CCTCCGCCTCCGCCTCCGCCGCCTCCGCCACGACCATCACCCACCACCC
Gtr2 3’ Flank Forward	TGCTATACGAAGTTATGGATCCGAGCTCGGGATTTCATCCGGTTGTTTG
Gtr2 3’ Flank Reverse	GCGGATAACAATTTCACACAGGAAACAGCCACCCAGCCAACCAAGTACC
TOR 5’ Flank Forward	GTAACGCCAGGGTTTTCCCAGTCACGACGGCAGCGACGGCAAGACATAC
TOR 5’ Flank Reverse	CCTCCGCCTCCGCCTCCGCCGCCTCCGCCCCAGAAACTGCACCATCCTA
TOR 3’ Flank Forward	TGCTATACGAAGTTATGGATCCGAGCTCGACAGTCTTTAGGGAGATGAA
TOR 3’ Flank Reverse	GCGGATAACAATTTCACACAGGAAACAGCTGATGGGACTGATGGTGTGAC
KOG-1 5’ Flank Forward (two)	GTAACGCCAGGGTTTTCCCAGTCACGACGACGGACCCTTCTTCAACTTCG
KOG-1 5’ Flank Reverse (two)	CCTCCGCCTCCGCCTCCGCCGCCTCCGCCGAAGGGGCCAACCTTCTCGT
KOG-1 3’ Flank Forward (two)	TGCTATACGAAGTTATGGATCCGAGCTCGATTACGAGAGGGGTGGCA
KOG-1 3’ Flank Reverse (two)	GCGGATAACAATTTCACACAGGAAACAGCCATACCAGGAAGAGAAGTC
Gtr2 ko Forward	GGACATACAAGCTAGTGCCT
Gtr2 ko Reverse	GCAAGTAGCCACAGAAAGTC
Gtr2 out of region Forward	TTTCTTGGTCCGTTGTGC

Gtr2 out of region Reverse	CTTGCTACTTTCTCCGTTC
Kog-1 out of region Forward	ATTATCTTGCTTCGCCTCC
Kog-1 out of region Reverse	GGTGTGCTTGTTCTATTCC
His-3 Forward	CTCATGTTCAACCCTTTGGATGG
His-3 Reverse	GTCATGCAGTTGGCTAAGGTTGAG
Hph Forward (A)	TCGGAGGGCGAAGAATCTCGTG
hph Reverse (A)	GCTTCTGCGGGCGATTTGTG
Hph Forward (B)	ACCTGCCTGAAACCGAACTG
hph Reverse (B)	CTGCTCCATACAAGCCAACC
Hph Reverse (1994)	AGCACTCGTCCGAGGGCAAA
Frq Forward (1994)	GAAGCATACTATCGCCAGCAGAC

2.2.6. Polymerase Chain reaction (PCR) using gDNA or Direct PCR

Q5 high fidelity DNA polymerase from New England BioLabs Inc. (NEB) was used following the manufacturer's instructions for PCR using gDNA templates.

Terra^{TM} PCR Direct Polymerase Mix (Takara Bio Inc) was used to amplify DNA fragments from bacterial colonies and while analyzing a large number of fungal strains. There is no need to extract gDNA when using this method, and fungal spores or bacterial and yeast colonies can be directly added into the PCR master mix. PCR tubes containing the kit materials and spore or colonies instead of the gDNA were subjected to the designed PCR protocol described by the manufacturer. A mixture of proteinase K and 6X loading dye was added to the final PCR product before loading on the agarose gel.

2.2.7. PCR product cleanup

PCR products were cleaned using Monarch PCR & DNA Cleanup Kit according to the manufacturer's recommendations. DNA was eluted in sterile dH2O.

2.2.8. Quantification of DNA

The concentration and purity of double-stranded DNA were determined using the Thermo-Fisher Scientific Nanodrop2000 UV/Visible spectrophotometer. The ratio of absorbance at 260 nm and 280 nm is used to assess the purity of DNA, and the ratio of ~1.8 is generally accepted as "pure" for DNA.

2.2.9. Restriction Enzyme digestion

All restriction digestions were carried out with enzymes obtained from New England Biolabs (NEB) and Thermo Fisher Scientific. The enzymes were used according to the manufacturer's guidelines in New England Biolabs website (https://www.neb.com).

2.2.10. DNA agarose gel electrophoresis

DNA agarose gel-electrophoresis was carried out according to standard procedures (Green and Sambrook 2012) using agarose dissolved in 1X TAE buffer by heating. 0.005% RedSafe^{TM} nucleic acid staining solution (iNtRON Biotechnology) was added. Gel electrophoresis was carried out in a horizontal tank containing 1x TAE buffer. Gels were imaged using the FluoroChem FC2 Imaging System (Alpha Innotech). Either a 100 bp ladder or a 1 kb ladder was used to identify the size of the DNA fragment.

2.3. Protein methods

2.3.1. Protein extraction

Protein extraction was conducted by grinding the frozen fungal mycelium in liquid nitrogen with a mortar and pestle. Powdered mycelium was then added to a microfuge tube containing 200µl of protein extraction buffer (PEB) (50mM tris pH 6.8, 2% SDS, 10% glycerol, 5mM EDTA, 1mM PMSF) (Appendix I), was vortexed and boiled for 5 min immediately, and was then left on ice. After extracting all samples, they were centrifuged for 5 min at 12000 x g at 25°C. Protein concentration was then assayed using Bio-Rad DC Protein Assay. Then a total volume of 20µl of the protein samples in PEB buffer containing 20µg of total protein, 1µl of 1% bromophenol blue, and 1/10 volume of 0.1M dithiothreitol was boiled for 2 min and were left at room temperature before loading on the gel.

2.3.2. Protein Assay

BioRad DC protein assay was performed according to the manufacturer's instructions. The

two closest replicates of the three for each sample were chosen for calculations. Dilutions of either 1/10 or 1/50 were chosen depending on which dilution fell in the middle of the BSA standard curve.

2.3.3. FLAG Western blotting and Detection

For FLAG detection, 20μg of total protein was run on 10% acrylamide SDS PAGE gels and was then transferred to Immobilon-P PVDF membrane (EMD Millipore) using a semi-dry blotting method. The membrane was incubated with blocking buffer containing 1% BSA in 1x TBST (150mM NaCl, 50mM Tris, pH 7.5 + 0.05% Tween-20) (Appendix I) for one hour at room temperature with shaking and was then incubated with 1/50,000 dilution in a blocking buffer of monoclonal anti-FLAG M2 antibody (Sigma-Aldrich). Membranes were washed three times for 5 min each in TBST and were then incubated with 1/50,000 dilution of HRP-conjugated goat anti-mouse secondary antibody (Bio-Rad) for one hour, and were then washed three times for 5 min each in TBST. Membranes were then detected using chemiluminescence reagent (Immobilon ECL reagents from Millipore), and the total amount of protein was quantified by using Coomassie blue or colloidal gold staining of the membrane.

2.3.4. FRQ Western blotting and Detection

Proteins were extracted from time-course samples with the same procedure as described, and 100μg of total protein was run on 7.5% acrylamide SDS PAGE gels, and was blotted to a PVDF membrane. Blocking was conducted in 5% skimmed milk in TBS (150mM NaCl, 50mM Tris, pH 7.5) (Appendix I), and anti-FRQ primary antibody (Alex Diernfellner and Michael Brunner generously provided the anti-FRQ antibody). Incubation was done with a 1/20 dilution for two hours at room temperature. The membrane was then washed three times with TBS for 5 min each time, and was incubated with HRP-conjugated goat anti-mouse secondary antibody diluted 1/10,000 in 5% milk/TBS at 4°C overnight. Finally, the membranes were washed three times with TBS for 20 minutes at room temperature and was then detected using chemiluminescence reagent and stained with Coomassie blue for total protein quantification. The phosphorylation state of FRQ protein was determined by the shift in the apparent molecular weight of the band.

2.3.5. GFP Western blotting and Detection

20 μg of total protein was run on 10% acrylamide SDS PAGE gels and was blotted to a PVDF membrane. Blocking was conducted in 3% BSA in TBST (20 mM Tris, 500 mM NaCl,

0.3% Tween-20, pH 7.5) for one hour and then primary anti body incubation was done using 1/5000 Abcam Rabbit polyclonal of Anti-GFP antibody in 3% TBST for another hour. The membrane was then washed three times with TBST for 5 mins each time and was incubated with goat anti-rabbit (Cedarlane) with diluted 1/5000 in 3 % BSA/TBST for one hour. Finally, the membranes were washed three times with TBST for 5 minutes at room temperature and was then detected using chemiluminescence reagent and stained for total protein quantification.

2.3.6. Colloidal Coomassie G-250 staining for proteins on membranes

If the membrane was dried, then it was placed in 100% methanol for 15 seconds and was then washed briefly with water for about 2-5 minutes. The washed membrane was then placed in 2-250 Coomassie blue stain (Appendix I) for about 1-2 minutes or longer until the bands appeared. It was then destained to remove the blue background using destain solution (Appendix I). After staining and destaining, the membrane was air-dried on a filter paper for about 15 to 30 minutes.

2.3.7. Membrane Staining using Bio-Rad's Colloidal Gold Total Protein Stain

Bio-Rad's Colloidal Gold Total Protein has a higher sensitivity than Coomassie blue. The PVDF membrane was washed three times for the duration of 20 minutes each with TTBS buffer (20 mM Tris, 500 mM NaCl, 0.3% Tween-20, pH 7.5) and was washed three more times with water to remove all salts that might interfere with the colloidal gold staining. Then colloidal gold protein stain was added to the container containing the membrane until the top of the membrane was covered with the dye (around 50 mL). The incubation time depends on the protein concentration, and the stain remains on the top of the membrane until bands appear and the background to band ratio is acceptable. The final membrane was then air-dried for about 20-30 minutes, and was scanned (Rohringer and Holden, 1985).

2.3.8. Protein expression quantitation for Western blots

To quantify the amount of expressed protein, protein levels were normalized against total protein by staining the membrane with Coomassie Blue or colloidal gold after immunodetection. Chemiluminescence was detected with a CCD camera, and Coomassie-stained membranes were scanned. Pixel densities of both images were quantitated with ImageJ software. The ratio between the chemiluminescent signal and the intensity of the staining for that sample was defined as the relative expression level of the protein. When three biological replicates of time

courses were carried out, each time course was normalized by determining the mean expression level as 1.0. The three-time courses were then averaged to get the mean of the three independent experiments (Ratnayake et al., 2018; Eskandari, Ratnayake, and Lakin-Thomas, 2021).

2.4. Coimmunoprecipitation and mass spectrometry analysis

Spores were inoculated on slants containing 1xVogel's salts, 2% glucose, 100µM choline, and 2% agar, and were incubated at 30°C. After 7 days, spores were transferred into 100ml liquid media containing Vogel's salts with 2% glucose and 100µM choline, and were incubated at 25°C with shaking at 150 rpm overnight. Samples were harvested and were washed three times with PBS (10mM phosphate, pH 7.4, 137mM NaCl, 2.7mM KCl) and with distilled water. on filter paper during vacuum filtration. Samples were immediately frozen in liquid nitrogen, and were stored at -80°C. Frozen samples were then ground in liquid nitrogen using a mortar and pestle, and were transferred to 500µl of IP lysis buffer (50mM HEPES, pH 7.5, 150mM NaCl, 10% (v/v) glycerol, 0.02% (v/v) NP40, 1mM EDTA, 1 µg/ml leupeptin, 1 µg/ml pepstatin A and 1mM PMSF) (Appendix I) and mixed by inversion for 20 seconds, left at 4°C for 5 min, and then centrifuged for 10 min at 15130 x g. Supernatants were collected. 5µl of the IP extracts were used to measure the protein concentration using the Bio-Rad DC Protein Assay.

Co-immunoprecipitation was carried out using 10 mg protein of the IP extracts. 50µl of Sepharose 4B beads (Sigma) were washed three times with the IP lysis buffer and were then incubated with 10 mg of protein to reduce nonspecific binding. Samples were incubated at 4°C with end-over-end agitation for one hour. Samples were then centrifuged at 500 x g for 1 minute, and the supernatant was collected.

10µl Anti-FLAG M2 Affinity Gel beads (Sigma–Aldrich) per sample were washed three times with IP lysis buffer at 500 x g at 4°C and then incubated in 1ml of 0.1M glycine-HCl pH 3.5 buffer for 10 minutes, and then washed another three times with IP lysis buffer. The supernatant was discarded, and the beads were incubated with IP extract containing 10 mg of the protein overnight at 4°C with end-over-end agitation. Samples were centrifuged at 750 x g for 1 min, and beads were washed with the IP lysis buffer three times. The beads were washed for the final two times with FLAG rinsing buffer (50mM NH_4HCO_3 pH8, 75mM KCl, 2mM Na_2EDTA) (Appendix I). Before the last wash and after adding 1 mL of FLAG rinsing buffer, beads were transferred to a 1.5 mL microfuge tubes. Frozen beads were sent to SPARC BioCentre (SickKids Proteomics, Analytics, Robotics & Chemical Biology Centre, Hospital for Sick Children,

Toronto, Canada) for mass spectrometry analysis. The results of mass spectrometry analysis were received as a Scaffold file (Scaffold 4.8.1 – Proteome Software Inc). Candidates were found through the Uniprot database, and NCU numbers were identified and searched in fungiDB. Proteins with 95% probability in the total spectrum count that were only bound to the protein of interest and not control samples analyzed at the same time were chosen as binding partners, and candidates that were repeatedly identified in two or three independent experiments bound to the same protein were listed as top binding partners (Eskandari et al., 2021; Ratnayake et al., 2018).

2.5. Microscopy

2.5.1. Fixed samples preparation

Fixed sample preparations were performed using 4% Paraformaldehyde in 1X PBS. Strains were grown in 35mm Petri plates in 4 mL of a minimal liquid medium with 1X Vogel's Salts, 2% glucose, and 100uM choline overnight at 22°C in light to obtain a small hyphal mat. The next day, the liquid medium was pipetted off, and 4mL of fresh media containing specific conditions, either inhibitors or nutritional supplements, were added to the fungal mat and incubated for another 4 hours at 22°C in constant light before fixation. Fixative was made by making 8% paraformaldehyde (Appendix I) in 60°C water, while stirring. The final homogenized mixture was neutralized by NaOH and was then diluted to 4% by adding PBS. The fungal mat was treated with 4 mL of the fixative for 10 mins. The fixative was washed off, and the fungus was washed three times with 1x pH 7.4 Phosphate Buffered Saline (PBS). Finally, one mL of 1X PBS was added to each plate to be able to move the fungal mat from the Petri dish and place it on a microscopy slide. Excess liquid was wiped off by gently tapping the slide on a Kim wipe. 2–3 drops of the pre-warmed (at room temperature) Prolong mountant was applied directly onto the specimen, and a coverslip was gently placed on the top of the sample and mountant. Slides were placed on a dry and dark surface, and were cured for 48 to 60 hours at room temperature before observation.

2.5.2. Live Sample preparation and imaging

Spores were inoculated on 1.5% Phytagel (2% Glucose, 1X Vogel's salt and distilled water) and were grown at 22°C in constant light for 48 hours. When the mycelium had grown 3–5 cm from the point of inoculation, an agar block bearing the colony margin was cut from the edge of the colony and was inverted onto 30 µl or a droplet of liquid MA medium (Appendix I) on a 1.5

mm thickness glass coverslip. This procedure makes the growing hyphae on the agar's surface as close to the coverslip as possible. (Hickey et al., 2004, 2002). To observe live samples using LSM 700 in different conditions and inhibitors, the agar block was removed using a forceps, and was placed gently on a new coverslip containing a droplet of the same media plus condition. Then the agar block was incubated for either 2, 5, 10 or 20 minutes. After the incubation time, agar blocks were replaced in a standard MA media (Appendix I) before imaging. This step was removed for SP8 microscopy. Images were taken using all incubation periods. 20 minutes of incubation time was found to be effective and reported in LSM 700 image section in Chapter 4.

2.5.3. Confocal microscopy imaging Using LSM 700

The LSM 700 microscope located at York microscopy facility, Life Science Building was used. 63X oil objective lens was used for imaging. The software in use was Zeiss black. To increase the quality of the image Averaging was set to 4 and pinhole was 1 AU (Airy unit). To increase the resolution of the picture, I increased the pixel size to 2048.2048. The picture obtained was then saved as a Carl Zeiss LSM image data format.

2.5.4. Confocal microscopy imaging Using SP8

2.5.4.1. Sample preparation

The same sample procedure as above was performed, without moving agar blocks to standard media before observing. A timer was used to count how much time was spent on each sample. After obtaining a time course interval of samples from 2 minutes to 30 minutes, images of about 15- 20 minutes incubation time in a selected media were chosen as the final image.

2.5.4.2. Leica SP8 Confocal Microscope settings

Leica TCS SP8 Confocal microscope / Leica Dmi8 CS inverted stand located at Advanced Optical Microscopy Facility (AOMF) in the MaRS building, PMCRT tower, 101 College St., Room 15-305, Toronto, ON, CANADA was used. I used HC PL APO 63x/1.40 NA Oil immersion CS2 for our research for all my images. HyD detectors were used for imaging. FIJI Software is used to process images obtained. I used mCherry and GFP for my samples, both using hybrid detectors. Line sequential setting was used and to take high resolution images laser power was kept in the range of 1-4%. A pixel size of 2048.2048 for better quality of images was used. To improve the quality of the image Averaging was established at 4 and pinhole was 1 AU.

2.6. Bioinformatics

Neurospora crassa sequences and all other information regarding the genomics and the proteomics of a gene of interest were obtained from the FungiDB database (http://fungidb.org/fungidb/) (Stajich et al., 2012). Database searches for homologs were carried out using NCBI BLAST software (https://blast.ncbi.nlm.nih.gov/Blast.cgi) (Madden 2013). Protein domains were identified using the NCBI Conserved Domain search tool (https://www.ncbi.nlm.nih.gov/Structure/cdd/cdd.shtml) (Marchler-Bauer et al., 2017). Mass spec data was identified using Uniprot database, and Domain similarity by using Pfam and Interpro databases.

2.7. Knock-in method at native loci

To investigate the function of different proteins, I used a knock-in method, which uses recombination-mediated plasmid construction in *S. cerevisiae* to make knock-in cassettes (Fig. 5). This method was used to make epitope-tagged proteins for the expression of genes at their native loci. I made knock-in vectors containing epitope tags followed by the selectable marker hph (resulting in hygromycin resistance) flanked by two loxP sites. These constructs can use the Cre/loxP system, allowing the selectable marker hph to be excised by introducing Cre recombinase into a strain containing a knock-in cassette, although this has not been done in my project. I used a modified version of the gene knock-out procedure (Dunlap et al., 2006) to function as a convenient knock-in strategy for *Neurospora crassa* genes (Honda and Selker, 2009).

2.7.1. Knock-in fragment construction

A 1.1 kb fragment including the 3'-end of the gene of interest coding region, without the stop codon, was amplified by PCR with forward primer 5' F, which contains 29 nt of homology at one end of the linearized pRS426 (Figure 6) , and reverse primer 5' R, which contains 29 nt of homology at the 5'-end of the knock-in module. A 500-bp fragment of the 3'-end of the gene of interest flanking region was amplified with forward primer 3' F, which contains 29 nt of homology with the 3'-end of the knock-in module, and reverse primer 3' R, which contains 29 nt of homology at the other end of the linearized pRS426.

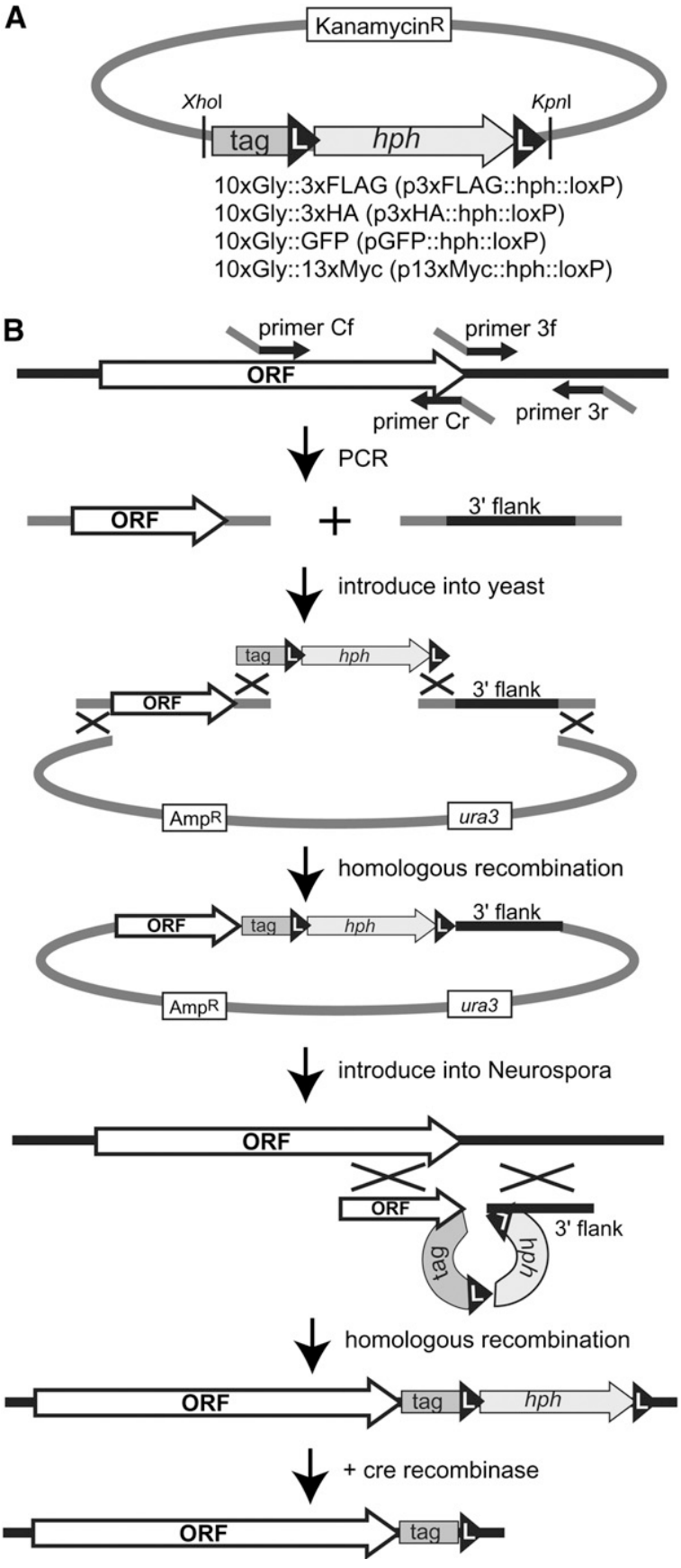
A
KanamycinR
XhoI
KpnI
tag
hph
10xGly::3xFLAG (p3xFLAG::hph::loxP)
10xGly::3xHA (p3xHA::hph::loxP)
10xGly::GFP (pGFP::hph::loxP)
10xGly::13xMyc (p13xMyc::hph::loxP)
B
primer Cf
primer 3f
ORF
primer Cr
primer 3r
PCR
ORF
3' flank
introduce into yeast
tag
hph
ORF
3' flank
AmpR
ura3
homologous recombination
ORF
tag
hph
3' flank
AmpR
ura3
introduce into Neurospora
ORF
ORF
3' flank
tag
hph
homologous recombination
ORF
tag
hph
+ cre recombinase
ORF
tag

Figure 5: Gene construction method. Adapted from (Honda and Selker, 2009).

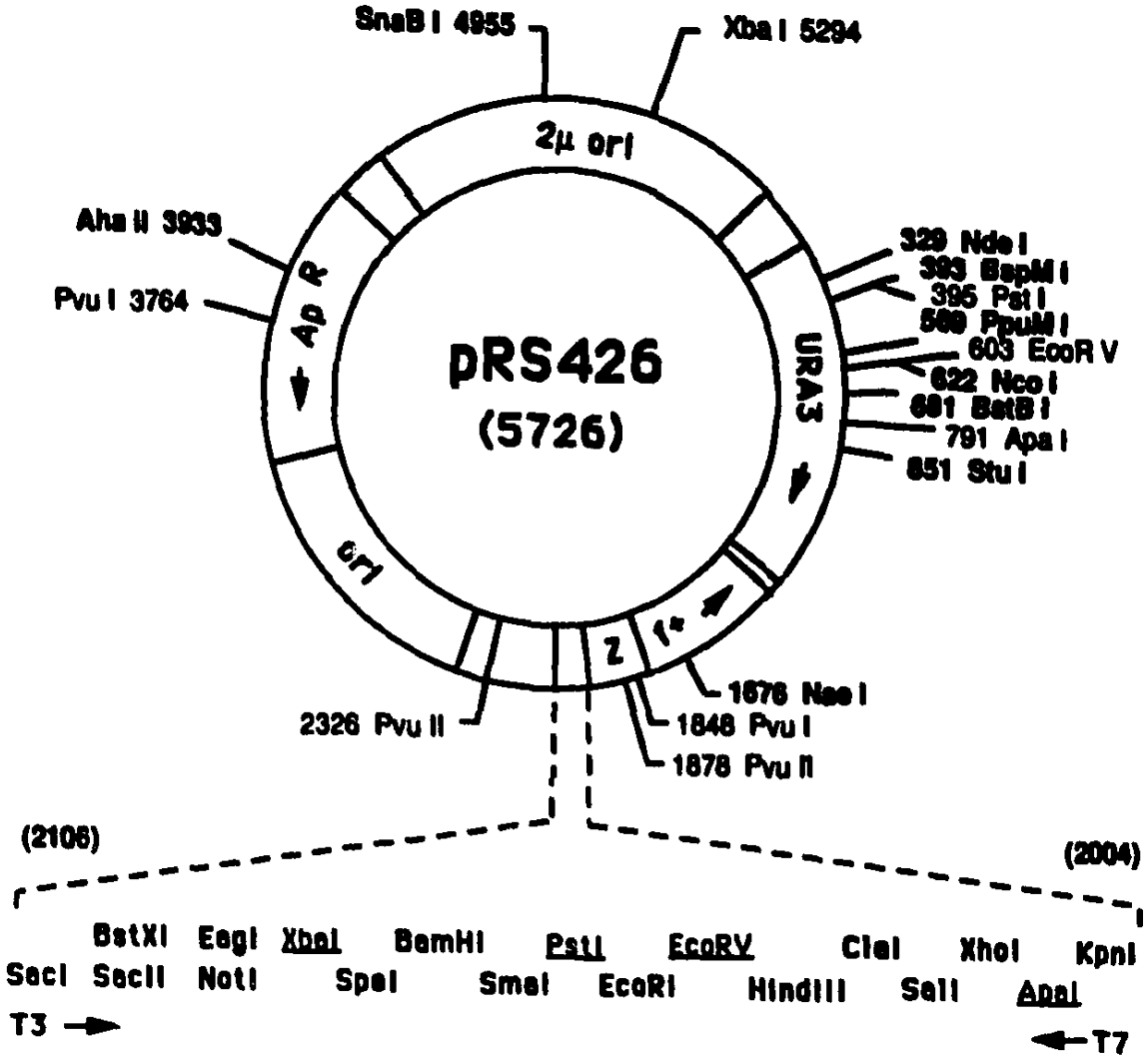

Figure 6: Map of the plasmid pRS426, showing key genes and selected restriction endonuclease sites. (Obtained from the FGSC)

2.7.2. Examples of the constructed plasmid maps (Fig. 7 and 8)

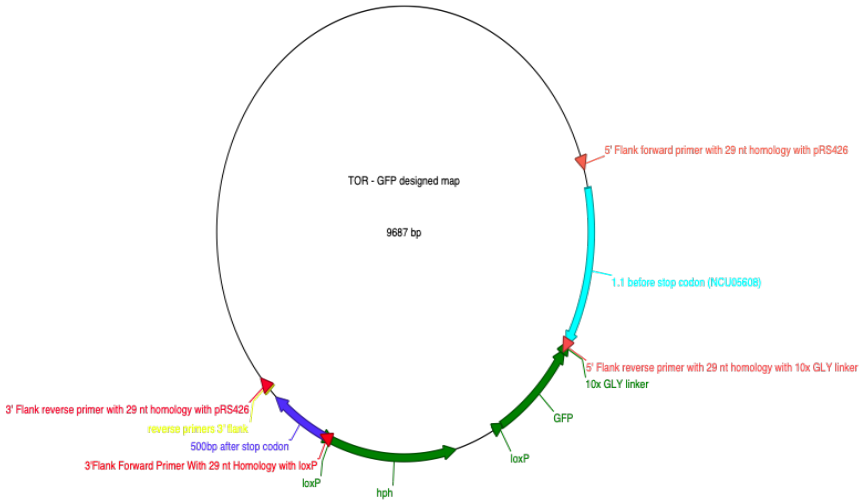

Figure 7: Tor-GFP plasmid map

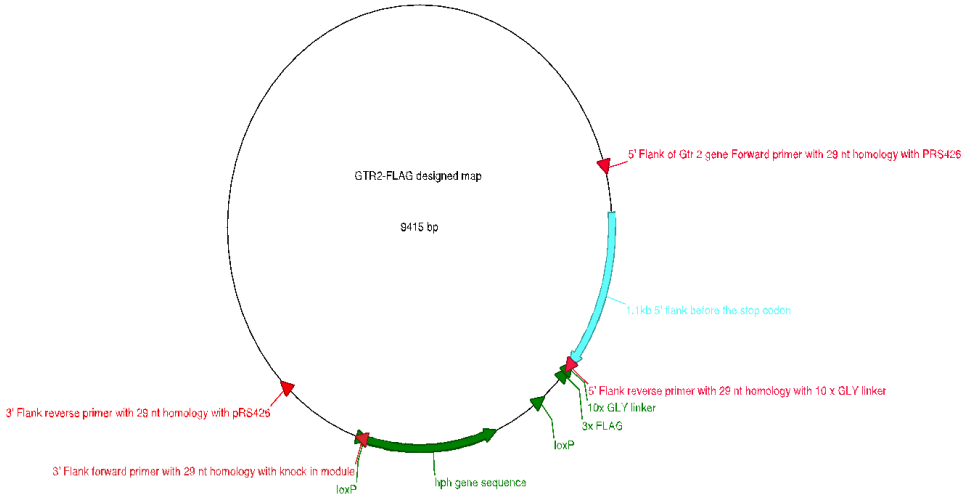

Figure 8: GTR2-FLAG plasmid map

2.7.3. Primer design for gene construction

ApE software was used to design suitable primers for this project. Primers used in this method were designed and synthesized with the following 5' common regions:

5f: GTAACGCCAGGGTTTTCCCAGTCACGACG...

5r: ATCCACTTAACGTTACTGAAATCTCCAAC...

3f: CTCCTTCAATATCATCTTCTGTCTCCGAC...

3r: GCGGATAACAATTTCACACAGGAAACAGC...

2.7.4. Plasmid preparation and Restriction Enzyme Digestion

In order to make the knock-in Cassette, the yeast shuttle vector pRS426 (Fig. 6), obtained from the Fungal Genetics Stock Center, was linearized by digestion with XhoI and EcoRI, (using standard NEB restriction enzyme digestion method). The knock-in module (GFP::loxP::hph::loxP), (3xFLAG::loxP::hph::loxP) or (mCherry::loxP::hph::loxP) was isolated from p tag ::hph::loxP by digestion with KpnI and XhoI.

2.7.5. Yeast transformation

Yeast strain FY834 was streaked in a fresh YPD plate (Appendix I) and left for 48 hours in a 30°C incubator until single colonies appeared. Single colonies were picked using an inoculation loop, restreaked in a fresh YPD plate, and incubated for another 48 hours at a 30°C incubator. A single colony from the second plate was picked and inoculated in YPD liquid media and incubated in 5-10 mL fresh YPD overnight at 30°C with shaking at 150 rpm. The next day, 1 mL of the overnight culture was added to 50 mL of fresh liquid YPD media and incubated again overnight at 30°C with shaking at 150 rpm. The day after O.D.600 was measured after 4 hr aiming for O.D.=1 and if it didn't reach the optimal OD, cultures were left on the shaker for another 6-8 hours. After this time, cultures were dispensed in 1mL microfuge tubes and were centrifuged at 1680 x g for 5 minutes. The supernatant was discarded, and the cell pellet was rinsed with 1mL of sterile H2O and was centrifuged again for another 5 minutes. The supernatant was discarded, and cells were re-suspended in 1mL of 100mM LiOAc and centrifuged for 30 sec. The supernatant was discarded again. Cell pellets were resuspended in 400 µl of 100 mM LiOAc and were left on the bench at room temperature until needed for transformation.

The yeast strain FY834 was cotransformed with linearized pRS426, the knock-in module, and the two PCR products for assembly in yeast by using its endogenous homologous recombination system (Figure 5). Transformation mixture was prepared by adding 360 µl of the mixture without the fragments (240 µl 50% PEG 3350, 36 µl 1 M lithium acetate, LiOAc) (Appendix I), 50 µl carrier DNA (sheared salmon sperm DNA) (Appendix I), and 34 µl sterile H2O. Pre-prepared yeast competent cells were vortexed again, and 50 µl of the cell pellet was

transferred into a new 1.5 mL microfuge tube. 360 µl of the transformation mixture was added to each tube. Finally, two µl of each PCR reaction (without clean up) and 100 ng of vector were added to the mixture and vortexed to completely dissolve the cell pellet. The final mixture was incubated at 30°C for 30 minutes. Tubes were then mixed by inverting and were placed in the water bath at 42°C for another 30 minutes. Tubes containing the transformation mixture and the cell pellet were centrifuged for 30 seconds at high speed, and the transformation mixture was pipetted off. Cells were resuspended in distilled water, mixed by pipetting, and centrifuged again for another 30 seconds at 1680 x g. Around 200 µl of the medium was left in the tube and mixed with the cell pellet by pipetting gently.

SC-URA plates (Appendix I) were prepared on the same day and sealed with parafilm, stored at 4°C, and warmed up to 30°C incubator before yeast transformation. 100-200 µl of the transformation mixtures were plated on the SC URA plates and were spread using sterile glass beads, and plates were left at 30°C for three days until the transformed colonies appeared. Single colonies were picked and were restreaked in a new SC-URA media and were left to grow in the 30°C incubator for another 2-3 days. The construction of the Cassette was confirmed by doing yeast colony PCR with the 5' forward and 3' reverse primers. Figure 7 and 8 shows examples of designed and constructed GFP and FLAG tagged plasmids using mentioned system.

2.7.6. Yeast DNA extraction using a combination of smash-and-grab and plasmid extraction method

1-2 mL of liquid SC-URA media (Appendix I) were added onto the SC-URA plates containing the transformant colonies, and the process was repeated by pipetting few times. A clean microscope slide was used to scrape down the colonies off the plate, and the mixture of colonies in SC-URA media was added to 1.5 microfuge tubes. From this step, the QIAGEN High-Speed Plasmid Mini kit protocol was followed with minor modification. 1.5 mL of the mixture (colonies + SC-URA liquid media) were added into a few 1.5 mL microcentrifuge tubes. Tubes were centrifuged at 14000 x g for 1 minute and the supernatant was discarded. 200 µl of PD1 buffer (including Rnase A) was added to the tube and vortexed to dissolve. To destroy the cell membrane and extract the DNA, 0.5 gr of 0.5mm diameter glass beads (Bio Spec) were added to new sets of microfuge tubes. The cell pellet and PD1 buffer mixture were added to the glass beads tubes and sealed and vortexed for 1-2 minutes. Then 200 µl of PD2 buffer was added on the top of the mixture. The tubes were inverted a few times to ensure that any residue was

dissolved and left at room temperature for another two minutes. 300 µl of the PD3 buffer was added and mixed immediately by inverting the tube ten times. Samples were centrifuged at 14000 x g for three minutes. A PD column was placed into a 2mL collection tube. The supernatant from the previous step was added at the column's center, centrifuged at 14000 x g for 30 seconds, and the flow-through was discarded. PD column was placed back into the same collection tube, and 600 µl of the wash buffer (ethanol was previously added) was added into the PD column. They were centrifuged at 14000 x g for 30 seconds, and flow-through was discarded. Then the PD column was placed back in the 2 mL collection tube and centrifuged again for another three minutes at 14000 x g to ensure that the column matrix was dry. PD column was placed into a new microfuge tube. Finally, 50 µl of the Elution buffer was added into the center of the PD column matrix and left at room temperature for two minutes to allow the elution buffer to be completely absorbed. The final centrifuge was performed at 14000 x g for at least 2 minutes to elute the purified DNA.

DNA was genotyped using cassette-specific primers to ensure the presence of the knock-in Cassette, and the size of the PCR products was compared to the 1 Kb DNA ladder to ensure the proper size of the Cassette. The quality and concentration of the DNA were measured using a Nanodrop machine.

2.7.7. Bacterial transformation and cassette preparation

1-5 µl (1pg-100 ng) of the yeast extracted DNA containing the desired knock-in Cassette was transformed into E-coli competent cells, and the final transformation mixture was plated on LB media (Appendix I) containing Ampicillin as a selectable marker. Single colonies were inoculated into an LB liquid media containing Ampicillin and were incubated overnight at 37 °C with shaking at 150 rpm. The day after, plasmid extraction was performed using a Qiagen midi plasmid extraction kit and the final DNA pellet was redissolved in an appropriate volume of TE buffer. The Cassette was amplified using the plasmid as a template with the 5' forward and 3' reverse primers. The correct size of the Cassette was confirmed by gel electrophoresis. The amplified Cassette was then used for *Neurospora crassa* transformation. PCR cleanup kit (Monarch PCR & DNA Cleanup Kit) was used to purify the PCR products containing the Cassette before *Neurospora crassa* transformation. To purify the DNA, samples were diluted using DNA Clean up Binding Buffer with a 2:1 ratio of buffer: sample.

2.7.8. Snap-Freezing the bacterial cultures

In order to freeze the bacterial cultures, 50% Glycerol (Appendix I) was prepared, and an equal amount of glycerol and bacterial cultures containing FLAG, GFP, or RFP knock-in cassettes were added to 1.5 Microfuge tubes and vortexed vigorously. Samples were then snap-frozen by immersing the tubes in liquid nitrogen (150°C) for 30 seconds and were transferred and stored in a -80°C freezer immediately.

2.7.9. Transformation of *Neurospora crassa* and progeny selection

2.7.9.1. Preparation of spores

The linkage of the target gene to *mus-51* or *mus-52* was checked. If there was linkage to one of the *mus* loci, the other *mus*^{ko} strain was used as the transformation recipient. 4 to 5 fresh slants of the *mus* knock-out strain on VM agar slants containing ignite (400 μg/ml) and histidine were grown at 30°C for 4-7 days. Mycelium from the slants was inoculated onto VM agar in a 250mL Erlenmeyer flask (without ignite for better growth). Flasks were incubated at 30°C in constant darkness for 3 days and then at 25°C for 7-10 additional days. Conidia were harvested using the same method as previously explained.

2.7.9.2. Transformation of Neurospora crassa

The Gene Pulser electroporation machine was adjusted at 1.5 kV (7.5 kV/cm), 25 μF capacitance, and 600 ohms resistance to start the *Neurospora* transformation. Spore suspension in 40 microliters of 1M sorbitol (Appendix I), 4mL of recovery media (2% yeast extract + 100 μg /mL histidine), purified DNA, and sterile electroporation cuvette were placed on ice. DNA was added to the conidia suspension, which was then added to the electroporation cuvette and was mixed gently by pipetting up and down few times and placed back on ice for another 5 minutes. The cuvette was wiped dry before inserting in the machine and tapped gently on the bench to endure the conidia settling down to the bottom. The cuvette was placed in the pre-cooled slide and pulsed. 1mL of cold Sorbitol was added to the cuvette immediately and mixed by pipetting up and down gently. The transformation mixture was then added to the cold recovery media in a 15 mL conical tube and was incubated at 30°C for two-four hours in constant darkness with shaking at 150 rpm.

20 mL of FGS agar (10x FGS, 2ml 500x L-histidine, and hygromycin) (Appendix I) was plated into 15 mm Petri dishes to solidify. Dilutions of recovered electroporation mixture and

regeneration agar (2% yeast extract + 100 μg /mL histidine) (Appendix I) were mixed in 15 mL conical tubes and were immediately poured on the top of FGS agar plates. Plates were sealed with micropore tape and were incubated at 30°C at constant darkness for seven days. Transformed colonies were picked and grown on slants containing Vogel's minimal media, including histidine (25 mg/mL) and choline (2 mg/mL) as supplements and hygromycin as a selection marker. Slants were left at 30°C for seven days.

2.7.9.3. Progeny selection and genotyping

To confirm the presence of the Cassette, spores were genotyped using Terra PCR Direct kit and cassette-specific primers. Heterokaryon strains were crossed into our lab strains either *(csp-1; chol-1 ras^{bd}) or (csp-1; chol-1 ras^{bd}; Δvta).*

After 4 weeks, ascospores from the cross were counted and heat-shocked at 60°C for 30 minutes to activate the ascospores. About 15-20 ascospores were plated on sorbose plating media containing hygromycin B. Colonies appeared after 2-3 days. They were then picked and grown in new slants containing appropriate supplements and were left at 30°C for 7 days. Around 800-1000 progenies were investigated from each cross. Slant cultures were genotyped for the presence/absence of *csp-1, his-3, chol-1, and mus-51,* first by inoculating *csp-1* progenies on three sets of microfuge tubes per progeny containing 200 μl of media containing liquid minimal media + choline, liquid minimal media + choline + histidine and liquid minimal media+ choline + histidine + ignite (160 μg/mL). Tubes were left at 30°C for 2 days, and the presence/ absence of each mutation was confirmed by comparing them with control strains for each condition.

Candidates that were able to grow on choline and histidine and could not grow on ignite (and were therefore *mus*$^{+}$) were chosen for gDNA extraction and the presence of desired cassettes and *vta* mutation were checked by PCR. Final candidates were then inoculated on race tubes to check the *ras^{bd}* genotype and confirm the normal function of the tagged protein to ensure that the tag's insertion did not disrupt the phenotype of the recipient strain.

2.8. Construction of tagged proteins at his-3 locus

The histidine-3 region of *Neurospora crassa* codes for an enzyme of the histidine biosynthesis pathway. Strains that will be used in this method carry the *his-3* mutation, which disrupts the biosynthetic pathway of histidine. To transform the *Neurospora crassa* at the *his-3* locus, plasmid vectors, which must carry the wild type *his-3* gene sequence, are digested and

linearized using appropriate restriction enzymes which cuts sequences away from the *his-3* region insert site and are transformed into a spore suspension of a strain which has a *his-3* mutation using electroporation (as above). The plasmid containing a wild type *his-3* gene sequence would replace the disrupted copy by homologous recombination, and the defect of the mutant will be rescued. Gene targeting at *his-3* is selected by growing the transformants in a histidine-free medium (Ratnayake et al., 2018; Tseng et al., 2017). Transformants were inoculated onto minimal agar stock tubes with the addition of choline. The successful transformants can grow on media without histidine. The genotype was confirmed using his-3 forward and his-3 reverse primers. Heterokaryons with the ability to grow on media without histidine were selected for further analysis.

Chapter 3. **Shared Components of the Frq-Less Oscillator and TOR Pathway Maintain Rhythmicity in *Neurospora***

The research discussed in the following chapter previously been published in the Journal of Biological Rhythms which included collaborations with another student (Eskandari et al, 2021). The research included in this chapter is all my own work.

3.1. Abstract

Molecular models for the endogenous oscillators that drive circadian rhythms in eukaryotes center on rhythmic transcription/translation of a small number of "clock genes." Although substantial evidence supports the concept that negative and positive transcription/translation feedback loops (TTFLs) are responsible for regulating the expression of these clock genes, certain rhythms in the filamentous fungus *Neurospora crassa* continue even when clock genes (*frq*, *wc-1*, and *wc-2*) are not rhythmically expressed. Identification of the rhythmic processes operating outside of the TTFL has been a major unresolved area in circadian biology. Our lab previously identified a mutation (*vta*) that abolishes FRQ-less rhythmicity of the conidiation rhythm and also affects rhythmicity when FRQ is functional. Further studies identified the *vta* gene product as a component of the TOR (Target of Rapamycin) nutrient-sensing pathway that is conserved in eukaryotes. TOR pathway components including GTR2 (homologous to the yeast protein Gtr2, and RAG C/D in mammals) were found as binding partners of VTA through co-immunoprecipitation (IP) and mass spectrometry analysis using a VTA-FLAG strain. In this chapter I report that reciprocal IP with GTR2-FLAG found VTA as a binding partner. Expression of GTR2 protein was found to be rhythmic across two circadian cycles, and functional VTA was required for GTR2 rhythmicity. FRQ protein exhibited the expected rhythm in the presence of GTR2 but the rhythmic level of FRQ dampened in the absence of GTR2. These results establish association of VTA with GTR2, and their role in maintaining functional circadian rhythms through the TOR pathway.

3.2. Introduction

The mechanistic TOR is a Serine/Threonine kinase, which consists of two separate complexes in mammals (mTOR) and yeast (TOR). TOR kinases are found in all domains of eukaryotic life. The primary function of the TOR signaling pathway is to integrate nutritional as well as growth signals and coordinate their effects at the cellular level. Activation of this pathway will lead to an increase in anabolic processes and a decrease in catabolic processes (Boutouja, Stiehm and Platta, 2019).

The TOR pathway has been intensively studied in yeast and mammals. In *Saccharomyces cerevisiae* (Figure 9), two multi-protein complexes have been identified (Loewith and Hall, 2011). TORC1, which is rapamycin sensitive and is located on the vacuolar membrane, is responsive to nutrient signals and controls a wide-ranging variety of readouts including protein synthesis and degradation, messenger RNA (mRNA) synthesis and degradation, ribosome bio-genesis, nutrient uptake, and autophagy. TORC2 controls the polarized organization of the actin cytoskeleton, endocytosis, and sphingolipid synthesis (Loewith and Hall, 2011).

The EGO complex is an important regulator of TORC1 in yeast, which consists of Ego1, Ego2, Ego3, Gtr1, and Gtr2 (Powis *et al.*, 2015). Gtr1 and Gtr2 are Ras-family GTPases and homologs of the metazoan Rag GTPases. Ego1 and Ego3 are homologs of the vertebrate proteins p18 (LAMTOR1) and P14+MP1 (LAMTOR2+LAMTOR3). In yeast, the EGO complex localizes to the vacuolar membrane and responds to intra-vacuolar amino acid levels. The $Gtr1^{GTP}$ $Gtr2^{GDP}$ combination activates TORC1, and activated TORC1 phosphorylates and activates Sch9, which is homologous to S6 kinase in mammals. TORC1 also regulates phosphatases in yeast through regulatory protein Tap42. Inactivation of TORC1 results in Tap42 dephosphorylation and a weak association with phosphatases that results in their activation or change in substrate preference (Loewith and Hall, 2011).

In mammals, extracellular growth factors produce their effects by using cell-surface receptors to activate the kinase AKT and the tuberous sclerosis complex (TSC), which in turn leads to the activation of mTORC1. The mTORC1 complex is also activated by amino acids by poorly characterized pathways that are not dependent on the cell-surface receptors and the TSC. The Ragulator-Rag GTPase complex (p18/ LAMTOR1, p14/LAMTOR2, MP1/LAMTOR3, p10/ LAMTOR4/C7orf59, HBXIP/LAMTOR5, RagA/B, and RagC/D) mediates amino acid

sufficiency signals to mTORC1(Yonehara *et al.*, 2017). Activation of mTORC1 leads to the phosphorylation of substrates including S6K, which further leads to the phosphorylation of the ribosomal protein S6. mTORC1 also phosphorylates translation inhibitor 4E-BP, which then leads to the release of eIF4E to increase translation (Jewell, Russell and Guan, 2013). It has been observed that in both mammals and yeast, localization of the TOR complex to the lysosomal/vacuolar membrane is required for its activation (Sancak *et al.*, 2010).

Our current research continues our effort to identify components of the FLO, and to expand our understanding of the function of VTA and its role in the *Neurospora crassa* TOR pathway. Our immediate goal was to answer the question: Do other components of the TOR pathway in *Neurospora crassa* also influence the circadian system?

Although the TOR pathway has been well-studied in yeast, very little is known about the components of this pathway in filamentous fungi such as *Neurospora crassa*. Genomic analyses have identified highly conserved putative TOR pathway genes in the fungal kingdom (Shertz *et al.*, 2010) but there are few functional studies. Rapamycin (or FK506) binding proteins (FKBPs) have been studied in *Neurospora crassa* (Pinto *et al.*, 2008). A survey of knockouts of putative Ser/Thr kinase genes in *Neurospora crassa* (Park *et al.*, 2011) identified STK-10 as a homolog of the TOR substrate Sch9/S6K and found that the knockout showed impaired growth and osmoregulation. A homolog of the TORC1/TORC2 kinase was identified in this study but no phenotypic analysis was carried out (Park *et al.*, 2011). Other components of the TOR signaling pathway, in particular potential components of an EGO or Ragulator complex, have not been described beyond our identification of VTA. We therefore began our investigation by looking for binding partners of VTA that are likely to be components of the *Neurospora crassa* homolog to the yeast/mammalian EGO/Ragulator complexes.

Our lab identified *Neurospora* gene NCU00376 as a homolog of yeast Gtr2 and mammalian Rag C/D, by the criteria of co-precipitation with VTA, sequence similarity, and requirement of the gene product for normal growth response to amino acid supplementation (Eskandari, Ratnayake and Lakin-Thomas, 2021). We have found that the rhythmic phenotype of the NCU00376 (*gtr2*) knockout is very similar to that of the vta^{ko}, in that it disrupts FRQ-less conidiation rhythmicity in two different assay systems and damps conidiation rhythmicity in the presence of FRQ (Eskandari, Ratnayake and Lakin-Thomas, 2021). As with *vta*, the $gtr2^{ko}$ also damps the rhythm of FRQ protein expression (this thesis). We therefore conclude that the protein

product GTR2 is another TOR pathway component in *Neurospora* that plays an important role in maintaining circadian rhythmicity in both FRQ-sufficient and FRQ-deficient backgrounds.

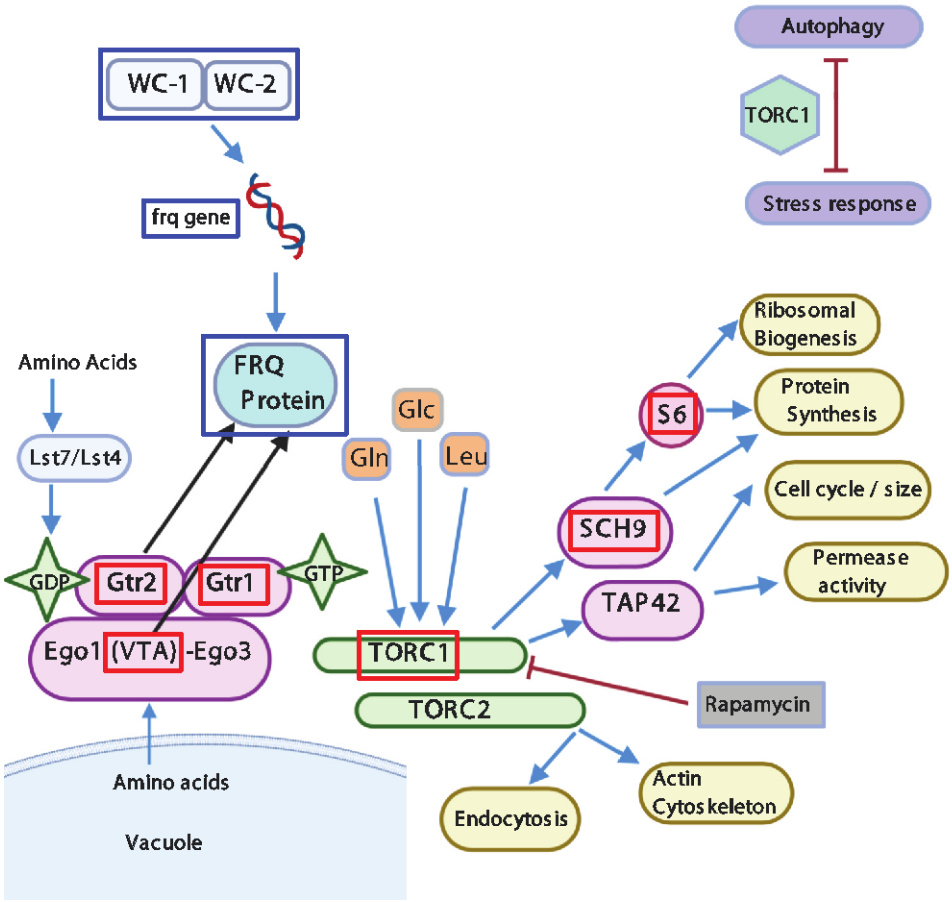

Figure 9: The TOR pathway as described in budding yeast (Created with BioRender.com.)

(Loewith and Hall, 2011; González and Hall, 2017; Saxton and Sabatini, 2017). Gln, Leu, Glc: glutamine, leucine, glucose. Arrows show activation and red blunt-ended lines show inhibition. *Neurospora crassa* proteins identified as probable components of the TOR pathway are outlined in red boxes. Blue boxes outline *Neurospora crassa* clock proteins WC-1, WC-2, and FRQ (not found in yeast). Black arrows suggest an influence of VTA and GTR2 on FRQ protein in Neurospora.

3.3. Results

3.3.1. VTA and GTR2 Bind to Each Other and to Another Probable TOR Pathway Component

3.3.1.1. Previous work

Our lab's previous work (Ratnayake *et al.*, 2018) identified VTA as a component of the TOR pathway in *Neurospora crassa*. To determine whether other components of this pathway also influence rhythmicity, we looked for binding partners of VTA that are likely to be TOR pathway components. Using a previously constructed VTA-FLAG fusion (Ratnayake *et al.*, 2018), we carried out co-IP followed by mass spectrometry. Three independent experiments were carried out using an unrelated FLAG-tagged strain and a strain without any FLAG tag as controls in each experiment. The top half of Table 4 presents the results of the co-IPs carried out by Lalanthi Ratnayake. Proteins were only included in Table 4 if spectrum counts were zero in both control strains in all three experiments.

The top hit was gene NCU00376. This gene is identified in the *Neurospora crassa* genome database FungiDB as guanine triphosphate binding-28 (*gtp-28*). Protein BLAST searches found that the closest homolog in *S. cerevisiae* is Gtr2p; one of the Ras-family GTPases found in the EGO complex that includes a homolog of VTA. We therefore refer to NCU00376 as *gtr2* and its product as GTR2. The closest homolog in mouse and human is RagD, a Ras-family GTPase found in the Ragulator-Rag GTPase complex. Both of these complexes function to transmit information about amino acid sufficiency to TOR.

3.3.1.2. Construction of GTR2-FLAG

To confirm the association of VTA and GTR2 by reciprocal co-IP, I constructed a FLAG-tagged GTR2 using knock-in techniques (Chapter II) to tag the endogenous gene. A 1.1 kb fragment including the 3′-end of the GTR2 (NCU00376) coding region, without the stop codon, was amplified from the genomic DNA of a *csp-1; chol-1 ras^{bd}* strain using the following forward primer (Chapter II) : GTAACGCCAGGGTTTTCCCAGTCACGACGCC TTCATTCTACCCTCATAC, which contains 29 nt of homology (indicated by underlining) at one end of the linearized pRS426 (shuttle vector, obtained from FGSC), and reverse primer: CCTCCGCCTCCGCCTCCGCCGCCTCCGCCACGACCATCACCCACCA CCC, which contains 29 nt of homology at the 5′-end of the 3xFLAG knock-in module. A 500 bp fragment of the 3′ GTR2 flanking region was amplified with the forward primer: TGCTATACGAAGTTATGGATCCGAGCTCGGGATTTCATCCGGTTGTTTG, which

contains 29 nt of homology with the 3′-end of the 3xFLAG knock-in module, and reverse primer: GCGGATAACAATTTCACACAGGAAACAGCCACCCAGCCAACCAAGTACC, which contains 29 nt of homology at the other end of the linearized pRS426. The rest of the process is as explained in Chapter II. Figure 10 shows PCR results of heterokaryon transformants into a mus mutant strain. The presence of two bands indicates the correct insertion of the cassette. Fragment sizes compared to a 1 Kb DNA ladder for confirmation. To ensure the normal expression of the GTR2- FLAG protein, immunoblotting was carried out with anti-FLAG antibodies. A strain without any FLAG (*csp-1; chol-1 ras^{bd}*) was used as the negative control. The FLAG-tagged GTR2 protein demonstrated expression in the expected region (48 KD) and no band was observed in the negative control lane (data not shown). Figure 11 indicates PCR results using cassette-specific primers and homokaryon progenies obtained from a cross of the *mus* transformant with a *csp-1; chol-1 ras^{bd}* strain.

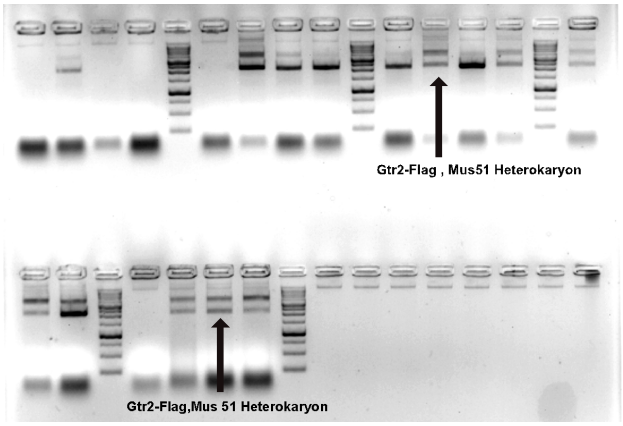

Figure 10: Spore PCR results of GTR2- Flag mus 51 transformants. 12 out of 19 transformants show correct size of the GTR2-Flag Cassette (3967 bp). Lanes number 7,8,12,13,14,16,17,18,21,22 and 23 are correct transformants.

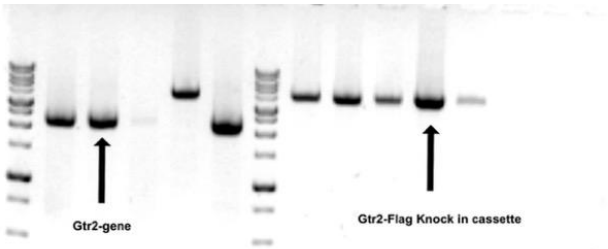

Figure 11: Spore PCR of GTR – FLAG progenies from a cross of *mus* transformant and a *csp-1; chol-1 ras^{bd}* strain. 5' Forward and 3' Reverse cassette primers used. Lanes number 5, 8,9,10,11,12 shows the correct size of the cassette.

3.3.1.3. Circadian phenotypes of transformants

Race tube assays were carried out to confirm the normal function of the GTR2-FLAG protein and to ensure that the insertion of the FLAG tag did not disrupt the phenotype of the recipient strain. The banding phenotype, period, and growth rate of GTR2-FLAG were similar to the control on high choline (Figure 12, Table 3). The GTR2-FLAG strain on low choline displayed a long-period rhythm, as expected for choline-deprived wild-type strains, but the period was significantly shorter than the control, indicating some effect of the FLAG tag under these conditions. In the conditions of choline supplementation used in the co-IP experiments, the C-terminal FLAG tag did not disrupt the growth or significantly impair the clock-related functions of GTR2 protein.

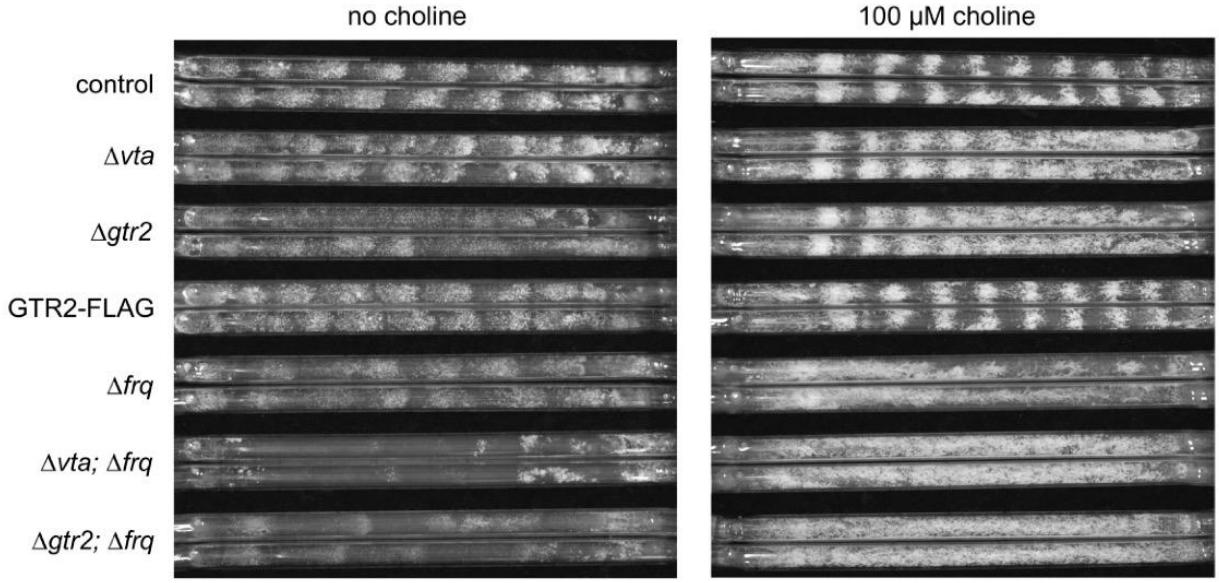

Figure 12: Effects of GTR2 deletion and FLAG tagging on free-running FRQ-less rhythms.

Choline-requiring (*chol-1*) strains were grown on solid agar with or without 100 µM choline in race tubes in constant temperature and constant dark. Growth is from left to right. Two replicate tubes are shown for each strain. All strains carry the *csp-1; chol-1 ras^{bd}* genotype as well as deletions of *frq, vta, or gtr2*, or GTR2-FLAG knock-in, as indicated.

	no choline		**100 µM choline**	
Strain	Period (h)	Growth rate (mm/h)	Period (h)	Growth rate (mm/h)
control	74.6 ± 3.32 (6)**	0.41 ± 0.01 (6)	21.0 ± 0.15 (6)	1.15 ± 0.01 (6)
Δ*vta*	73.5 ± 7.97 (6)**	0.40 ± 0.01 (6)	21.6 ± 0.14 (6)*	1.10 ± 0.01 (6)
Δ*gtr2*	NR	0.41 ± 0.02 (6)	22.0 ± 0.28 (6)**	1.03 ± 0.01 (6)
GTR2-FLAG	48.9 ± 3.35 (6)**†	0.48 ± 0.01 (6)	20.7 ± 0.09 (7)	1.16 ± 0.01 (7)
Δ*frq*	83.6 ± 4.73 (6)**	0.45 ± 0.01 (6)	NR	1.18 ± 0.01 (6)
Δ*vta;* Δ*frq*	NR	0.51 ± 0.01 (6)	NR	1.20 ± 0.01 (6)
Δ*gtr2;* Δ*frq*	NR	0.52 ± 0.05 (5)	NR	1.16 ± 0.01 (5)

Table 3: Growth phenotypes of Δ*gtr2* and GTR2-FLAG strains. All strains carry the *csp-1; chol-1 ras^{bd}* genotype in addition to indicated genotypes. Data are reported as mean ± SEM (N) where N is the number of race tubes. NR = not rhythmic. *: Period is significantly different from control on high choline at $p < 0.05$ (*) or $p < 0.01$ (**). †: Period on low choline is significantly different from control on low choline at $p < 0.01$.

3.3.1.4. Co-IP with GTR2-FLAG

As shown in Table 4, the uncharacterized protein NCU04811 was the top binding partner with GTR2- FLAG, and NCU05950 (VTA) was the second-most frequent binding partner, followed by GTR1. These results confirm the physical association between VTA and GTR2 and suggest a functional relationship between these proteins.

Binding Partners of VTA									
Locus ID	Gene product	MW (kDa)	Exp. 1		Exp. 2		Exp. 3		total counts
			peptides	counts	peptides	counts	peptides	counts	
NCU00376	GTR2	48	3	9	9	13	12	16	38
NCU04811	Hypothetical Protein	33	9	13	2	2	5	6	21
NCU01099	GTR1	45	2	2	3	3	6	6	11
NCU04376	Hypothetical protein	52	2	2	-	0	2	2	4
Binding Partners of GTR2									
NCU04811	Hypothetical Protein	33	1	5	2	4	2	3	12
NCU05950	VTA	17	3	4	-	0	2	2	6
NCU01099	GTR1	45	-	0	1	1	2	2	3

Table 4. Co-immunoprecipitation and mass spectrometry results. Binding partners of each FLAG-tagged bait protein are listed in descending order of total spectrum counts. An unrelated FLAG-tagged strain and a strain without any FLAG tag were used as controls in each experiment. NCU number represents the ID of the gene in the *N.crassa* genome database (FungiDB). Results are shown for three independent experiments. Experiments with VTA-FLAG (top half of table) were carried out by Lalanthi Ratnayake.

3.3.2. GTR2 Protein Levels Are Rhythmic

To determine whether GTR2 protein is rhythmic, a time-course experiment was conducted using the GTR2-FLAG knock-in strain and an anti-FLAG antibody. Samples were harvested every 4 h across two circadian cycles from 24 to 72 h in darkness. Figure 13 demonstrates rhythmic expression of the protein. The peaks are at approximately 24-28, 48-52, and 68 h in darkness, which is close to the 21-22 h circadian period of *Neurospora crassa* (Table 3). This low-amplitude rhythm is not obvious by visual inspection of the blots (Figure 13 b) but is reproducibly found after quantitation (Figure 13 a). A one-way analysis of variance (ANOVA) of the three replicate experiments found a significant effect of time, $p < 0.001$. Whether this rhythm is biologically significant remains to be determined. It has been reported that the RNA levels of

GTR2 are rhythmic with a peak in the afternoon/ evening at about 24 h in DD, or shortly after subjective dusk (Hurley *et al.*, 2014). Assuming a period of about 21 h (Table 3), we would expect RNA peaks at about 24, 45, and 66 h in our culture system, a few hours before the protein peaks we observe (Figure 13a). GTR2 protein was also detected in a proteomics data set designed to identify rhythmic proteins (Hurley *et al.*, 2018), although this data set failed to detect rhythmicity of the protein. This may be due to lower sensitivity of the proteomics method or differences in the culture systems and growth media used.

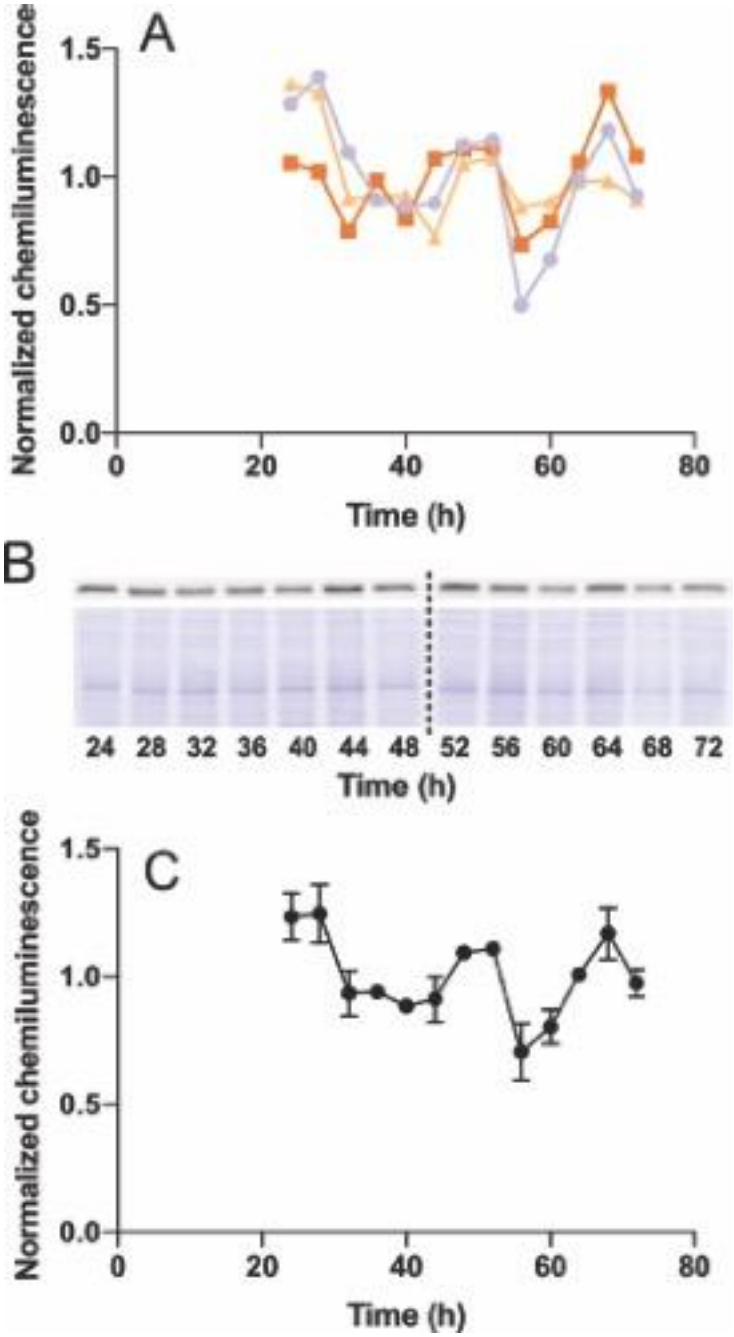

Figure 13: Rhythmic expression of GTR2 protein. (a) GTR2-FLAG (*csp-1; chol-1 ras*^{bd}) protein expression from three independent experiments across 24-72 h in constant conditions. (b) Immunoblot of one experiment showing GTR2-FLAG levels (above) and Coomassie blue staining (below). Dotted line indicates separation between two gels blotted to the same membrane. (c) Mean ± SEM from three independent experiments.

3.3.3. VTA is Essential to Maintain Rhythmicity of the GTR2 Protein

I next tested the hypothesis that the close physical association between VTA and GTR2 might affect the levels of GTR2 protein. To determine whether VTA protein is necessary to

maintain the rhythmic expression of the GTR2 protein, three independent time-course experiments were conducted on a GTR2-FLAG strain in the absence of VTA. As shown in Figure 14, the rhythmicity of the protein was completely disrupted. Figure 14a shows that none of the three independent trials with the Δ*vta* strain show similarity with each other nor do they with the VTA wild type (Figure 13). A one-way ANOVA of the three replicate experiments found no significant effect of time, $p > 0.5$. To determine whether Δ*vta* changes the total amount of the GTR2 protein or just disrupts rhythmicity, one time point (28 h) was chosen which was at high levels in all experiments and three independent biological trials were loaded on the same gel, three samples of the wild type and three of Δ*vta* (data not shown). The relative amount of the GTR2 protein was quantified by calculating the ratio of chemiluminescence of each sample to its total protein by Coomassie staining. The mean of the three independent samples demonstrated similar ratios of 0.94 ± 0.08 (SEM) for GTR2-FLAG (*csp-1; chol-1 ras*^{bd}) and 0.82 ± 0.20 (SEM) for GTR2-FLAG (*csp-1; chol-1 ras*^{bd}; Δ*vta*). A paired two-tailed Student's *t* test gave a *p* value of 0.65, indicating that the difference is not statistically significant. It can be concluded that VTA protein does not control the total level of expression of GTR2 protein, but that the presence of VTA is required to maintain rhythmic expression of GTR2 protein.

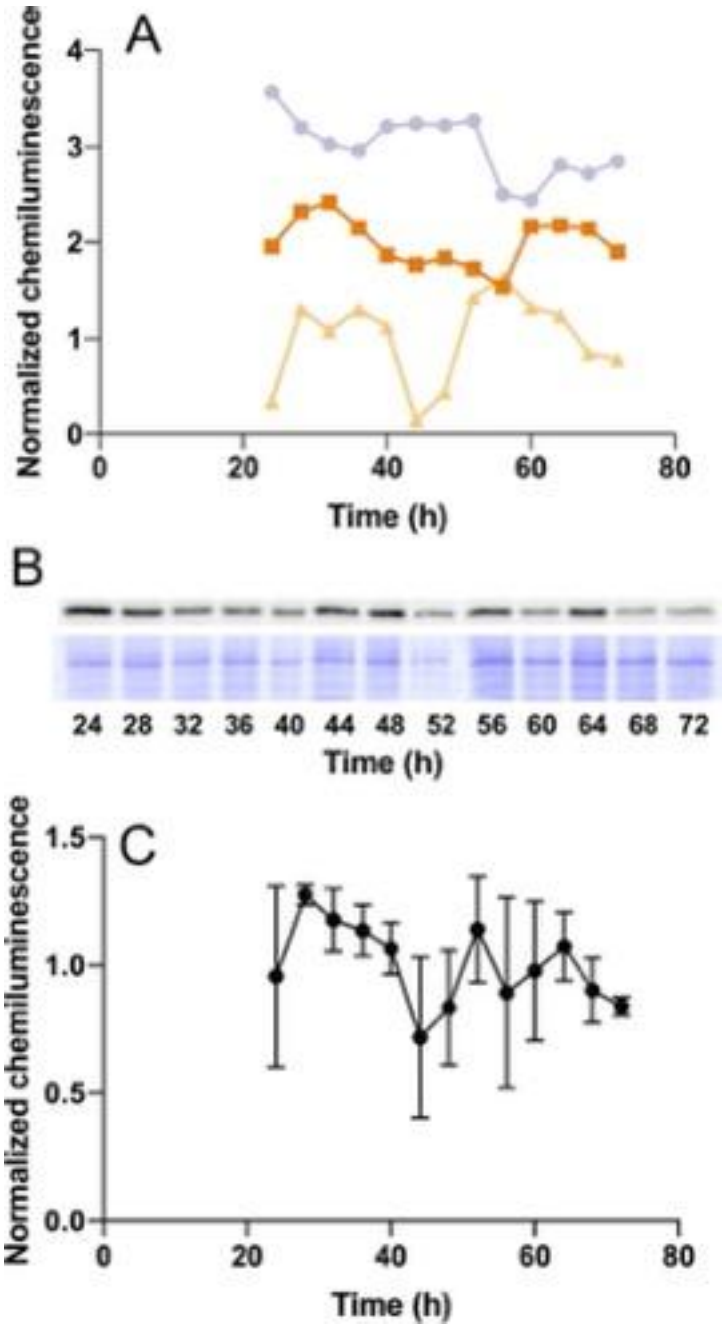

Figure 14: Expression of GTR2 protein in Δvta background. (a) GTR2-FLAG (*csp-1; chol-1 ras^{bd}; Δvta*) protein expression from three independent experiments across 24-72 h in constant conditions. Replicates were offset by +1.0 or +2.0 vertically for clarity. (b) Immunoblot of one experiment showing GTR2-FLAG levels (above) and Coomassie blue staining (below). Dotted line indicates separation between two gels blotted to the same membrane. (c) Mean ± SEM from three independent experiments.

3.3.4. GTR2 Is Essential to Maintain Expression Level and Rhythmicity of the FRQ Protein

To first confirm that the FRQ/WCC TTFL is functional in our time-course samples, immunoblotting with anti-FRQ antibody was conducted on the same biological samples as in Figure 13, and FRQ protein demonstrated the expected rhythm in protein amount and phosphorylation state across two circadian cycles in the GTR2 wild-type strain, GTR2-FLAG (*csp-1; chol-1 ras* ; *bd* Figure 15). A one-way ANOVA of the three replicate experiments found a significant effect of time on protein levels, $p < 0.001$. To determine whether GTR2 is essential for the rhythm of FRQ protein, another time-course experiment was conducted on a Δ*gtr2* (*csp-1; chol-1 ras*^{bd}) strain. It was found that the FRQ protein level was rhythmic but appeared to dampen over time (Figure 16). A one-way ANOVA of the three replicate experiments found a significant effect of time on protein levels, $p < 0.001$.

To quantitate the effect of the absence of GTR2 on the total level of expression of FRQ, I re-ran selected GTR2 wild type and Δ*gtr2* protein samples and blotted the two gels on one membrane for immunodetection with anti-FRQ antibody and direct comparison of FRQ protein levels. Three time points were chosen near the peaks of expression at 24, 44, and 60 h. The membrane was stained with Ponceau Red before immunodetection and the relative amount of the FRQ protein in each lane was calculated relative to total protein in that lane. The results indicated that in the absence of GTR2 protein, the expression level of the FRQ protein tends to be lower than GTR2 wild type and is significantly lower at the third time point (Figure 17). I conclude that the presence of GTR2 is essential for normal FRQ expression levels, and the rhythm of FRQ protein levels damps out in the absence of GTR2.

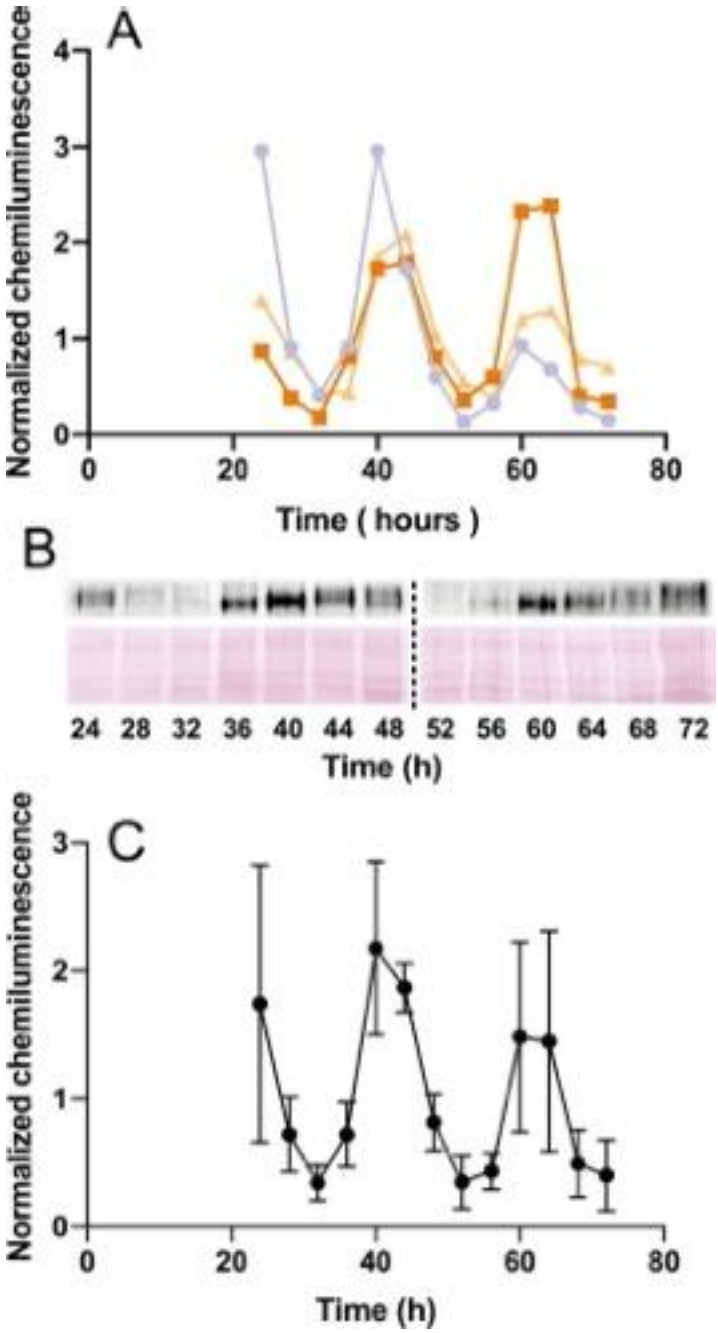

Figure 15: FRQ protein levels in the presence of GTR protein. (a) FRQ (*csp-1; chol-1 ras*^{bd}) protein expression from three independent experiments across 24-72 h in constant conditions. (b) Immunoblot of one experiment showing rhythm of FRQ levels (above) and Ponceau Red staining (below). Dotted line indicates separation between two gels blotted to the same membrane. (c) Mean ± SEM from three independent experiments. The phosphorylation state of FRQ protein can be determined by the shift in the apparent molecular weight of the band.

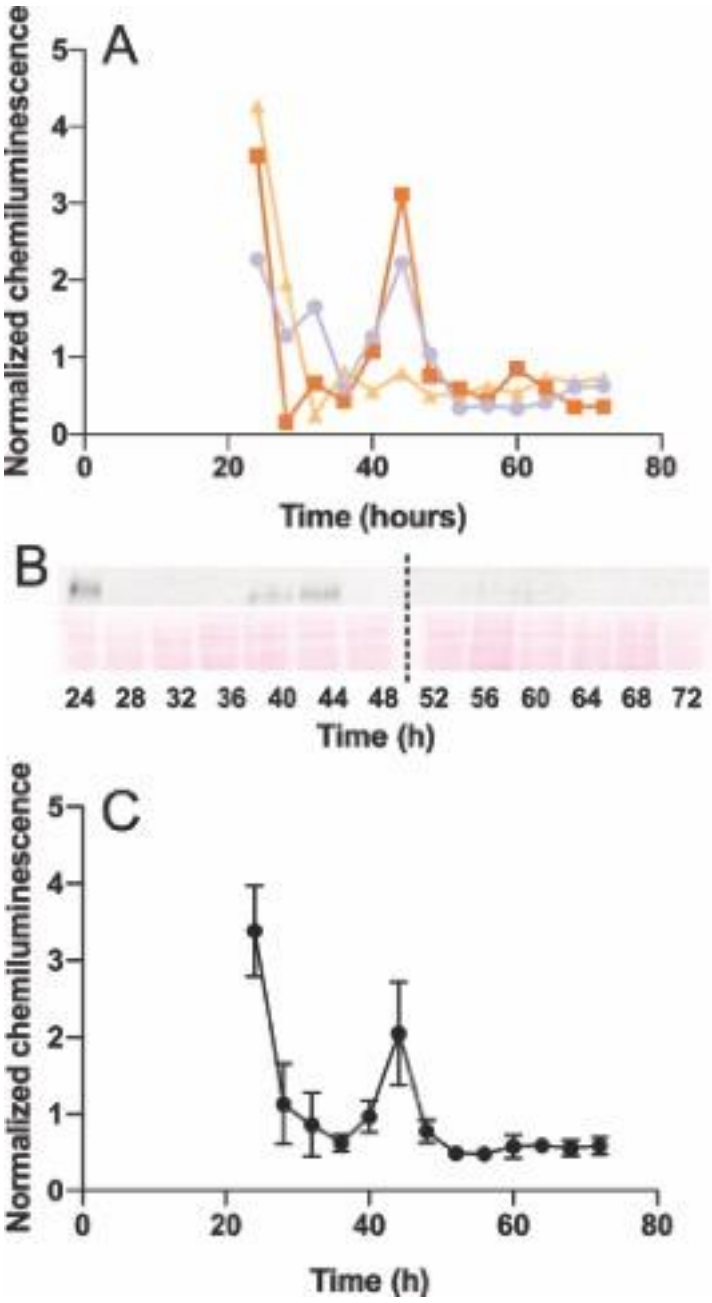

Figure 16: FRQ protein levels in the absence of GTR2 protein. (a) FRQ (*csp-1; chol-1 ras^{bd}; Δgtr2*) protein expression from three independent experiments across 24-72 h in constant conditions. (b) Immunoblot of one experiment showing rhythm of FRQ levels (above) and Ponceau Red staining (below). Dotted line indicates separation between two gels blotted to the same membrane. (c) Mean ± SEM from three independent experiments.

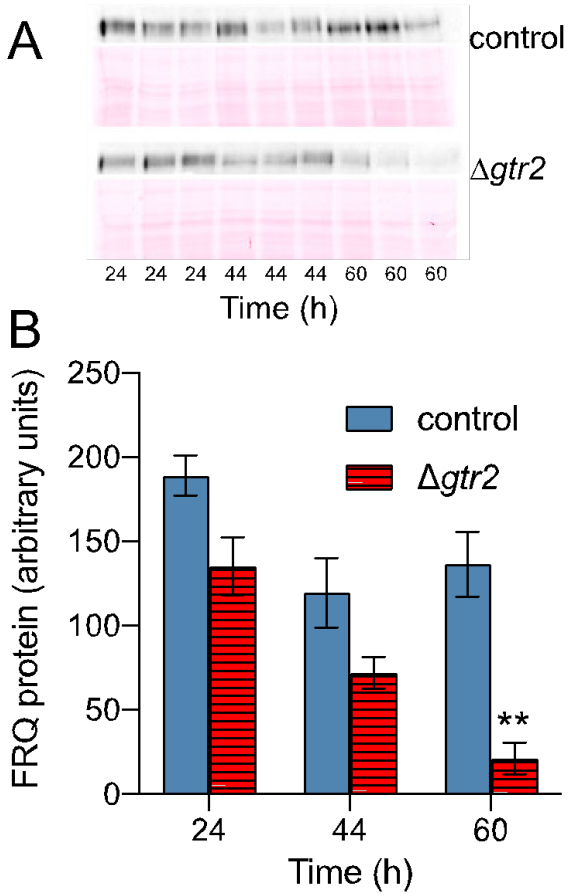

Figure 17: FRQ protein levels in the presence and absence of GTR2. 24, 44, and 60 h samples were chosen to compare the total amount of FRQ protein between strains. (a) Immunoblot showing FRQ protein (above) and Ponceau Red staining (below) for control (*csp-1; chol-1 ras*^{bd}) and GTR2 deletion (*csp-1; Δgtr2; chol-1 ras*^{bd}) with three replicates for each time point. Two gels were blotted to the same membrane for immunodetection. (b) Mean ± SEM from three independent samples for each strain. **Control significantly different from Δgtr2, $p < 0.001$.

3.4. Discussion

This research enhanced our knowledge of the components of the FLO and TTFL and their interaction and the role of the TOR pathway. Our lab previously found NCU05950 as VTA, homologous to Ego1 in yeast and LAMTOR1 in mammals. We have now identified the product of NCU00376 as GTR2, homologous to one of the Rag GTPases found in the EGO or amino acid–sensing complexes of yeast and mammalian TOR pathways. Another protein of interest that showed up in our mass spec results as a binding partner of VTA and Gtr2 was NCU01099, known as Gtr1. Gtr1 is a Rag GTPase in the same complex as VTA and GTR2. We also found a

new binding partner for all our components as NCU 04811, which we were not able to find any homologs for. Future work on its function should give us clues about the interaction of these proteins. We have demonstrated that these proteins can be found in a complex.

Over the past few years, there has been increasing interest in identifying the links between circadian rhythms and metabolism. There is considerable evidence for the existence of metabolic oscillators that might be present in addition to the TTFL. One potential biochemical link between these two is the TOR signaling pathway (Lakin-Thomas, 2019). TOR signaling has been linked to circadian clocks in several organisms (Lakin-Thomas, 2019), both as an output pathway and in a more direct role in generating or maintaining rhythmicity. Evidence for these more immediate effects of TOR on clocks comes from studies on *Drosophila* (Zheng and Sehgal, 2010), human cell lines (Feeney *et al.*, 2016; Walton *et al.*, 2018) and both SCN and peripheral tissues of mice (Lipton *et al.*, 2017; Cao, 2018). In recent studies on *Arabidopsis*, TOR was found to be essential for glucose- and nicotinamide- mediated control of the circadian period (Zhang *et al.*, 2019), and knocking down TOR activity with inhibitors, micro-RNA or RNAi was found to lengthen the circadian period (Wang *et al.*, 2020).

Our previous work (Ratnayake *et al.*, 2018) demonstrated that deletion of *vta* dampens conidiation rhythmicity in FRQ wild-type strains and abolishes FRQ-less rhythms. These results provided evidence of a role for the TOR pathway in the rhythmicity of *Neurospora crassa* in the presence or absence of a functional FRQ/WCC TTFL. In our work with the GTR2 deletion, similar results were obtained from assays of conidiation rhythmicity (Eskandari *et al.,* 2021). Our findings raise attention to questions about the roles of VTA and GTR2 in the circadian system and whether VTA and GTR2 function in the same pathway to maintain circadian rhythms.

Time-course experiments with the anti-FRQ antibody have revealed exciting insights into the interaction of these TOR pathway components with the FRQ/WCC TTFL. Our previous results demonstrated that the FRQ protein rhythm dampens over time in the absence of VTA protein (Ratnayake *et al.*, 2018). In my current work with GTR2, similar results were obtained, and the presence of GTR2 was shown to be essential to maintain the regular expression of the FRQ protein.

In related research (Diernfellner *et al.*, 2019) , the clock-controlled gene *prd-4* was found to be essential for FRQ phosphorylation in response to translation inhibition. This phosphorylation requires an upstream kinase of PRD-4, which was identified as TORC1 using phosphorylation of

S6 as an assay for TORC1 activity (Diernfellner *et al.*, 2019). We have not characterized the pathway through which VTA and GTR2 affect FRQ, but our work is consistent with the work of Diernfellner et al. and suggests a pathway: VTA> GTR2 > TOR > PRD4 > FRQ.

Overall, it can be concluded that the presence of both VTA and GTR2 is necessary for the normal function of FRQ and the circadian system, demonstrating a strong connection between the TOR pathway and circadian rhythms. We propose that GTR2 and VTA maintain circadian rhythmicity through the complementary interaction of FLO with the FRQ/WCC TTFL, supporting our model that the TTFL is not adequate to explain circadian rhythms in *Neurospora crassa*. We hypothesize that FLO may work through the TOR pathway, an essential metabolic signaling pathway in all eukaryotes (Fig. 18). Our results are expected to have implications for enhancing the understanding of the circadian systems of other organisms and for understanding the fundamentally important process of timekeeping in eukaryotes.

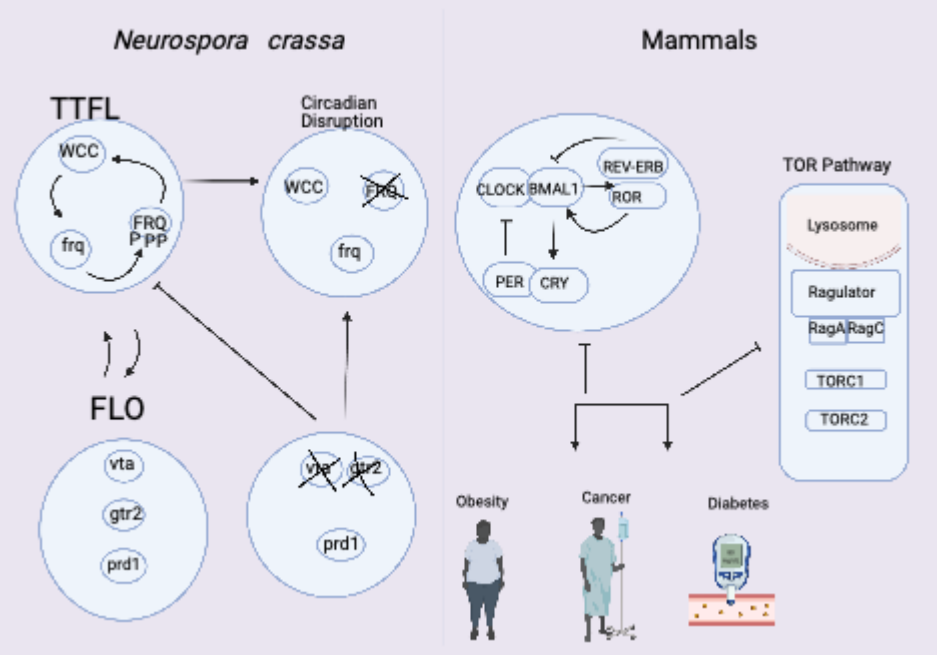

Figure 18: Mutual interaction of TTFL and FLO. Knock out of mutual FLO and TOR pathway components will lead to dysfunctional circadian rhythmicity. Inhibition of circadian clock and TOR pathway in mammals will lead to metabolic disorders such as diabetes, cancer, and obesity. (Li *et al.*, 2011; Saxton and Sabatini, 2017; Pilorz, Helfrich-Förster and Oster, 2018; Ratnayake *et al.*, 2018; Boutouja, Stiehm and Platta, 2019; Eskandari, Ratnayake and Lakin-Thomas, 2021). Created with BioRender.com.

Chapter 4. Localization of TOR Pathway Components in *Neurospora*

4.1. Abstract

In this chapter, I report the subcellular localization of VTA and GTR2 in different nutritional states, and the presence and absence of TOR pathway inhibitors. Kog1/Raptor is a regulator for TOR1 activity in yeast and mammals, and I observed localization of KOG1in standard condition, in the presence of arginine as well as TOR pathway inhibitors in *Neurospora crassa*. My data indicates that GTR2-RFP localizes close to the structures identified as vacuolar membranes but is cytoplasmic in the absence of VTA. KOG1-GFP looks similar to GTR2-RFP. In the presence of arginine, KOG1-GFP and GTR2-RFP are localized around the vacuolar membrane. Starvation using media without glucose looks similar to the *vta* ^{ko} condition in the GTR2 strain. In KOG1-GFP, a drop in the expression and the presence of P bodies around the edges of the vacuole were observed in the absence of glucose. In the presence of TOR pathway inhibitors Torin I and Torin II, an abnormal structural morphology was observed in both cases, thereby indicating that the presence of inhibitors damages the vacuolar and internal network, and moves the KOG1 protein expression signal to the outer membrane.

Our images from ATG8-RFP strains indicate the accumulation of autophagosomes in the absence of VTA and in the presence of TOR pathway inhibitors suggesting a role of VTA in induction of autophagy.

4.2. Introduction

4.2.1. Previous research on the role of VTA and GTR2 as mutual components of the TOR pathway and circadian rhythms

Our lab's previous work indicated that a GFP fusion of the NCU05950 (VTA) protein is localized to vacuolar membranes and deletion of putative acylation sites abolishes this localization, suggesting that fatty acids anchor it to the membrane as these acyl groups anchor the yeast and mammalian homologs. These deletions failed to rescue the *vta* mutant phenotype, demonstrating that vacuolar localization is required for normal clock function (Ratnayake et al., 2018).

Our previous study using coimmunoprecipitation of a VTA-FLAG strain conducted by a former lab member indicated that some TOR pathway components are associated with VTA. One of the top binding protein candidates is GTR2, which is homologous to the yeast protein and is known as Rag C/D in mammals. Further reciprocal coimmunoprecipitation of GTR2-FLAG with VTA indicates that VTA and components of the TOR pathway also coimmunoprecipitated with GTR2. Additional experiments on GTR2 protein suggest that the protein expression was rhythmic across 24 to 72 hours of the circadian cycle, with a period close to the 21.5-hour circadian cycle time of *Neurospora crassa.* FRQ protein demonstrated the expected phosphorylation rhythms in the presence of GTR2. However, such rhythm of phosphorylation dampens in the absence of GTR2, which is consistent with the observation with VTA (Eskandari et al., 2021; Ratnayake et al., 2018).

4.2.2. Goal of the present study

My research aimed to investigate other dimensions of our FLO model, and further understand the function of VTA and its role in the *Neurospora crassa* TOR pathway. I also investigated the localization of the TOR pathway components in different conditions, which would help us to understand the TOR pathway in *Neurospora crassa*. Until now, our focus was on the upstream effectors of TORC. My research would assist to further understand the relationship between the EGO complex and TORC1, as well as the role of VTA as a mutual component of FLO and TOR pathway.

4.2.3. KOG1 protein as a key regulator of the TOR complex and autophagy

In humans and yeast, mTORC1/TORC1 consists of three essential components: Raptor/

kog1, mLST8/Lst8, and mTOR/Tor. The presence of Kog1/Raptor is necessary to recruit substrates to the TOR kinase and it acts a regulator for TOR1 activity (Figure 19). mLst8/Lst8 is assumed to stabilize the complex. The presence of growth hormones and of nutrients causes activation of TORC1, which leads to an increase in anabolic processes, such as protein synthesis and mRNA synthesis through phosphorylation of downstream substrates. In contrast, starvation or TORC1 inhibitors such as Rapamycin led to a drop in substrate phosphorylation and decreased TORC1 activity. Inhibition of TORC1 causes cells to switch from anabolic to catabolic metabolism and enter a quiescent state (Hughes Hallett et al., 2015).

In mammals and yeast, amino acid and nitrogen signals act through a complex that contains small proteins known as Gtr1/2 in yeast and RagAB/CD in mammals. These complexes are localized on the vacuolar or lysosomal membrane, and mediate and respond to these signals by binding and activating TORC1 (Sancak et al., 2010). In the presence of sufficient nutrition, Kog1/Raptor binds and recruits substrates of TORC1, and this is an essential regulator of the activation of TOR1.

These signals inhibit TOR during energy starvation through the AMPK pathway. An essential function of the activation of AMPK is the phosphorylation of the Kog1/Raptor component of TORC1 in yeast and mammals. Glucose starvation leads to AMPK activation and phosphorylation of Kog1 through Snf1, which leads to disassembly of TORC1 in yeast and the separation and movement of Kog1 from its original location on the vacuolar membrane to a single body on the edge of the vacuole (Hughes Hallett et al., 2015)

Autophagy is a catabolic process that includes a ubiquitous, non-selective degradation process to recycle cellular components that allows survival under limited conditions. (Miller-Fleming et al., 2014). Autophagy has a crucial role in filamentous fungi, which impacts their growth, morphology, and development (Pollack et al., 2009).

During autophagy, the cargo is engulfed by the phagophore. Upon completion, the phagophore matures into an autophagosome, transports, and releases the cargo into the vacuole, where it gets degraded. The autophagosome formation starts at the PAS (pre-autophagosomal structure) with the assembly of several autophagy related proteins and subsequent nucleation and expansion of the double membrane (Miller-Fleming et al., 2014).

In yeast, there are two different autophagy mechanisms: the first is microautophagy, in which the cytoplasm is transferred to the vacuole by invagination of the vacuolar membrane. The

second is macroautophagy, which involves the de novo formation of double-membrane structures called autophagosomes. Both forms of autophagy are regulated by TORC1. In yeast, regulation of the macroautophagy by TORC1 activity includes signaling by the TORC1 to the Atg1 kinase complex, which is necessary for inducing macroautophagy. When TORC1 is active, Atg13 is hyperphosphorylated, which inhibits the interaction of Atg13 with Atg1, Atg17, Atg31, and Atg29. Inhibition of TORC1 results in dephosphorylation of Atg13, assembly of the Atg1 protein kinase complex, phosphorylation and activation of Atg1 and, consequently, macroautophagy mediated by as yet unidentified Atg1 substrates (Loewith and Hall, 2011)

Atg8 is an autophagy related gene found in Saccharomyces cerevisiae and plays a key role in forming autophagosomes. Atg8 is localized in the membranes of pre-autophagosomal structures (PAS), autophagosomes, and autophagic bodies, and has therefore been used as a marker of these organelles (Shpilka et al., 2011). The product of the *Atg8* gene (gene ID =NCU01545) is a marker of autophagosomes in *Neurospora crassa* (Fleißner et al., 2016).

In *Neurospora crassa*, the vacuole is the compartment of degradation and recycling in aging and starvation conditions. During autophagy, fungal vacuoles adopt the role of animal lysosomes. Autophagy can be induced in *Neurospora crassa* by starvation or the presence of the macroloid antibiotic Rapamycin (Fleißner et al., 2016). Since TORC1 is a significant regulator of the autophagy process, the absence of one of its main components (VTA) is proposed to induce autophagy.

4.2.4. The role of KOG1 protein and the autophagy process in *Neurospora crassa*

In the present study, my hypothesize was that KOG1 protein in *Neurospora crassa* acts as its homologs in mammals and yeast, and starvation or EGO component mutants such as *vta* changes its localization from the vacuolar membrane to puncta structures on the vacuole (Hughes Hallett et al., 2015).

In another approach, I studied autophagy induction as a downstream effect of the TOR pathway. My hypothesis is that the absence of *vta* might mimic the outcome of the presence of TOR pathway inhibitors or starvation.

4.2.5. Experimental approach

The goal of my experiments was to find the role of a key component in the TORC1 (KOG1), and to observe interactions between EGO and TORC. To meet the objective, I constructed

KOG1-FLAG to conduct time course experiments, and coimmunoprecipitation with KOG1-FLAG to get more information about the function of TORC1 components and how they interact with VTA and GTR2. I also constructed GTR2-RFP, and a former lab member has previously constructed VTA-GFP. I observed their localization in different nutritional states and in the presence and absence of TORC inhibitors such as Torin I and Torin II, which provided information about the activity of the TOR pathway in *Neurospora crassa*. Additionally, microscopy was done in the presence of different concentrations of Torin I, Torin II, and the TORC1 activator arginine, and the absence of glucose as a factor in starvation. Importantly, observations in the presence and absence of VTA were made to investigate the effect of the presence of VTA on the localization of TOR pathway components. To investigate the relationship between the EGO complex component and TORC1, coimmunoprecipitation and mass spectrometry were performed to find the binding partners of proteins in the presence and absence of VTA.

To investigate autophagy, I examined the localization of ATG8-RFP in the presence and absence of VTA, and the presence of Torin II as TOR complex I and II inhibitor. This goal was achieved by constructing ATG8-RFP in the *vta* ^{ko} and *vta* wild-type background.

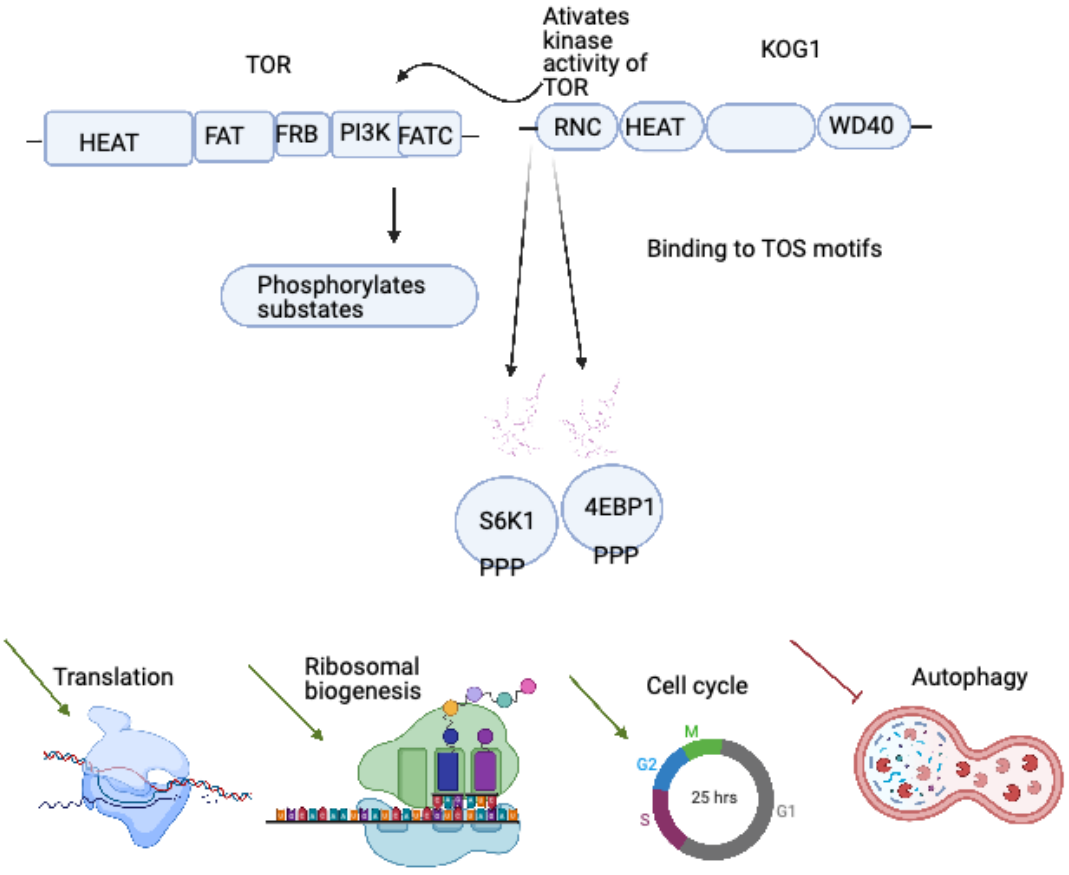

Figure 19: The presence of Kog1/Raptor is necessary to recruit substrates to the TOR kinase and is a regulator for TOR1 activity. In mammals RAPTOR binds to the HEAT repeat region in the amino-terminal half of mTOR. It functions as substrate adaptor, because it binds to the TOS (TOR signaling) motif that is present in several TORC1 substrates. Moreover, it is also involved in the correct lysosomal targeting of TORC1. Disruption of KOG1/Raptor interaction with its two main substrates, S6K1/ SCH9 and 4EBP1 leads to TOR pathway inhibition and impaired transcription, ribosomal biogenesis, cell cycle arrest and activation of autophagy (Boutouja et al., 2019; Hughes Hallett et al., 2015). Created with BioRender.com

4.3. Results

4.3.1. Construction of GTR2-RFP, GTR2-GFP, KOG1-GFP, KOG1-RFP and KOG1-FLAG in native chromosomal locations.

4.3.1.1. Transformation of Neurospora and progeny selection

The KOG1-GFP, KOG1-FLAG, KOG1-RFP and GTR2- RFP, GTR2-GFP plasmids were constructed using a knock-in method, which uses recombination-mediated plasmid construction in Saccharomyces cerevisiae to make knock-in cassettes (Figure 20 and as explained in chapter II). KOG1-GFP, KOG1-FLAG, KOG1-RFP, GTR2-RFP, and GTR2-GFP plasmids were extracted from yeast (Figure 21) and amplified in *E. coli*. The bacterial plasmid of KOG1-RFP

was constructed to use in case KOG1-GFP was not functional. Knock-in cassettes were amplified from bacterial plasmids using 5' forward and 3' reverse specific primers, and the PCR products were then transformed by electroporation into the *mus-51 his-3* strain of *Neurospora crassa* deficient in non-homologous end joining (Honda and Selker, 2009). Transformed colonies were picked and grown on slants. To confirm the presence of the cassette, spores were genotyped using Terra PCR direct kit, and *gtr2* and *kog-1*-specific primers (Figure 22). Heterokaryon strains were crossed into our lab strain (*csp-1; chol-1 ras*^{bd}; Δ*vta)*. Around 800-1000 progenies were investigated from each cross. Slant cultures were genotyped for the presence and absence of *csp-1,his, chol-1, mus-51.* gDNA extraction was performed on candidates, and the presence of desired cassettes (Figure 23) and *vta* mutation (Figure 24) were investigated by PCR.

Homokaryons were obtained from GTR2-RFP, KOG1-GFP and KOG1-FLAG strains. KOG1-FLAG protein expression was investigated using anti-flag antibody (Figure 25). GTR2-GFP was not present in any of the progenies from different crosses. The GTR2 C-terminal GFP homokaryon might be lethal for an unknown reason such as the presence of a mutation during transformation or an interference with protein function that is unknown at this point.

4.3.1.2. Backcrosses

In all cases in the GTR2-RFP and KOG1-GFP knock-in cassette's presence, the *vta* mutation was also present, which might be caused by adding hygromycin into our selection plates. Both the knock-in cassette and the *vta* knockout allele carry the hygromycin resistance gene. To find a progeny without *vta* mutation in the background, I backcrossed GTR2-RFP (*csp-1, chol-1, ras*^{bd}*, vta*) and KOG1-GFP (*csp-1, chol-1, ras*^{bd}*, vta*) strains into a *ras*^{bd} strain. Ascospores were picked and analyzed for the presence and absence of *vta* and *csp-1* mutation using direct spore PCR. Genomic DNA was extracted from *vta* wild type strains and was used for knock-in cassette investigation. The KOG1 FLAG strain was initially crossed to a *csp-1, chol-1, ras*^{bd} as well as to *csp-1, chol-1, ras*^{bd}*, vta* strain. By conducting the process, I obtained KOG1-FLAG in the *vta* wild type and *vta* ^{ko} backgrounds without the need to make a backcross.

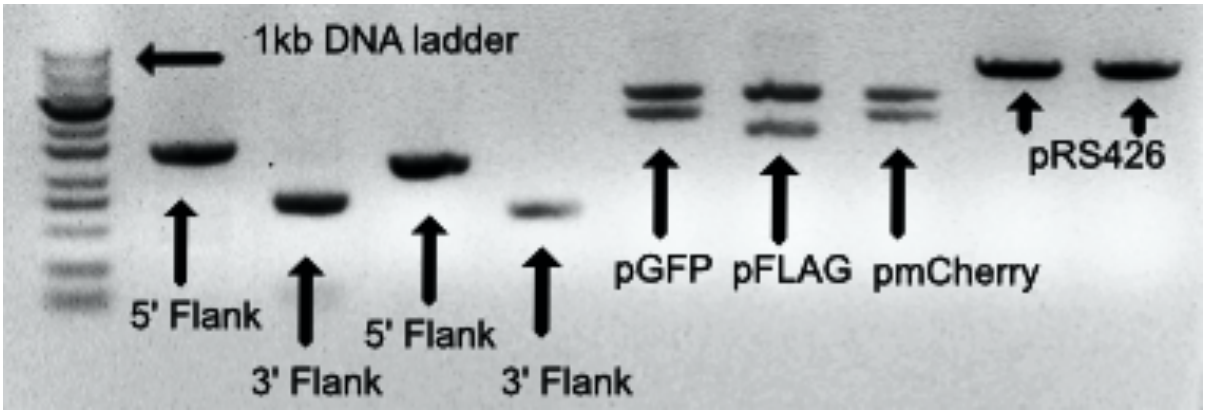

Figure 20: Restriction enzyme digestion before yeast transformation. Digestion results of pRS426 by XhoI and EcoRI and a knock-in module (GFP::loxP::hph::loxP), (3xFLAG::loxP::hph::loxP) or (mCherry::loxP::hph::loxP) isolated from plasmid tag ::hph::loxP by digesting with KpnI and XhoI are shown in the last 5 lanes. Confirmation of 5' and 3' flank of *gtr2* (2nd and 3rd lanes) and *kog1* (4th and 5th lanes) genes.

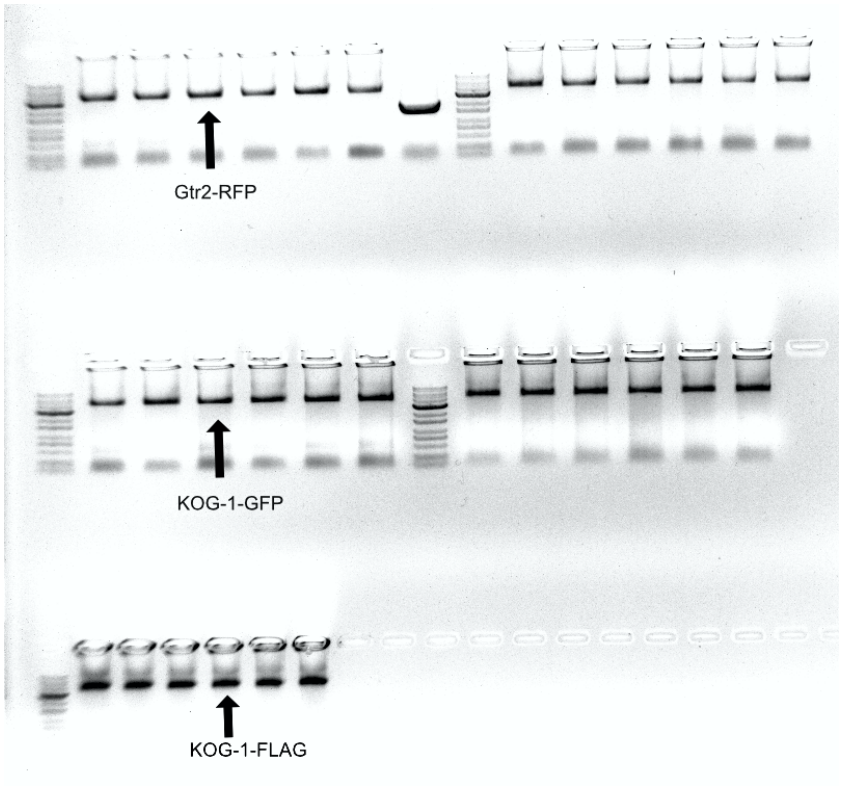

Figure 21: Genotyping of plasmid extraction from yeast colonies and before E-coli transformation on 1% agarose gel. In all cases transformants indicate expected sizes. 1 kb ladder was used as a reference.

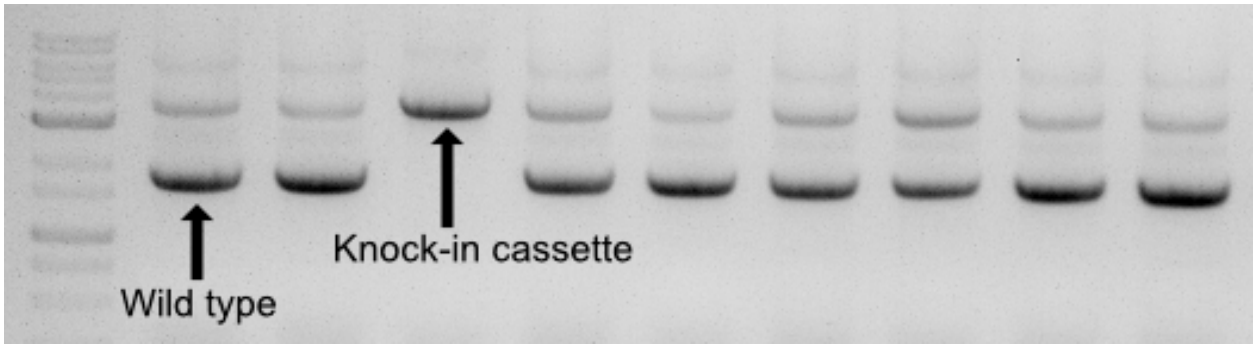

Figure 22: Gel electrophoresis of direct PCR on KOG1- FLAG transformants into a *mus-51* mutant strain. Heterokaryons are selected by presence of two bands, which shows two copies of the gene (with knock-in and without knock in cassette). Lane 4 indicates a positive control for the presence of a KOG1-FLAG homokaryon.

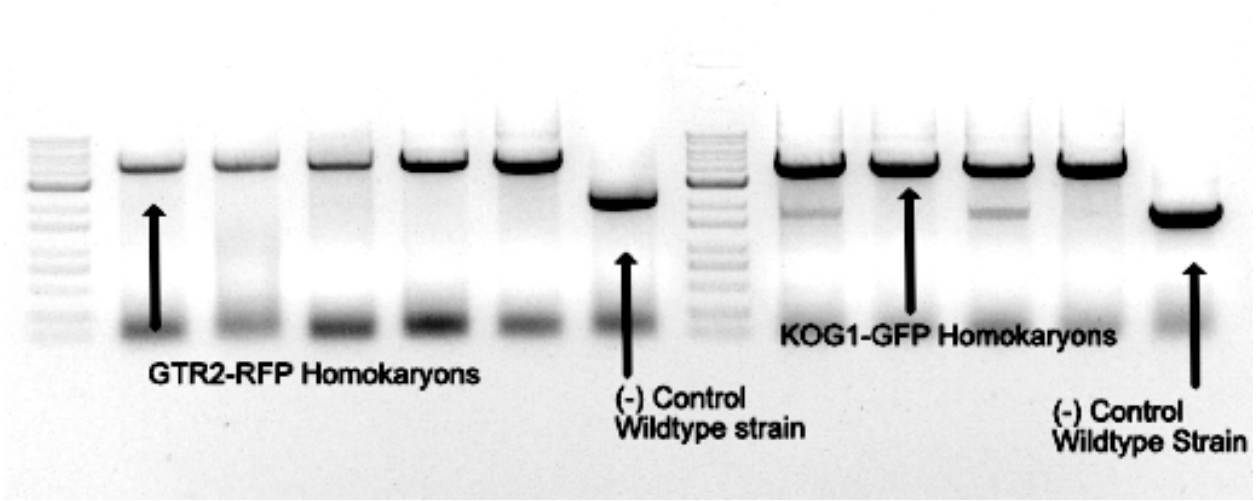

Figure 23: Agarose gel electrophoresis using GTR2-RFP and KOG1-GFP knock-in cassette specific primers. 1Kb DNA ladder was used to observe band size. In both cases, the knock-in cassette produces fragments above 3.5 Kb, and wild type strain is 2.5 kb.

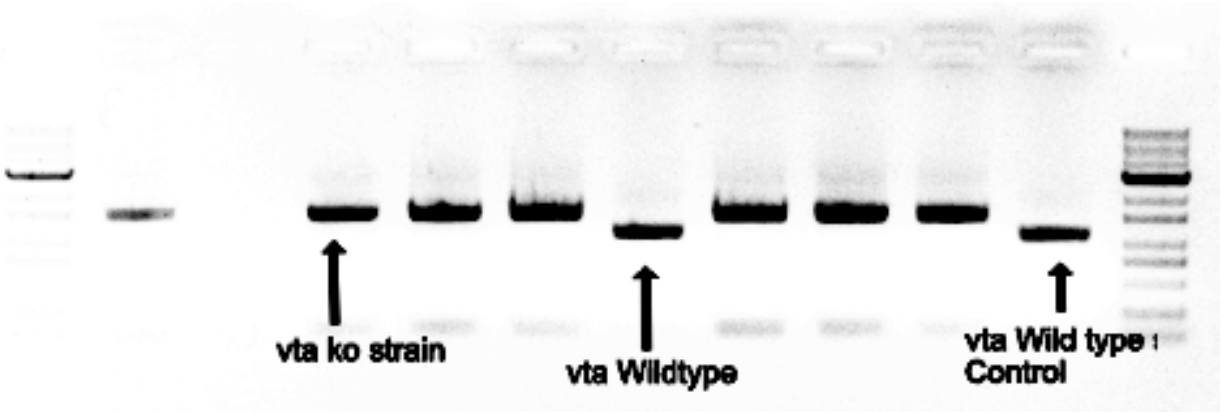

Figure 24: Agarose gel electrophoresis of GTR2-RFP and KOG1-GFP progeny using *vta*^{ko} specific primers. 1Kb DNA ladder was used to observe band size. Using these primers, *vta* wild type strain is 1096 bp and *vta* ^{ko} is 1500 bp.

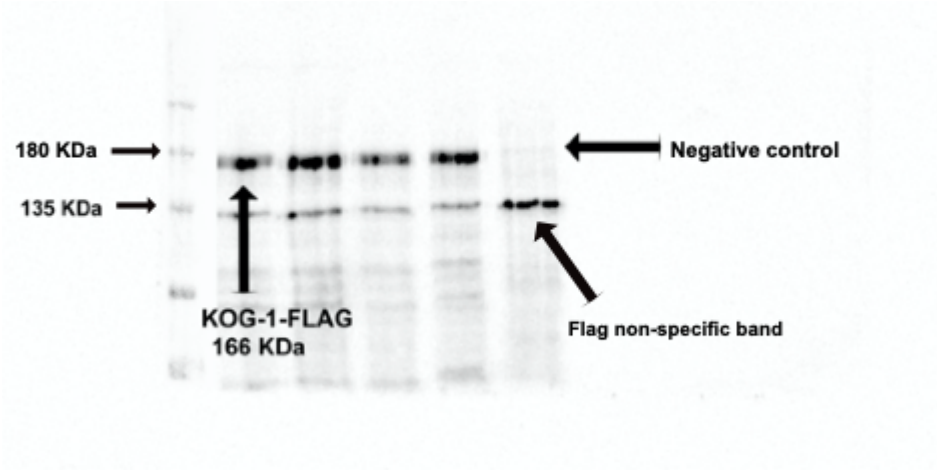

Figure 25: Western blotting results indicating the expression of KOG1-FLAG. KOG1-FLAG protein is 166 kDa. From left to right: protein ladder with the upper and lower band sizes indicated as 180 kDa and 135 kDa. Lanes 2, 3, 4, 5 are different strains of KOG1-FLAG with the same genetic background. Lane 6 is a negative control, which does not have the FLAG tag. The bottom band around 135 kDa is a non-specific band, which is always present in our flag immunodetection results.

4.3.1.3. Race tube analysis

Final candidates were inoculated on race tubes to check the *ras*^{bd} phenotype and to confirm the tagged protein's normal function in order to ensure that the tag's insertion did not disrupt the phenotype of the recipient strain (Figures 26 & 27).

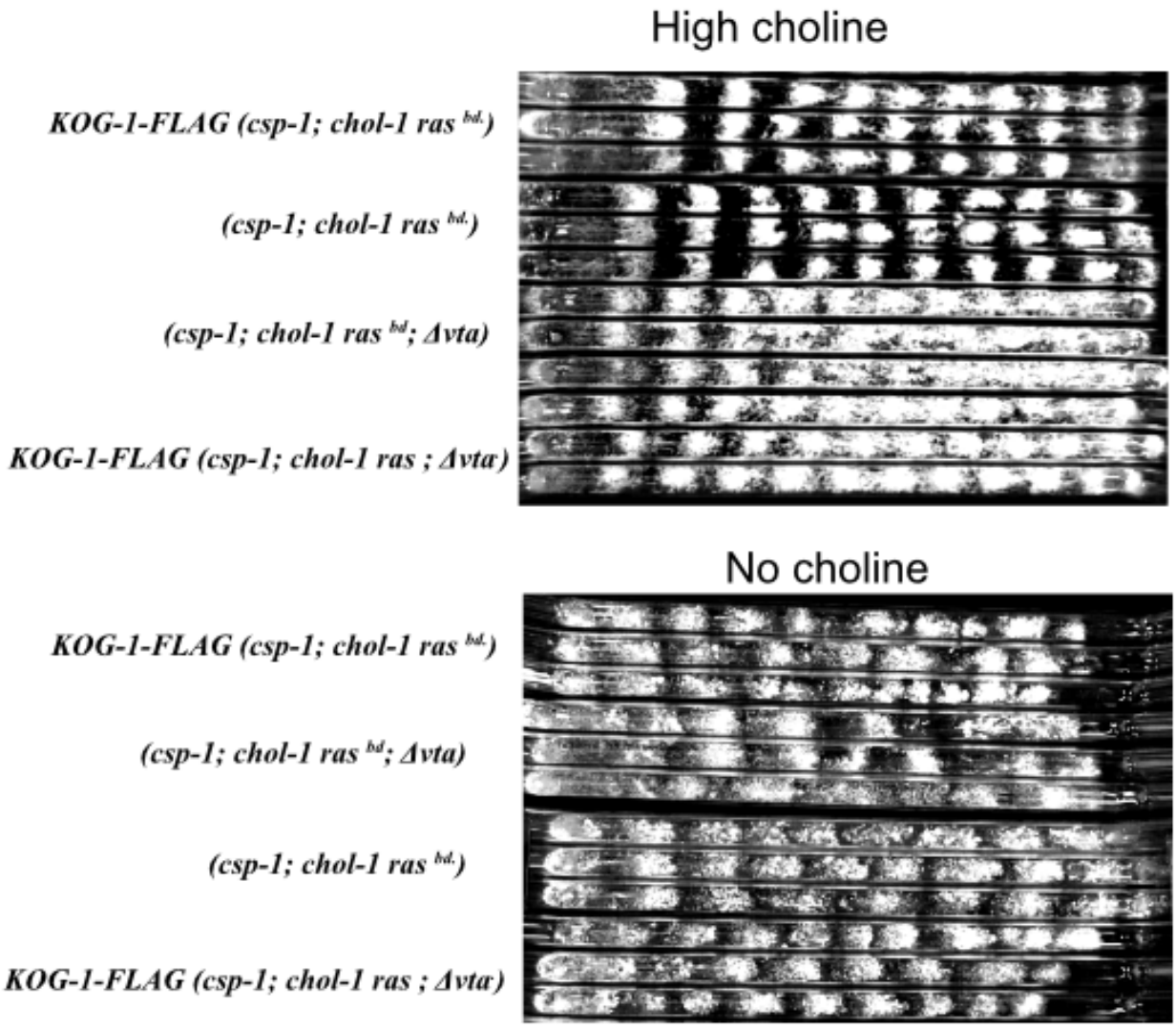

Figure 26: Race tubes indicating the growth phenotype of different KOG1-FLAG strains. Strains are carrying *csp-1; chol-1 ras*^{bd} genotype as well as deletions of *frq* or *vta.* Controls were (*csp-1; chol-1 ras*^{bd}), (*csp-1; chol-1 ras*^{bd} , *vta*^{ko}) and an Oak Ridge wild-type strain lacking any mutation. Choline-requiring (*chol-1*) strains were grown on solid agar with or without 100 μM choline in race tubes in constant temperature at 22°C and constant DD. Growth is from left to right. Three replicate tubes are shown for each strain.

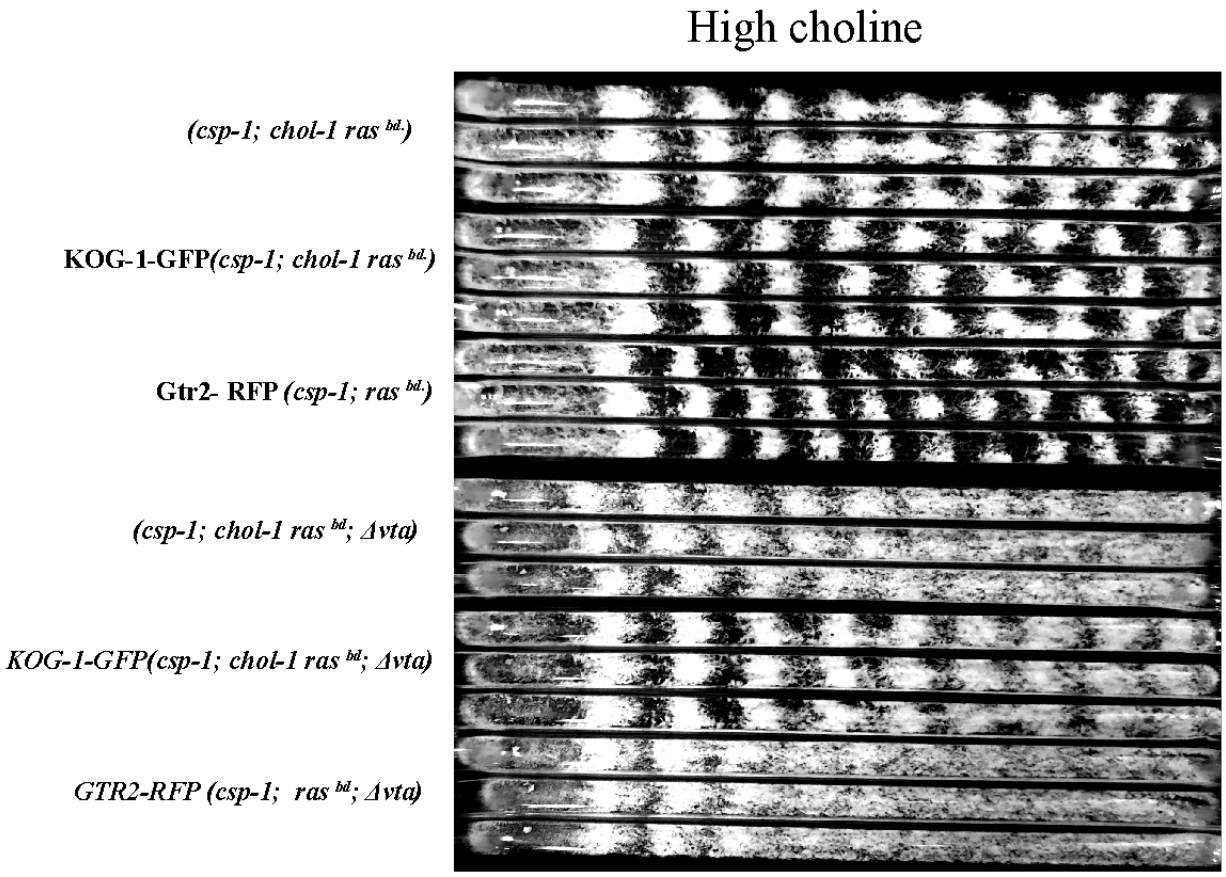

Figure 27: Race tubes indicating the growth phenotype of different KOG1-GFP and GTR2-RFP strains. Conditions as for the previous figure.

Race tube assays were performed to confirm the normal function of the KOG1-FLAG, KOG1-GFP, and GTR2-RFP proteins and to ensure that the insertion of the tag did not disrupt the phenotype of the recipient strain. All strains were compared to controls to ensure that the tag proteins do not produce a phenotype similar to mutants. Some of my strains, such as GTR2-RFP and KOG1-GFP, were only used for microscopy. The presence of the *chol-1* mutation was not essential for microscopy. Therefore, for some strains, only high choline media was used to observe the phenotype. Figure 26 and 27 and Table 5 show the banding phenotype, period, and growth rate of the strains used in this research.

Table 5: Race tube data indicating the period and growth rate of different strains and in the presence and absence of choline.

	HIGH CHOLINE		NO CHOLINE	
Genotype	**Growth rate by regression (mm/h)**	**Period by regression (hours)**	**Growth rate by Regression (mm/h)**	**Period by regression (hours)**
Bd; csp-1; chol-1; vta^{+}	1.18 ± 0.02 (3)	21.06 ± 0.38 (3)	0.42 ± 0.02 (3)	82.20 ± 2.85 (3)
Bd; csp-1; chol-1; vta^{KO}	1.10 ± 0.02 (3)	22.83 ± 0.08 (3)	0.44 ± 0.05 (3)	84.55 ± 30.53 (3)
Oak Ridge wild type	2.65 ± 0.08 (3)		2.59 ± 0.03 (3)	
Gtr2-RFP Bd; csp-1	1.03 ± 0.02 (3)	20.43 ± 0.60 (3)		
KOG-1-GFP ras^{bd}; csp-1	1.26 ± 0.02 (3)	21.11 ± 0.19 (3)		
Bd; csp-1; chol-1; vta^{ko}; Gtr2-RFP	1.06 ± 0.22 (5)	32.07 ± 3.66 (5)	0.48 ± 0.03 (5)	57.01 ± 7.02 (5)
KOG-1-FLAG ras^{bd}; csp-1 chol-1	1.33 ± 0.01 (3)	21.54 ± 0.48 (3)	0.48 ± 0.03 (3)	62.37 ± 10.38 (3)
KOG-1-GFP ras^{bd}; csp-1 chol-1	1.05 ± 0.02 (3)	21.59 ± 0.28 (3)	0.48 ± 0.03 (3)	56.74 ± 2.56 (3)
KOG-1-FLAG rasbd; csp-1; chol-1	1.29 ± 0.05 (3)	21.34 ± 0.35 (3)	0.44 ± 0.10 (3)	75.68 ± 28.87 (3)
KOG-1-FLAG ras^{bd}; csp-1; chol-1	1.37 ± 0.02 (3)	21.40 ± 0.24 (3)	0.46 ± 0.06 (3)	69.76 ± 8.44 (3)

4.3.2. Construction of ATG8-RFP strain

In order to make a strain carrying ATG8-RFP in the presence and absence of *vta*, plasmid vector pAtg8 (Figure 28) was used in this study and the vector carries the wild type *his-3* gene

sequence. *his-3* targeting *Neurospora crassa* transformation methods were used. Following the transformation, the wild type *his-3* sequence replaced the disrupted copy, and the defect of the *his-3* mutant was rescued. Gene targeting at *his-3* is selected by growing the transformants in histidine-free medium (Tsang, 2014).

I have transformed our lab *vta* knock out (*bd; csp-1 chol-1 his-3 vta* ^{ko}) and *vta* wild type (*bd ; csp-1 chol-1 his-3 vta* $^{+}$) strains with an atg8-mCherry plasmid digested with specific restriction enzymes (Figure 29). Transformation method was conducted as explained for *his-3* targeting *Neurospora crassa* transformation (Chapter II). Transformant colonies were picked from sorbose plates containing histidine and were inoculated in slants containing Vogel's minimal media with choline but no histidine. The presence of the ATG8 marker were confirmed by the ability of the transformant to grow on media without histidine. DNA was then extracted from successful candidates and genotyping by applying PCR using his-3 forward and reverse primers confirmed the presence of Atg8-RFP. Two bands indicated the successful transformants (Figure 30). Final strains were found to be heterokaryons.

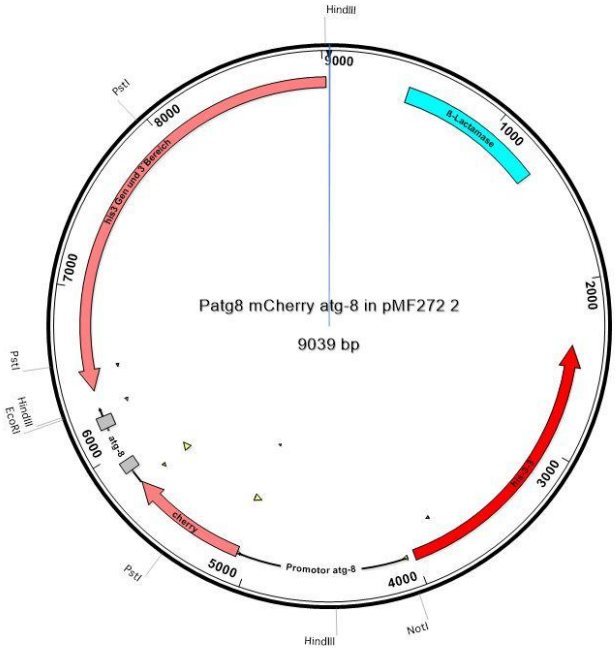

Figure 28: Map of the plasmid Atg8-mCherry, showing key genes and selected restriction endonuclease sites (Andre Fleisner, Personal communication)

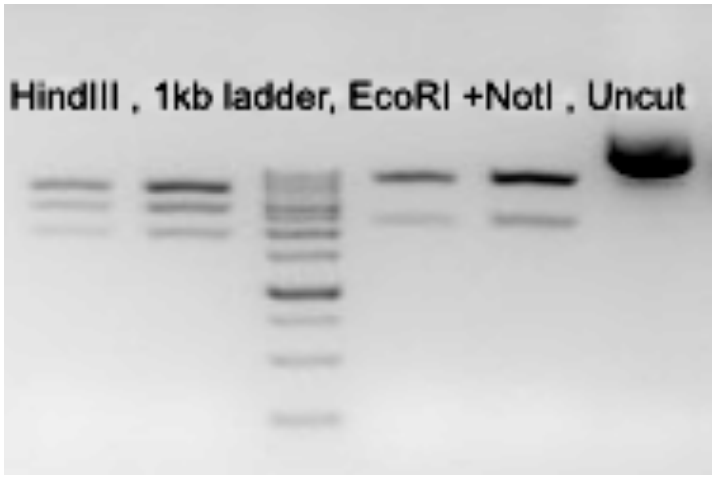

Figure 29: Gel electrophoresis results of restriction enzyme digestion of bacterial extracted Atg8–mCherry plasmid. Digestion with HindIII restriction enzyme (lanes 1 and 2) results in 3 DNA fragments (lengths: 1821 bp, 2714bp and 4504 bp). Double digestion of the plasmid with EcoRI and NotI restriction enzymes results in 2 DNA fragments (lengths: 2242bp and 6797 bp).

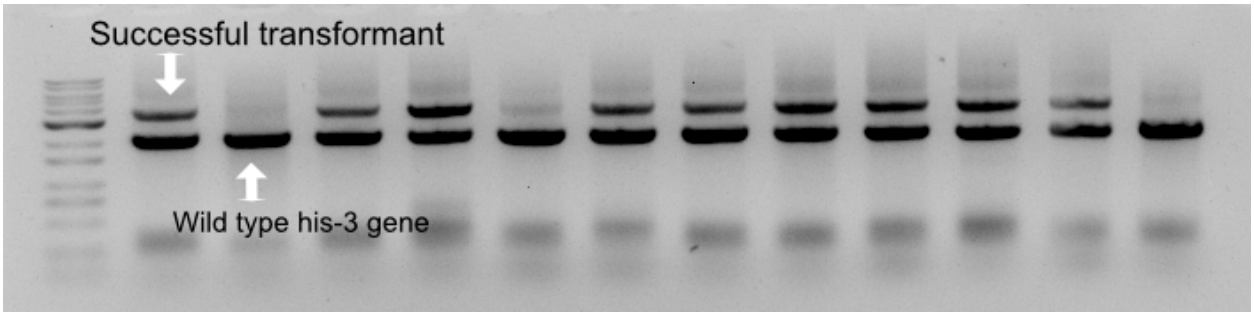

Figure 30: PCR results using his3 forward and reverse primers to confirm the presence of ATG8-RFP. Lane 1 is the 1kb DNA ladder, and lane 2 shows the positive control (Atg8-RFP) or the successful transformant, and lane 3 is the negative control (*Atg*8 gene).

4.3.3. Imaging

The first goal of this project was to optimize the best method of sample preparation for microscopy and find a suitable microscope compatible with our samples to obtain high-quality pictures. *Neurospora crassa* grows at a rapid rate and the cytoplasm flows towards the hyphal tip. Due to such growth pattern, long exposures under the microscope are difficult. I started by using fixed samples and observed them using LSM 700 at York University's microscopy facility. Unfortunately, after many attempts to obtain the best fixation method, including using different concentrations of PFA and washing steps and sample preparations, I was not able to get excellent

images. Due to the artifacts that came from the fixation method and the high quench in the fluorescence signal, I gave up on using fixed samples.

I started using live samples using the same LSM 700 Microscope. After optimizing the method and using different sample preparation, the results were still not optimal. The internal cellular network in the hyphae such as vacuoles and the exact expression location were not observable. I then began using the Leica SP8 microscope at the Advanced Optical Microscopy Facility in MaRS building to take high-quality images.

4.3.4. Fixed samples

In order to observe the localization of GTR2-RFP and KOG1-GFP, fixed samples were prepared as described in the general methods (Chapter II). Their localization was observed in different conditions such as: in the presence and absence of *vta*, after incubation with Torin II (5 µM) for 4 hours, after incubation in arginine for 4 hours (5 mM), after incubation in Rapamycin for 4 hours (500 nM), and after 4 hours incubation in liquid minimal media without glucose.

4.3.4.1. Observation of KOG-GFP using LSM 700

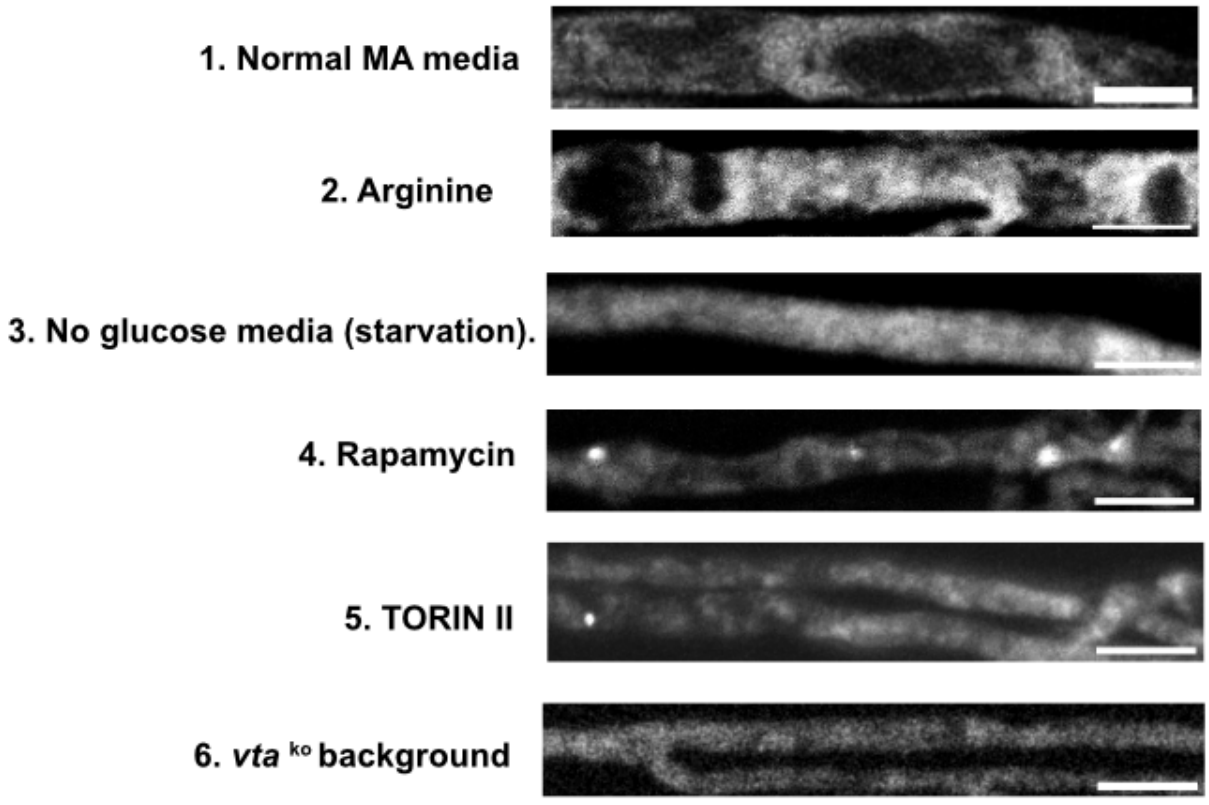

Figure 31: Subcellular localization of KOG1 protein in different conditions using the fixative method and LSM 700 microscope. KOG1:: GFP tagged and expressed from the native chromosomal location was observed in different conditions and in the presence and absence of VTA. In all cases, 63 X objective lenses were used. 1- in normal MA media 2- In the presence of 5mM arginine 3- In no glucose media (starvation), 4- in the presence of 500nM Rapamycin 5- In the presence of 5 Micromolar Torin II and 6- In the *vta* ^{ko} background. The scale bars are 10 µm.

As shown in Figure 31, the fixative method did not provide high-quality images and made the identification of localization difficult. In general, the expression is accumulated more around the vacuole, and the vacuolar structures are more visible in the presence of arginine compared to normal media. Cytoplasmic localization is seen in the absence of glucose. Inconsistent results were obtained using Rapamycin. In the presence of either inhibitor (Rapamycin and Torin II), there was an abnormal and damaged structure, and an uneven expression along the hyphae was observed. In the presence of Torin II, there was an indication of the presence of body formation at the edge of the vacuole. There was an even expression of protein all over the cytoplasm in the *vta* ^{ko} background, which indicates it to be cytoplasmic.

4.3.4.2. Observation of GTR2-RFP using LSM 700

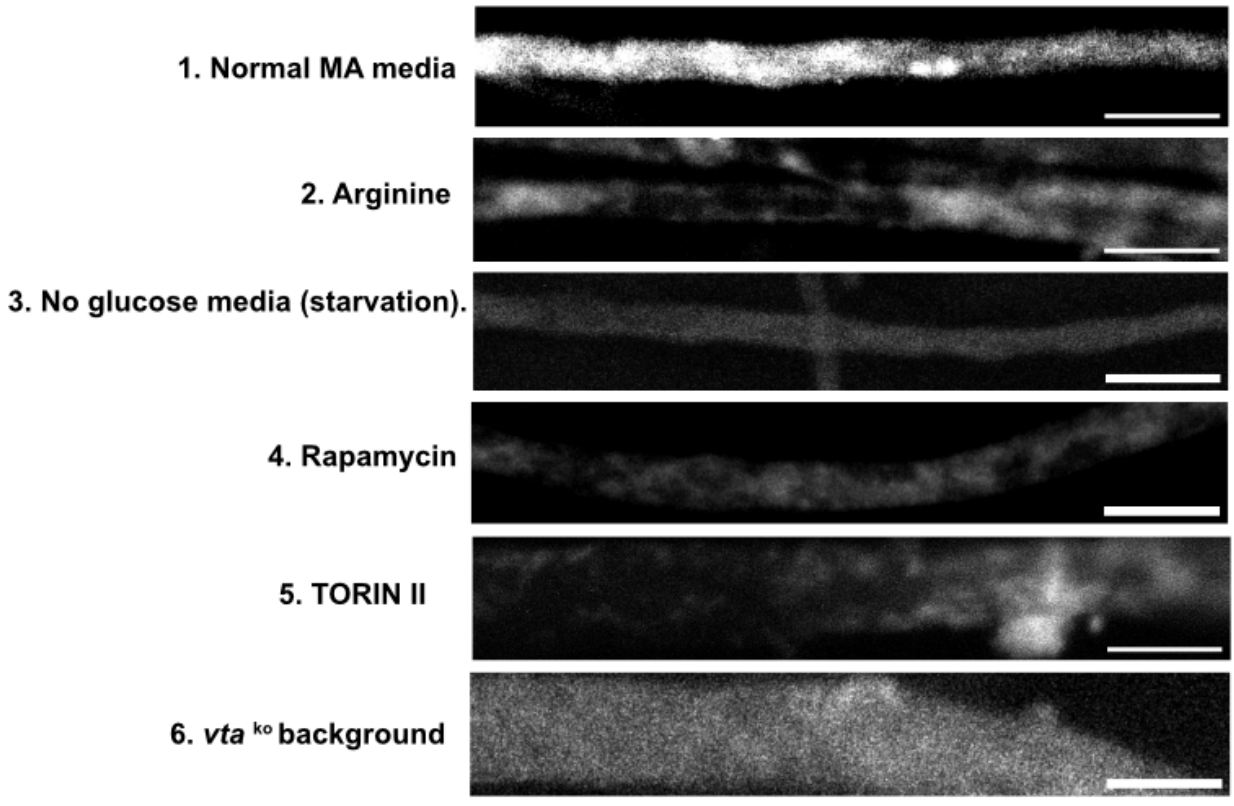

Figure 32: Subcellular localization of GTR2 protein in different conditions using the

fixative method and LSM 700 microscope. GTR2:: RFP tagged and expressed from the native chromosomal location was observed in different conditions, and in the presence and absence of *vta*. In all cases, 63 X objective lenses were used. 1- in Normal MA media, 2- In the presence of 5mM arginine, 3- In no glucose media (starvation), 4- in the presence of 500nM Rapamycin, 5- in the presence of 5 μM Torin II, 6-in the *vta* ^{ko} background. The scale bars are 10 μm.

The fixative method did not provide high-quality images and made the identification of localization difficult (Figure 32). Cytoplasmic localization is observed in the absence of glucose. Inconsistent results were obtained using Rapamycin. In the presence of either inhibitor (Rapamycin and Torin II), there was an abnormal and damaged structure. There was an even expression of protein all over the cytoplasm in the *vta* ^{ko} background, which indicates it to be cytoplasmic.

4.3.5. Live sample Observation using Confocal LSM 700

To observe the localization of GTR2-RFP, KOG1-GFP, and ATG8-RFP, live samples were prepared on the surface of Phytagel (Appendix I) with required supplements as described in the general methods. Their localization was observed in different conditions as follows: in the presence and absence of *vta*, after incubation of Torin II (0.5 μM), after incubation of Torin 1 (1μM), after incubation in arginine (5 mM). 20 minutes incubation time was chosen for the observations.

4.3.5.1. KOG1-GFP localization under different conditions using LSM 700

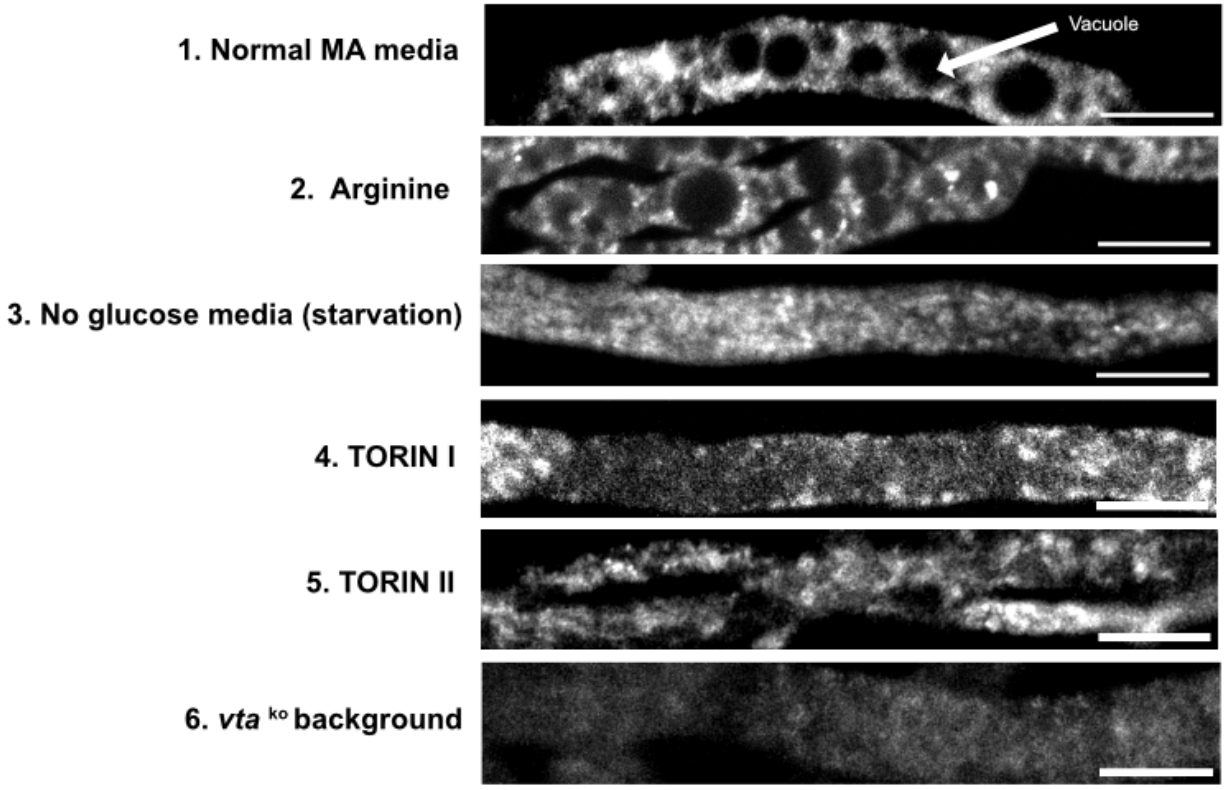

Figure 33: Subcellular localization of KOG1 expressed from the native chromosomal location. 1- KOG1-GFP localization in 1.5% Phytagel (Appendix I) and treated with minimal liquid media, including 2% glucose and choline as supplements for growth. 2- KOG1-GFP localization after 20 minutes arginine (5mM) treatment. 3- KOG1-GFP localization after 20 minutes incubation with no glucose media (starvation). 4- KOG1-GFP localization after 20 minutes Torin I (1 μM) incubation. 5- KOG1-GFP localization after 20 minutes of Torin II (0.5 μM) incubation. 6- KOG1-GFP localization in the *vta* ^{ko} background. The scale bars are 10 μm.

As shown in Figure 33, in glucose medium and with arginine, KOG1 is localized around the vacuole and on the vacuolar membrane. Torin I disrupted the vacuolar localization, and the hyphae was not found to have a normal phenotype. Torin II also disrupted the vacuolar localization of KOG1, damaged the normal hyphae structure of *Neurospora crassa*, and KOG1 showed an uneven expression along the hyphae. In the *vta* ^{ko} background, no detailed structure was obvious. In both cases, young hyphae and old hyphae, the protein seemed cytoplasmic, and the expression was found to be even across the hyphae.

4.3.5.2. GTR2-RFP localization under different conditions using LSM 700

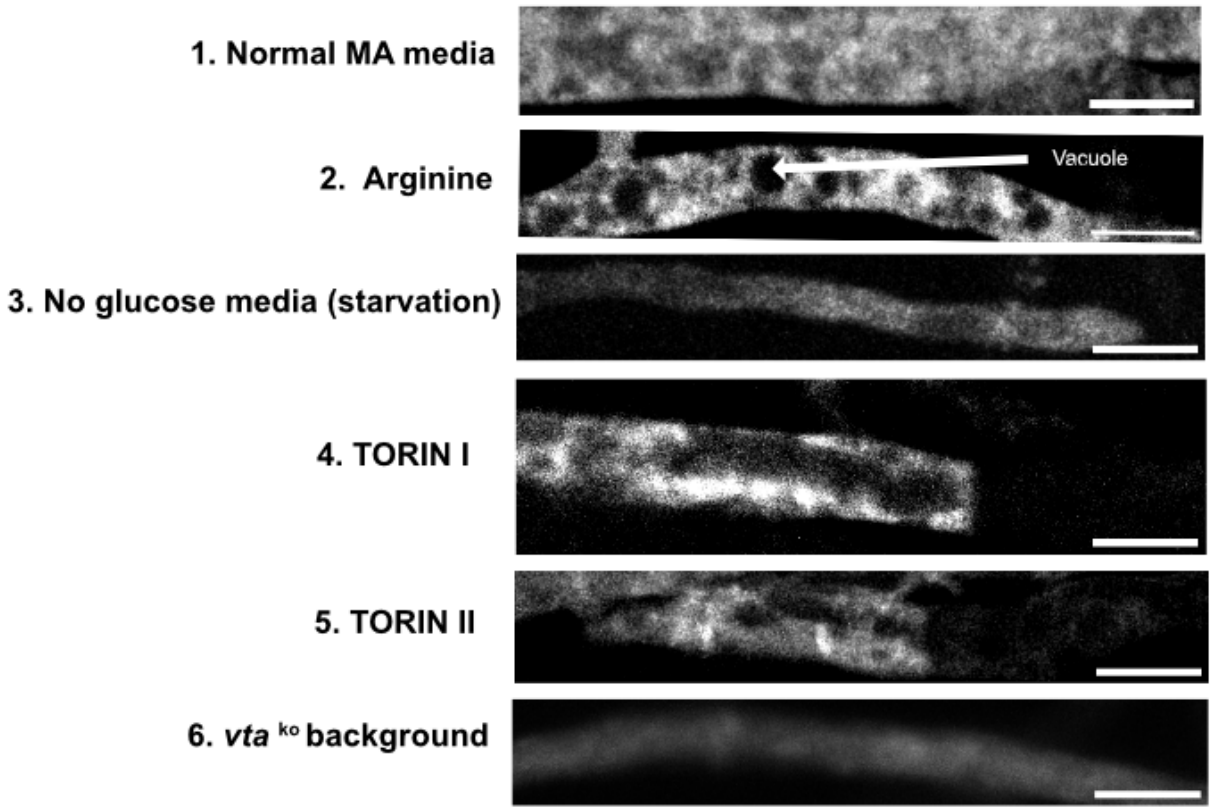

Figure 34: Subcellular localization of GTR2-RFP protein expressed from the native chromosomal location. 1-normal MA media, 2- in the presence of 5mM arginine, 3- in the absence of Glucose (starvation), 4- in the presence of 1 µM Torin I, 5- after 20 minutes incubation in 0.5 µM Torin II, 6- in a *vta* ^{ko} background. The scale bars are 10 µm.

As shown in Figure 34, in normal media, GTR2 was found around the vacuolar membrane and filamentous structures. In the presence of arginine, it was found to be brighter around the vacuole. In the absence of glucose (starvation), there were no significant structures visible, and protein was found to be cytoplasmic. With Torin I and Torin II, the structure of the normal hyphae was found to be disrupted and there was uneven expression along with brighter expression around the outer membrane. In a *vta* ^{ko} background, similar to the starvation condition, there were no significant structures visible, and protein was found to be cytoplasmic.

4.3.5.3. ATG8-RFP localization under different conditions using LSM 700

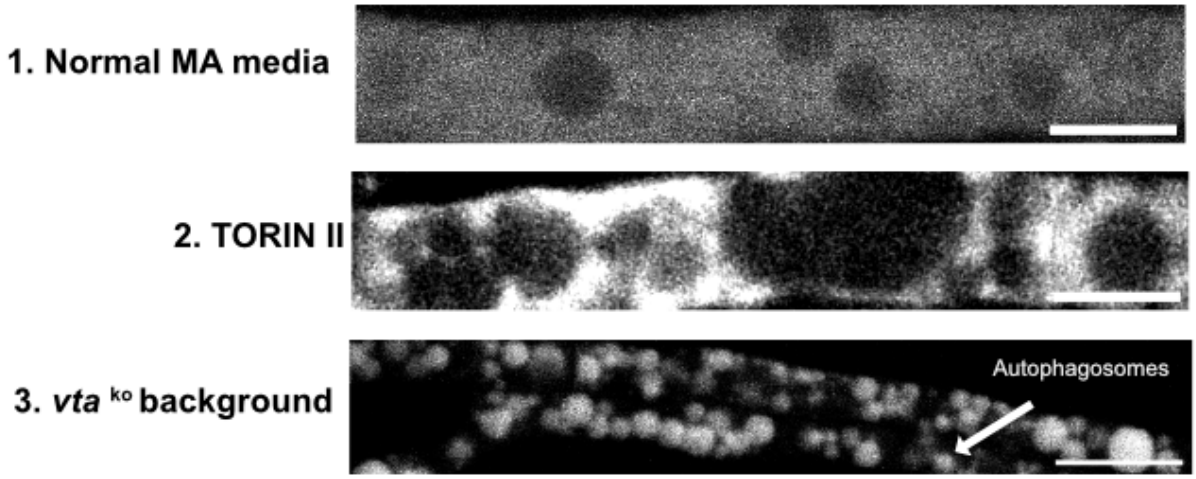

Figure 35: Subcellular localization of ATG8 protein in different conditions. 1- normal MA media, 2- in a *vta* ^{ko} background and 3- after 20 minutes incubation in 0.5 µM Torin II. The scale bars are 10 µm.

A strain with the genotype *csp-1 his-3*+::pccg-1::NCU01545+::mCherry; *chol-1 rasbd*; that expresses ATG8-RFP from the *ccg-1* promoter at the *his-3* locus was constructed in the *vta*$^{+}$ as well as *vta* ^{ko} background. As shown in Figure 35, ATG8-RFP, which is an indicator of the presence of autophagosomes, is evenly distributed in the cytoplasm in the *vta* wild-type strain. In the middle picture, there are bright dots, or autophagosomes, in the *vta* ^{ko} background. In the presence of 0.5 micromolar Torin II, there are signs of accumulation of autophagosomes in the hyphae in the picture.

4.3.5.4. VTA-GFP imaging using Leica SP8

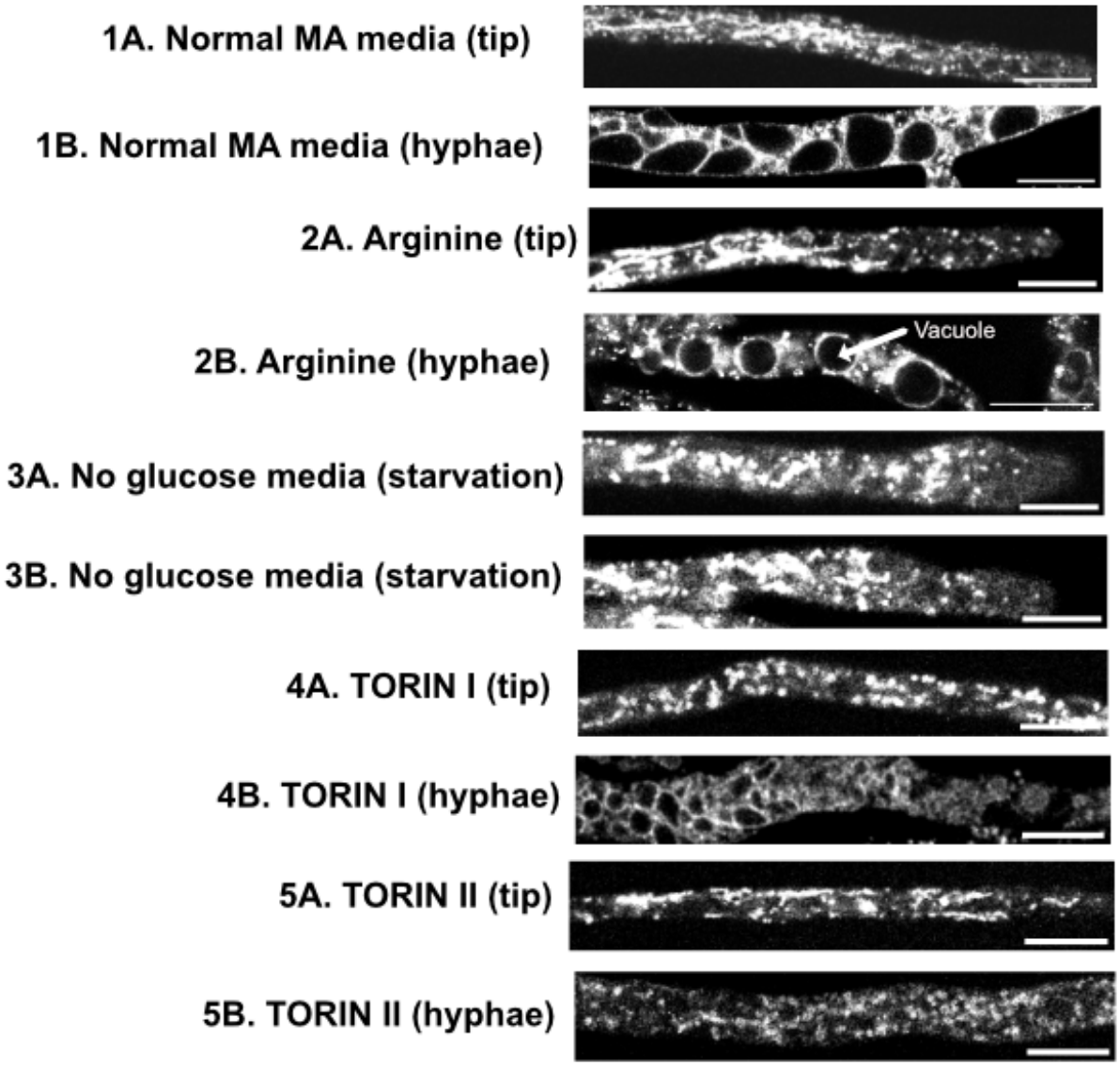

Figure 36: Subcellular localization of VTA protein in different conditions. 1- in Normal MA media, 2- in the presence of 5mM arginine 3- in the absence of glucose (starvation), 4- 2500 nM Torin I, 5- 500 nM Torin II. A represents the tip of growing hyphae, while B indicates older hyphae structures. The scale bars are 10 μm.

The VTA::GFP strain with the genotype *csp-1 his-3+::pccg-1::NCU05950+::GFP; chol-1 ras^{bd}; NCU05950^{ko}* a that expresses the wildtype NCU05950::GFP fusion protein from the *ccg-1* promoter was made by former Ph.D. student Lalanthi Ratnayake (Ratnayake et al., 2018). As shown in Figure 36, in all conditions, there was very little effect on the localization of VTA. It is

consistent with the previous finding that VTA is a membrane protein, and it is expected to stay attached to the membranes even in the presence of TOR pathway inhibitors or starvation. The normal localization of VTA was previously reported (Ratnayake et al., 2018).

4.3.5.5. KOG-1-GFP imaging using Leica SP8

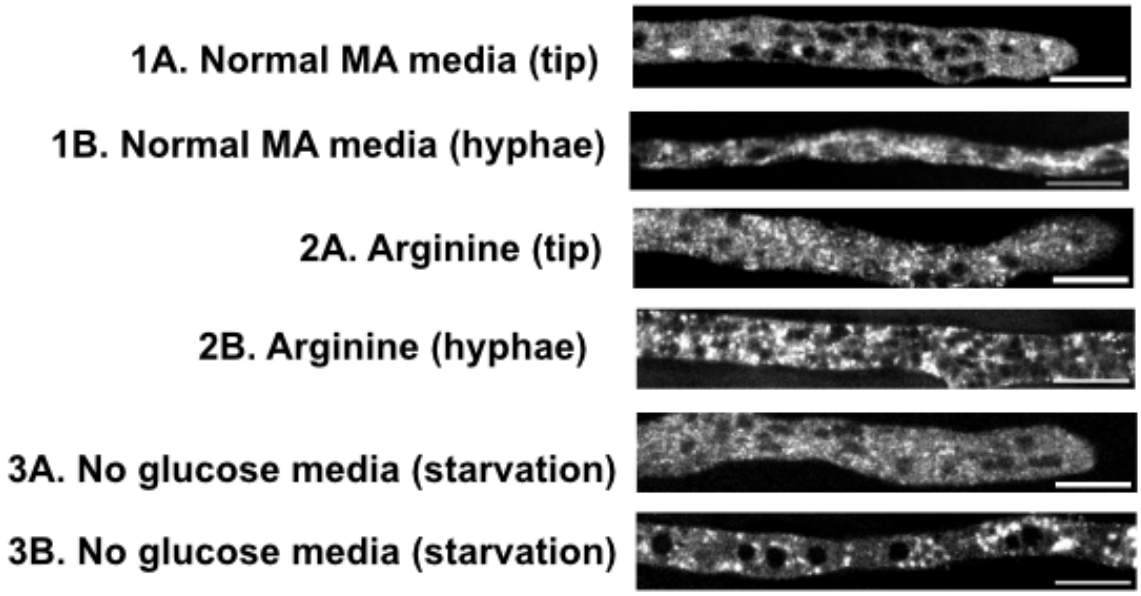

Figure 37: Subcellular localization of KOG1 protein in different conditions. 1- in Normal MA media, 2- in the presence of 5mM arginine, 3- in no glucose media (starvation). A represents the tip of growing hyphae while B indicates older hyphae structures. The scale bars are 10 μm.

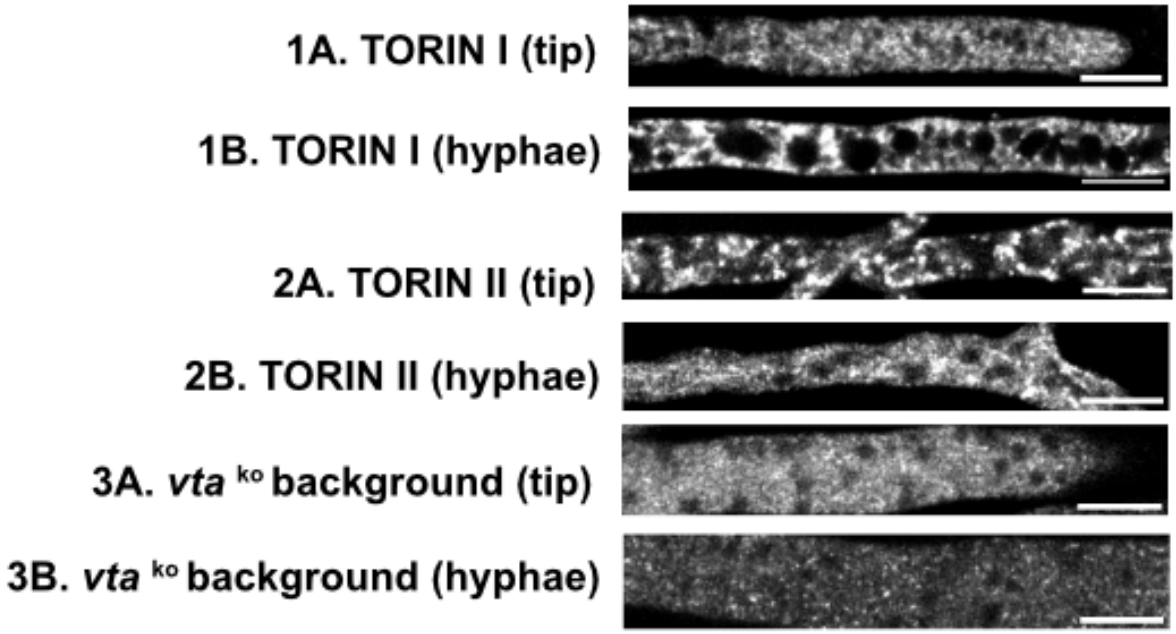

Figure 38: Subcellular localization of KOG1 protein in different conditions. 1- in the presence of 2500 nM Torin I, 2 - 500 nM Torin II, 3 – in the *vta* ^{ko} background. A represents the tip of growing hyphae, while B indicates older hyphae structures. The scale bars are 10 μm.

KOG1::GFP tagged and expressed from the native chromosomal location was observed in different conditions and in the presence and absence of *vta*. As shown in the standard media (Figure 37), there was an expression and localization of KOG1 protein around the vacuolar structures, while in the presence of 5mM arginine, the KOG1-GFP was also observed to be located on the vacuolar membrane. In the absence of glucose, there was less expression of the protein, and there was a KOG1 body formation looking like a bright dot at the edge of the vacuole. In the presence of 2500 nM Torin I and 500 nM Torin II, KOG1 protein did not look significantly different from standard condition, which suggests that Torin does not change its localization. In the *vta* ^{ko} background, KOG1 protein does not localize on the vacuole anymore and it was spread out in the cytoplasm, which suggests that the vacuolar localization of KOG1 depends on the presence of *vta* (Figure 38).

4.3.5.6. Gtr2-RFP imaging using Leica SP8

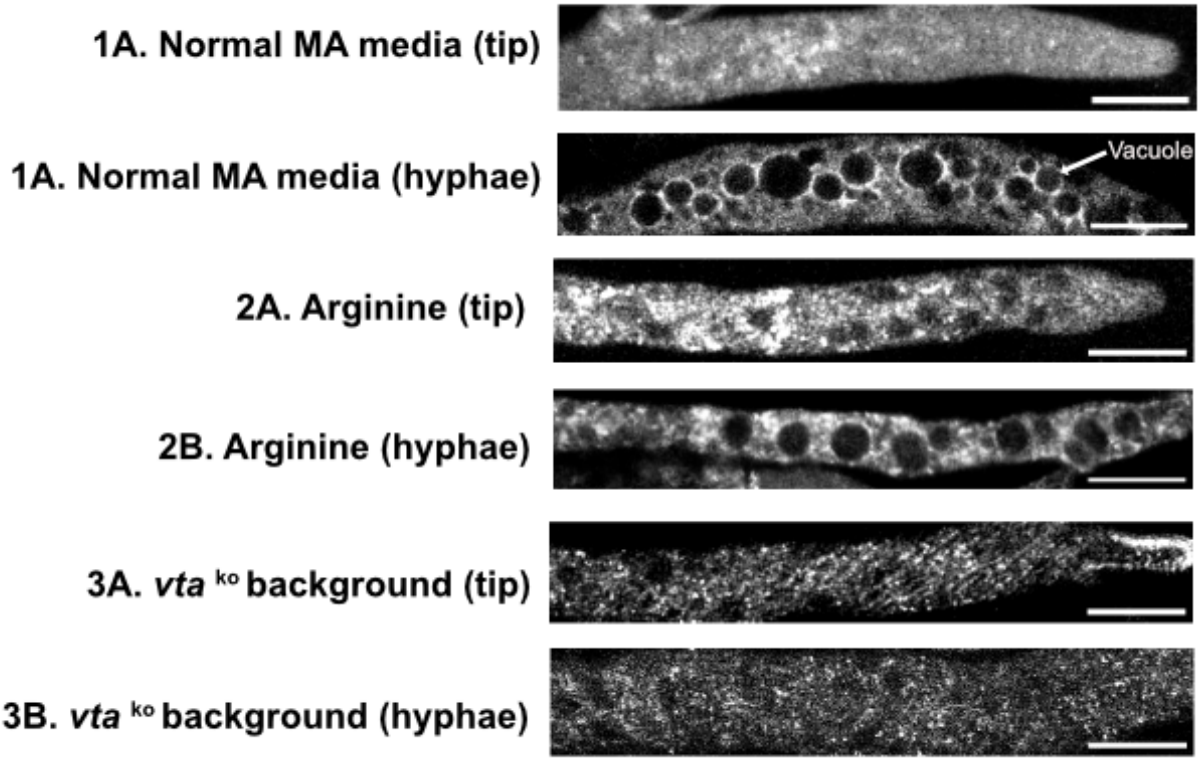

Figure 39: **Subcellular localization of GTR2 protein in different conditions.** 1- in Normal MA media, 2- In the presence of 5mM arginine, 3 – in the *vta* ^{ko} background. A represents the tip of growing hyphae, while B indicates older hyphae structures. The scale bars are 10 μm.

GTR2:RFP tagged and expressed from the native chromosomal location was observed in different conditions, and in the presence and absence of *vta*. My data indicates that GTR2 accumulates around the vacuoles normally and in arginine, and it is cytoplasmic in the absence of *vta* (Figure 39).

4.3.6. KOG1-FLAG protein expression

To observe protein expression rhythm across two circadian cycles (from 24-72 hours in DD), three independent time-course experiments were conducted using a KOG1-FLAG strain in the presence and absence of VTA (Figure 40 & 41). The results demonstrate that although the expression of KOG1-FLAG protein does not seem to be equal across different times of the day, it does not exhibit the characteristics of rhythmic expression among three independent trials in the presence or absence of VTA.

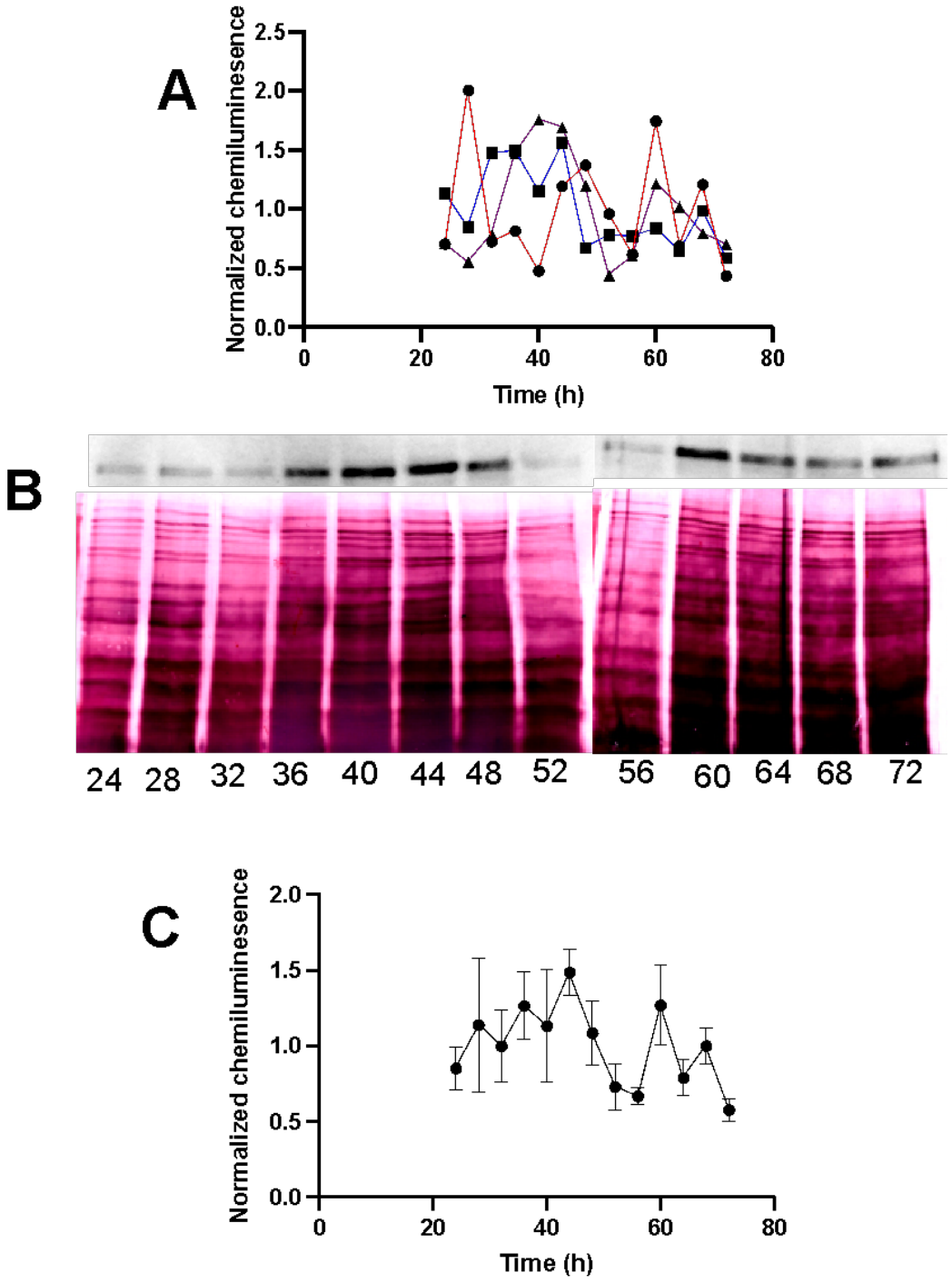

Figure 40: Expression of KOG1 protein in the *vta* wild type background. (a) KOG1-FLAG (*csp-1; chol-1 ras*^{bd}) protein expression from three independent experiments across 24-72 hours in constant conditions. (b) Immunoblot of one experiment showing KOG1-FLAG levels (above) and Colloidal Gold Total Protein Stain (below). (c) Mean +_SEM from three independent experiments.

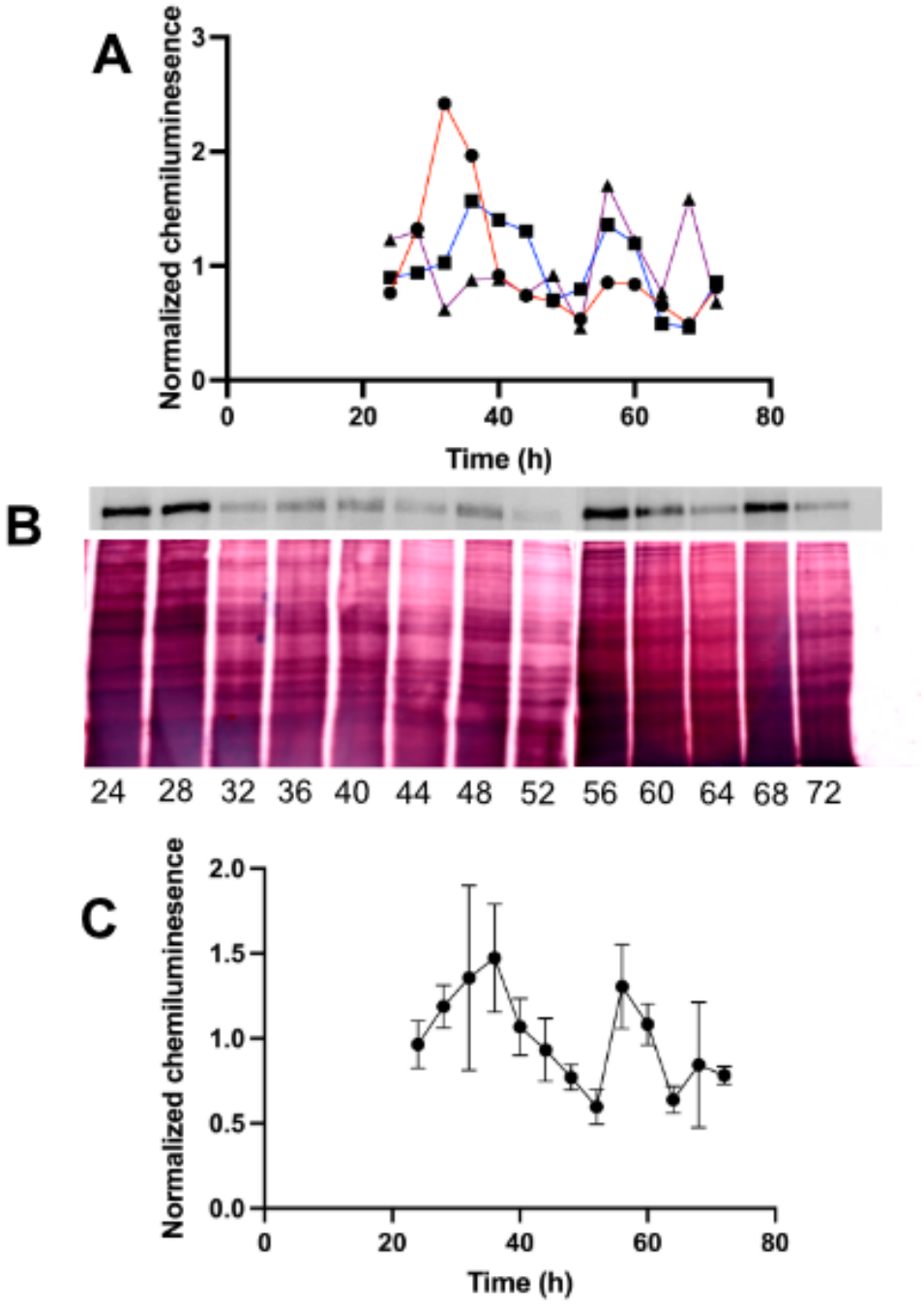

Figure 41: Expression of KOG1 protein in *Δvta* background. (a) KOG1-FLAG (*csp-1; chol-1 rasbd; Δvta*) protein expression from three independent experiments across 24-72 hours in constant conditions. (b) Immunoblot of one experiment showing KOG1-FLAG levels (above) Colloidal Gold Total Protein Stain (below). (c) Mean+- SEM from three independent experiments.

4.3.7. Coimmunoprecipitation and mass spectrometry of KOG1-FLAG and GTR2-FLAG

Coimmunoprecipitation and mass spectrometry were conducted to determine the mutual binding partners among KOG1-FLAG, GTR2-FLAG, and VTA–FLAG. This revealed the association of the EGO complex and TORC1 in *Neurospora crassa* and allowed us to investigate the possibility of the presence of a mutual component, which might be important for the normal functioning of the clock. Additionally, coimmunoprecipitation on the same proteins without VTA helps us to understand whether the binding partners would change in the absence of VTA. This experiment provides insights on the importance of the VTA, and how it affects the binding partners and the association of TOR pathway components.

Binding partners of each FLAG-tagged bait protein are listed in descending order of total spectrum counts (Table 6). An unrelated FLAG-tagged strain and a strain without any FLAG tag were used as controls in each experiment. NCU number represents the ID of the gene in the *Neurospora crassa* genome database (FungiDB). The following table exhibits the results of two independent experiments.

Table 6: Coimmunoprecipitation and mass spectrometry results

Binding Partners of KOG1							
Locus ID	Gene product	MW (kDa)	EXP.1		Exp.2		Total counts
			Peptides	Counts	peptides	Counts	
NCU05608	Serine/threonine -protein kinase TOR	278 kDa	2	187	2	11	198
NCU04795	TCO89	76 kDa	2	91	2	12	103
NCU00915	asparstyl-trna SYNTHETASE	65 kDa	2	4	2	29	33
NCU04281	MLST8	36 kDa	2	17	2	3	20
NCU00018	CDC48		2	7	2	11	18
NCU03387	SEC18	91 kDa	2	4	2	5	9
NCU09700	T-complex protein 1	60 kDa	2	4	2	4	8

	subunit beta						
NCU07580	Cyclin-dependent protein kinase	38 kDa	2	4	2	4	8
NCU08336	Succinate dehydrogenase	71 kDa	2	4	2	3	7
Binding Partners of KOG1 *vta* ^{ko}							
Locus ID	Gene product	MW (kDa)	EXP.1		Exp.2		Total counts
			peptides	Counts	peptides	Counts	
NCU05608	Serine/threonine-protein kinase TOR	278 kDa	2	143	2	7	150
NCU04795	TCO89	76 kDa	2	82	2	12	94
NCU04640	eIF2B	32 kDa	2	5	2	17	22
NCU08336	Succinate dehydrogenase	71 kDa	2	5	2	8	13
NCU02639	Argininosuccinste synthase	46 kDa	2	7	2	2	9
NCU08390	Acetyltransferase	27 kDa	2	3	2	6	9
NCU09116	Aromatic amino transferase	62 kDa	2	3	2	6	9
NCU04790	ERF-3	79 kDa	2	3	2	6	9
NCU00483	HYPOTHETICAL protein	33	2	3	2	6	9
NCU03561	Mitochondrial carrier protein	33 kDa	2	5	2	3	8
NCU05235	RLP24	26 kDa	2	3	2	5	8
NCU09111	G6PD	58 kDa	2	3	2	5	8
NCU04799	PABP	82 kDa	2	5	2	2	7

NCU03690	Nucleoporin-37	104 kDa	2	3	2	3	6
NCU09700	T-complex protein 1 subunit beta	60 kDa	2	3	2	2	5
NCU08550	HYPOTHETICAL protein	32 kDa	2	3	2	2	5
Binding Partners of GTR2 *vta* ^{ko}							
Locus ID	Gene product	MW (kDa)	Exp.1		Exp.2		Total counts
			peptides	Counts	peptides	counts	
NCU09116	Aromatic aminotransferase Aro8	62 kDa	2	26	2	36	62
NCU05410	Acetylornithine transaminase	33 kDa	2	14	2	24	38
NCU01632	Pentafunctional arom polypeptide	170 kDa	2	4	2	30	34
NCU04640	Probable translation initiation factor eIF-2 beta chain	32 kDa	2	11	2	20	31
NCU01099	Gtr1_RagA	45 kDa	2	21	2	5	26
NCU08390	N-acetyltransferase domain-containing protein	27 kDa	2	6	2	11	17
NCU03561	Mitochondrial carrier	33 kDa	2	10	2	5	15
NCU04811	Uncharacterized protein	32 kDa	2	11	2	3	14
NCU02284	nucleolar ATPase	118 kDa	2	3	2	11	14

	Kre33						
NCU00915	Aspartyl-tRNA synthetase	65 kDa	2	6	2	7	13
NCU08663	nonsense-mediated mRNA decay protein 3	58 kDa	2	4	2	8	12
NCU08336	Succinate dehydrogenase flavoprotein subunit	71 kDa	2	6	2	6	12
NCU06301	CENP-V/GFA domain-containing protein	18 kDa	2	6	2	5	11
NCU00021	Clustered mitochondria protein homolog	142 kDa	2	3	2	8	11
NCU01454	mitochondrial hydrolase	37 kDa	2	7	2	3	10
NCU04277	Homoserine kinase	38 kDa	2	7	2	3	10
NCU00043	serine/threonine-protein phosphatase PP1	35 kDa	2	6	2	4	10
NCU01485	KOW domain-containing protein	45 kDa	2	4	2	6	10
NCU03548	Mannose-1-phosphate guanylyltransferase	64 kDa	2	3	2	7	10

NCU03112	NADH-cytochrome b5 reductase-2	37 kDa	2	3	2	6	9
NCU03979	biotin synthase	48 kDa	2	3	2	6	9
NCU05390	Mitochondrial phosphate carrier protein	33 kDa	2	4	2	4	8
NCU00018	cell division control protein Cdc48	90 kDa	2	3	2	5	8
NCU08952	translation 6	44 kDa	2	3	2	5	8
NCU02438	tricarboxylic acid-19	46 kDa	2	3	2	4	7
NCU01894	hypothetical protein	39 kDa	2	3	2	4	7
NCU04924	HAD-superfamily hydrolase	55 kDa	2	4	2	3	7
NCU08299	60S ribosomal protein L3	48 kDa	2	4	2	3	7
NCU03117	inosine-5'-monophosphate dehydrogenase IMD2	57 kDa	2	3	2	3	6
NCU02634	Pru domain-containing protein	41 kDa	2	3	2	3	6
NCU07549	Mitochondrial ribosomal protein L43	15 kDa	2	3	2	2	5
NCU02804	mitochondrial 60S ribosomal protein L25	18 kDa	2	3	2	2	5

NCU05813	mitochondrial large ribosomal subunit	41 kDa	2	3	2	2	5
NCU07953	alternative oxidase	41 kDa	2	3	2	2	5

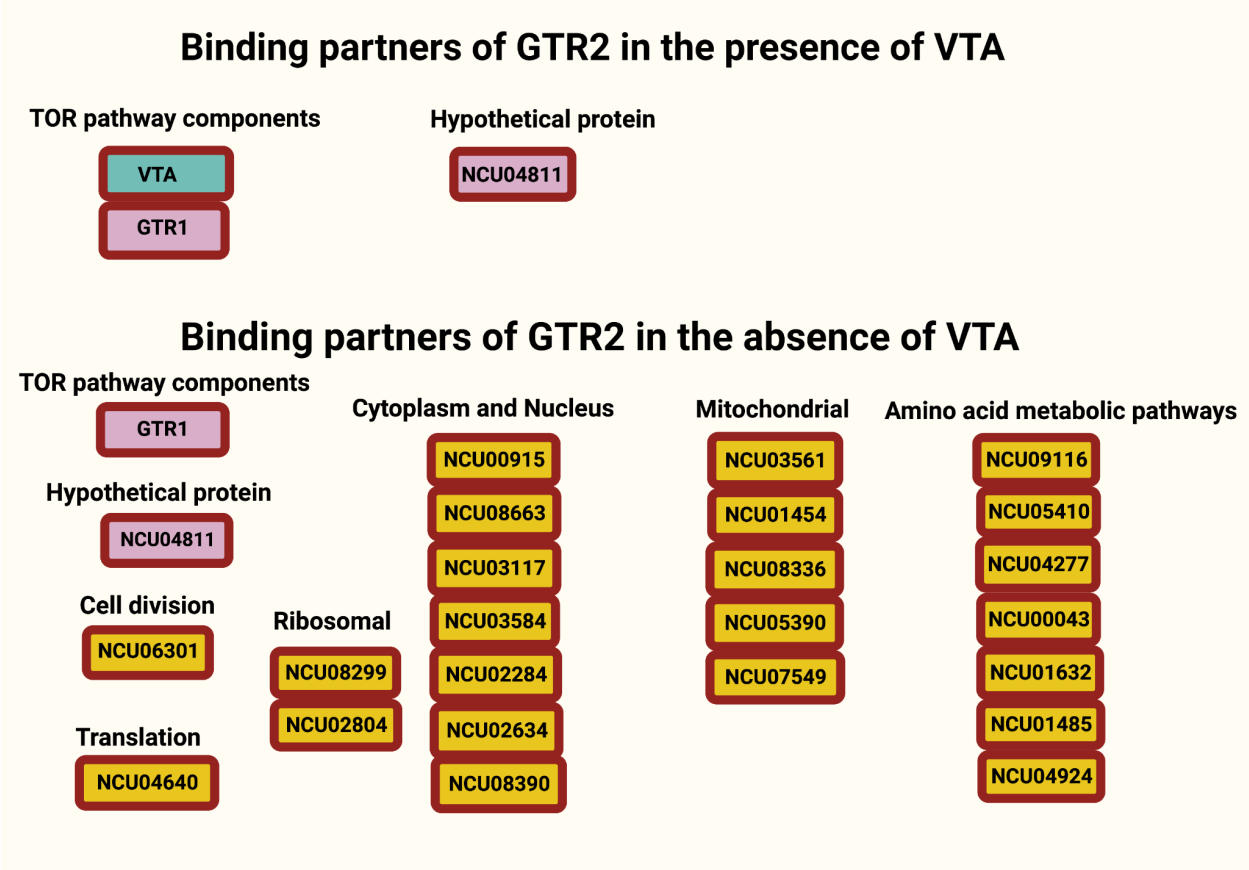

Figure 42: Co-IP and mass spec results of GTR2-FLAG in the presence and absence of VTA. Binding partners indicated with NCU number. Known and important binding partners are labeled with their names. Dark pink color: proteins present in the presence and absence of VTA. Light blue: proteins present in the GTR2-FLAG wild-type strain but absent in the absence of VTA. Yellow: new binding partners that were only present in the absence of VTA. Created with BioRender.com.

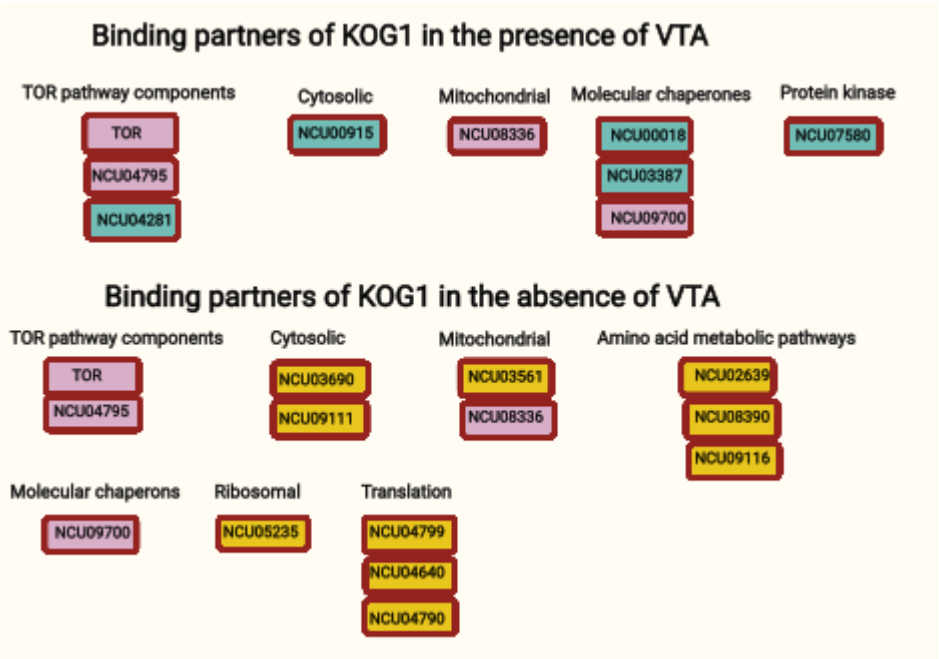

Figure 43: Co-IP and mass spec results of KOG1-FLAG in the presence and absence of VTA. Binding partners indicated with NCU number. Known and important binding partners are labeled with their names. Dark pink color: proteins present in the presence and absence of VTA. Light blue: proteins present in the KOG1-FLAG wild-type strain but absent in the absence of VTA. Yellow: new binding partners that were only present in the absence of VTA. Created with BioRender.com.

4.4. Discussion

In this chapter, my approach was to use tagged proteins to observe the localization of TORC1 components in live cells to further study a signaling pathway, which might demonstrate different roles and re-localization of proteins to different parts of the cell (Yadav *et al.*, 2013). By observing the localization of KOG1-GFP and GTR2-RFP under different conditions, we can see the difference between the KOG1 and GTR2 protein localization in the presence and absence of VTA, which shows the critical role of VTA protein in the localization EGO and TORC1 components. Pull-down experiments are also strong evidence of the interaction between TORC1 components (Long *et al.*, 2005).

The data presented in this chapter indicate that GTR2-RFP localizes in structures identified as vacuolar membranes but is cytoplasmic in the absence of VTA. KOG1-GFP looks similar to GTR2-RFP. In the presence of arginine, KOG1 is localized around the vacuole. Starvation using no glucose media looks similar to the *vta*^{ko} condition in the GTR2 strain, and in KOG1-GFP, there is the presence of bodies around the edges of the vacuole. VTA-GFP does not seem to

change its localization in different conditions.

A study showed that Raptor (homologous to KOG1) interacts directly with mTOR but not with Rheb and the mTOR-raptor interaction is unaffected by Rapamycin (Yadav *et al.*, 2013). This is consistent with my results and the absence of VTA (which might mimic the effect of TOR pathway inhibitor and / or starvation) does not affect the interaction of TOR and KOG1 protein. A protein blast search in NCBI data base shows rheb small monomeric GTPase RhbA as the closest homolog in Neurospora as NCU01444 and it is called gtp19. Initial results I obtained with Rapamycin were inconsistent, therefore I changed my approach and decided to use Torin I and Torin II as TOR pathway inhibitors. In the presence of TOR pathway inhibitors both Torin I and Torin II, an abnormal structural morphology was observed. It indicates that inhibitors damage the vacuolar and internal network and move the fluorescence signal to the outer membrane.

Another study in yeast showed that Kog1 moves from its localization (vacuolar membrane) to a single body near the edge of the vacuole in the glucose starvation condition (Hughes Hallett, Luo, & Capaldi, 2015). Kog1-body formation is a separate process from P-body and granule formation, and it is a rapid and reversible process. AMPK activates Snf1, which phosphorylates glutamine-rich prion-like motifs in Kog-1. Interestingly it was found that in a high number of organisms lacking TSC1/2, such as yeast and C elegans, the Snf1-dependent phosphorylation sites were present. Therefore, it appears that regulation of TORC1 in early eukaryotes is by using Kog1-body formation, while higher eukaryotes use TSC1/2. In *Neurospora crassa* TSC1/2 is not expressed.(Diernfellner *et al.*, 2019) Kog1-bodies then serve to increase the threshold for TORC1 activation in cells that might have been starved for a significant period. Kog1-bodies create hysteresis (memory) in the TORC1 pathway and help ensure that cells remain committed to a quiescent state under suboptimal conditions. (Hughes Hallett, Luo and Capaldi, 2015) The hypothesis is entirely consistent with my results, and we can see the formation of single bodies close to the edges of the vacuole in the absence of glucose.

We previously tested the effect of VTA on the expression patterns of GTR2 and found a significant impact of VTA on the rhythmic expression pattern of GTR2 across two circadian cycles (Eskandari, Ratnayake and Lakin-Thomas, 2021). FRQ protein expression was also tested in the presence and absence of GTR2, and the presence of GTR2 protein was found to be essential for normal FRQ expression. (Eskandari, Ratnayake and Lakin-Thomas, 2021) To see

the effect of VTA on the normal KOG1 expression, which would give us a clue about the association of VTA and TORC1 components, we examined the protein expression of KOG-1-FLAG protein across two circadian cycles and in the presence and absence of VTA. Comparing the expression level of KOG1-FLAG protein in the presence and absence of VTA shows a slightly different expression pattern. However, the KOG1 protein was not rhythmic across two circadian cycles from 24-72 hours, even in the *vta* wild-type strain. These results and our microscopy results indicate that the presence of VTA is required for normal KOG1 subcellular localization and function. Still, it does not affect the expression pattern of KOG1 protein.

One of the primary activators of TORC is the presence of nutrients, especially amino acids, which eventually promotes cell growth, increases anabolic process, and inhibits catabolic process in the cell (González and Hall, 2017; Saxton and Sabatini, 2017). Nevertheless, the complete mechanism that activates TORC1 in response to different amino acids in different organisms is yet to be understood. Various research elucidates the vital role of evolutionarily-conserved heterodimeric small GTPases: RagA/B,RagC/D (the Rag complex) in mammals and Gtr1-Gtr2 (the EGO complex) in yeast (Sancak *et al.*, 2008, 2010; Tanigawa *et al.*, 2021). Based on the results of previous experiments conducted by our lab on *Neurospora crassa*, the main amino acid that activates TORC1 is arginine. Arginine was less effective at increasing *gtr2* and *vta* mutant growth in *Neurospora crassa* (Ratnayake *et al.*, 2018; Eskandari, Ratnayake and Lakin-Thomas, 2021). In the present study, arginine increases the vacuolar membrane localization of KOG1 protein and accumulation of GTR2 protein from cytoplasm around the vacuolar structures.

Glutamine is most effective in activating the yeast TORC1, while leucine and arginine are most effective for activation of mammalian TORC1 (Boutouja et al., 2019). In contrast, *Neurospora crassa* growth is inhibited by leucine, not activated, and growth does not respond to added glutamine in the presence of another nitrogen source (Ratnayake *et al.*, 2018). The activation of growth by arginine, and the lack of effect of arginine in the Δ*gtr2* strain, both might be related to the role of arginine in *Neurospora crassa* as a storage compound in vacuoles (Ratnayake *et al.*, 2018; Eskandari, Ratnayake and Lakin-Thomas, 2021).

Atg8 is an autophagosomal marker, and is believed to increase with the same rate of the accumulation of autophagosomes (Fleißner *et al.*, 2016). Autophagy is a catabolic process downstream of the TOR pathway, and it is induced when the TOR pathway is inhibited (Boutouja, Stiehm and Platta, 2019). I introduced an ATG8-RFP plasmid to our strains and

obtained strains in a *vta* wild type and *vta* ^{ko} background. Results of ATG8-RFP microscopy in the absence of VTA indicate an increase in the accumulation of autophagosomes, and also the presence of TOR pathway inhibitor Torin II. However, in the presence of VTA, the hyphae look to have even expression along the cytoplasm. This suggests a role of VTA in the autophagy process. The absence of VTA may mimic the effect of starvation and/or TOR pathway inhibitors.

Conducting coimmunoprecipitation and mass spectrometry using KOG1-FLAG in the presence and absence of VTA, and GTR2-FLAG in the absence of VTA produced interesting results. Binding partners of GTR2-FLAG in the *vta* wild-type background were previously published (Eskandari, Ratnayake and Lakin-Thomas, 2021). This study analyzed and compared the results of these FLAG tagged proteins in their wild type and *vta*^{ko} background (Figure 42 & 43).

The most abundant common binding partner shared by KOG1-FLAG and KOG-1-FLAG *vta*^{ko} is NCU05608, which based on a search on fungiDB, is known as phosphatidylinositol 3-kinase tor2, div-18. A uniport search identifies it as Serine/threonine-protein kinase TOR. The results of mass spectrometry and coimmunoprecipitation therefore show a strong connection between the KOG1 protein and TOR. This is expected due to KOG1 being a key regulator of TORC1 activation and directly bound to the TOR protein. The next common protein is NCU04795, which is annotated as a hypothetical protein in fungi DB but was found to be TORC1_cplx_su_TCO89 in InterPro. TCO89, as a family and a domain, is described as a component of the TORC1 complex. It was reported that amino acid starvation does not affect the localization or the direct interaction of mTOR with Raptor (Yadav *et al.*, 2013). This is consistent with my mass spectrometry results, and we can see that KOG1, a homolog of Raptor, is still firmly bound to TOR protein in the presence and absence of VTA.

Another common component in the presence and absence of VTA is NCU09700 or T-complex protein 1 subunit beta, identified as cpn-6 in fundi DB, and as T-complex protein 1 subunit in uniprot. The role of the protein as the tailless complex polypeptide 1 (TCP-1) is a highly structurally conserved molecular chaperone located in the cytosol (Ursic and Culbertson, 1991). The protein has also been shown to bind to Golgi membranes and microtubules, signifying a role in mitotic spindle formation in dividing cells (Trent *et al.*, 1991). The last common binding partner is NCU08336, identified as Succinate dehydrogenase flavoprotein subunit, tca-12 in fungi DB and Succinate dehydrogenase [ubiquinone] flavoprotein subunit,

mitochondrial in uni prot database. Succinate dehydrogenase or SDH is an enzyme in the citric acid cycle. It has a direct association with the aerobic respiratory chain. In eukaryotes, SDH is inserted in the inner mitochondrial membrane. The mechanism of FAD-dependent oxidation of succinate to fumarate and the reduction of ubiquinone to ubiquinol is catalyzed by SDH (Kim *et al.*, 2012).

The two important binding partners found only in the KOG1-FLAG *vta* wild type were NCU04281 and NCU03387. NCU04281 or LST8/MLST8 is a common component of both mTORC1 and mTORC2, complexes, which in response to nutrients, regulate growth. Additionally, in mTOR1, MLST8 has the role of direct interaction with mTOR to increase its kinase activity (Loewith *et al.*, 2002). The same protein is found as the target of rapamycin complex subunit wat1 (pop3 or wat1) from Schizosaccharomyces pombe, a component of yeast TORC1 and TORC2 complexes. Wat1 consists of seven ED repeats, and it is a conserved protein. The homolog of wat 1 in budding yeast is lst8, which is a crucial gene for survival and acts as a positive regulator of the TOR complex (Verma *et al.*, 2014) NCU03387 is identified as vesicular-fusion protein SEC18 in fungiDB. One of the top bonding partners of KOG1-FLAG that is present in the presence of VTA but is lost in the absence of VTA is NCU00018. A search in fungiDB indicates it as a cell division control protein Cdc48. CDC48 was primarily found in a yeast cell division cycle that coordinates many degradative and ATP-dependent cellular mechanisms to maintain cellular homeostasis. Lack of CDC48 expression leads to cell death and vacuoles formation derived from ER (Imamura, Yabu and Yamashita, 2012). Another top binding partner of KOG1-FLAG, which is also absent in the absence of VTA, is NCU00915, annotated as Aspartyl-tRNA synthetase in fungidb. tRNA synthetases are specifically important catalyzes of reactions responsible for charging tRNAs with the correct amino acid, which is essential for the standard translation of mRNA into a protein (Fröhlich *et al.*, 2018).

A comparison of the GTR2-FLAG vta^{ko} mass spectrometry results with previous results (Eskandari, Ratnayake and Lakin-Thomas, 2021) indicates that GTR2-FLAG is still binding to the two main proteins that it bound in the presence of VTA, including GTR1 NCU01099 and a hypothetical protein NCU04811. These results emphasize the role of VTA as a membrane protein, anchoring GTR2 to the vacuolar membrane. When VTA is not present, the binding proteins are still attached to GTR2, however, I found many binding partners for GTR2 in the absence of VTA. From these observations, I hypothesized that the dissociation of GTR2 from

VTA does not affect the interactions of GTR2, GTR1, and the hypothetical protein. However, it does dissociate the GTR2-GTR1 complex from the vacuolar membrane, which increases the interaction of GTR2 with numerous other proteins. This is also consistent with the results of my microscopy observations, as we can see in the absence of VTA, there is no localization of the GTR2 protein around the vacuole and the expression is cytoplasmic.

These results support the hypothesis that a connection exists between the mutual components of the clock and TOR pathway. These results further indicate that for the proper functioning of the signaling pathway and the circadian clock, interactions between these proteins are required (Figure 44).

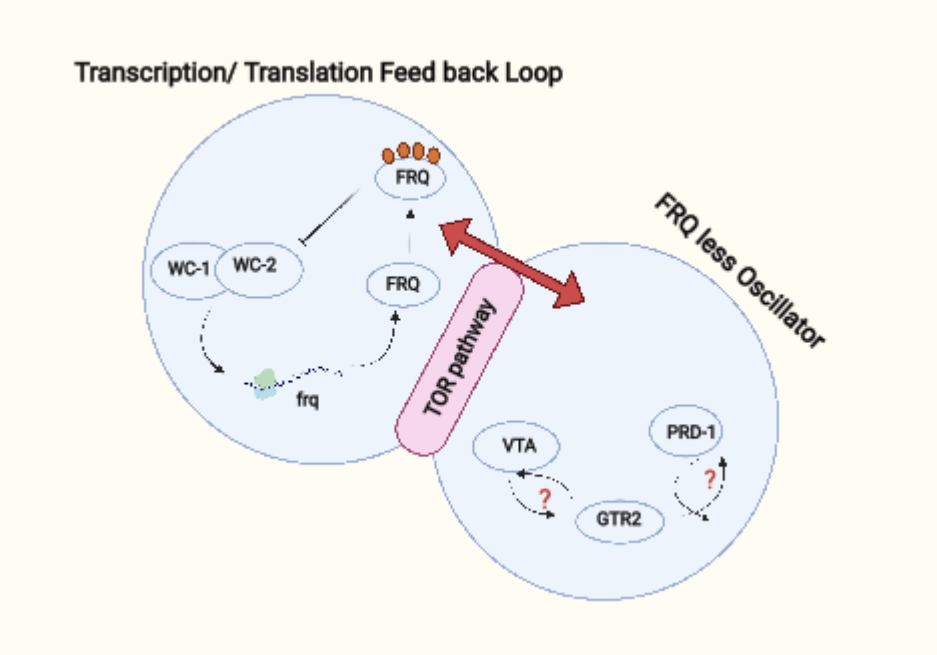

Figure 44: Interaction of FLO and TTFL through the TOR pathway. Our results indicate a direct connection between FLO and TTFL through the TOR signaling pathway. Created with BioRender.com.

Chapter 5. Future Directions and Significance of the Research

5.1. Future Directions

In my thesis work, protein partners of VTA-FLAG, GTR2- FLAG (in both *vta*$^{+}$ and *vta*^{ko} background), and KOG1 FLAG (in both *vta*$^{+}$ and *vta*^{ko} background) were identified by co-immunoprecipitation and mass spectrometry. A follow-up approach would be cross-linking before IP to identify transient protein interactors. This might help identify unexpected protein interactors that could give clues to clock-related functions of VTA. Once interactors are identified, further work can include knockouts or knockdowns to look for effects on rhythmicity. Also, performing Co-IP at different times of the day would be interesting to determine if the interactor proteins change at various times of the day. This is another approach to explore the TOR pathway's association and the circadian clock.

Now that we know the binding partner of GTR2, investigating the nucleotide-binding status of the GTR1/GTR2 combination to see how it activates TORC1 would be very useful. To investigate GTP binding of GTR1 and GTR2, one might make mutants in the GTPase domain to prevent it from hydrolyzing GTP and make a protein stuck in the GTP-bound form, then look for the phenotype. In addition, a comparison could be made between the GTR2 sequence and other GTPases to find non-conserved sequences.

Now that we know the localization of VTA with its function and association with its main binding partners, an interesting approach would be to use deletion mutants of VTA that do not localize to the vacuole and see if other proteins still associate with VTA in co-IP and mass spectrometry.

From my mass spec results, we were able to identify some other components of the TOR pathway in *Neurospora crassa*, and it would be of interest to assay their effects on the circadian clock by making different tagged proteins using our established gene construction method. It would be exciting to look at their rhythmicity, expression, and localization in *frq* and *chol-1* mutant presence and absence.

To have a deep understanding of the TOR pathway function, the best approach is to look at downstream effects, especially its direct downstream substrates. The most widely used assay for TORC1 activity is phosphorylation of one of its targets, S6K (mammals) or Sch9 (yeast), which phosphorylate ribosomal protein S6. Our lab now has a tool (unpublished) to look at S6

phosphorylation in different conditions, times, and genetic backgrounds, and it will be fascinating to study its rhythmicity and see whether its rhythmicity is preserved in the *frq*+ and *frq*^{ko} strains. This would be essential to study interactions between the TOR pathway and the circadian clock directly.

To observe microscopy samples from different times of the day, samples can be prepared using the same method for the Time Course experiment (Chapter II). This is an interesting experimental approach to determine whether TOR pathway components' localization changes at different times of the day and if there is a rhythmic pattern in their localization. Samples could be harvested in darkness and at several times of the day, for example from 24-72 hours, and imaged. The only problem with this method would be that the microscopy should be done immediately since the samples should be observed at a specific time. To make this work, one can use a better-fixed sample preparation method that does not use paraformaldehyde. In the case of live sample observation, the samples could be kept in a dark space and transferred to the microscopy room before starting the microscopy and taking images quickly.

To observe autophagy in a better and more accurate way it's better to consider other factors and genes involved in the process in addition to ATG8 and investigate their role in autophagy. It might also be interesting to determine whether or not the whole autophagy process is rhythmic using the system explained above for time course samples. Chloroquine and its derivative hydroxychloroquine (HCQ) are an example of FDA-approved drugs used as lysosomal inhibitors that inhibit autophagy by impairing autophagosome fusion with the lysosome (Mauthe et al., 2018). This drug could be used to quantifiably measure the rate of autophagy by counting the autophagosome accumulation, using special microscopy tools and expertise. With this method, one can observe and count the number of autophagosomes in the wild type, *vta*^{ko} strains in the presence and absence of Tor pathway inhibitors and different mutant backgrounds, and before and after treatment with CQ. The next step would be to make knock-in ATG8-FLAG or ATG13-FLAG to assay the expression of the proteins in the autophagy induced samples and assay the expression of the autophagy proteins at different times the day to see if autophagy is rhythmic.

5.2. Significance of the Research

Almost all organisms, including humans, have biological clocks (also known as circadian rhythms). Circadian rhythmicity is found in single-celled organisms and in isolated cells from multicellular organisms and is, therefore, a fundamental property of cellular physiology. The

clock can regulate the daily cycle, so fungi, plants, animals, and humans adapt their biological rhythms to Earth's revolutions. For example, our internal clock determines when we get tired and hungry, the time of the day we learn best, the appropriate time to wake up, rest, and sleep. The clock also impacts our key biological functions such as nutrition, mental focus, heart functions, appetite, and the occurrence of diseases. Due to the modern and busy lifestyle, when humans are unable to maintain such a rhythmic clock (also known as circadian disruption), then that could lead to jetlag, reduced fertility, premature aging, obesity, heart disease, cancer, autism, Alzheimer's, and other such life-threatening diseases.

For the year 2017, the Nobel Prize in medicine was awarded for research on circadian biology. A better understanding of circadian rhythms is expected to add a new dimension to the existing treatment of numerous diseases. Over time, predictive algorithms are expected to be developed that could predict how deviations from the biological clock might impact future changes in an individual's health.

The circadian clock and TOR pathway are evolutionarily conserved among organisms, and their impacts on human health are undeniable. Disruption in the circadian clock and TOR pathway lead to severe metabolic disorders. Most of the mutual components of the FLO and TOR pathway have sequence similarities and are conserved among eukaryotes. My research helps better understand the relationship between FLO and TTFL and their connection through the TOR pathway. This would allow researchers to apply and test these effects on higher model organisms, eventually leading to translational applications.

REFERENCES

Adamovich, Yaarit, Liat Rousso-Noori, Ziv Zwighaft, Adi Neufeld-Cohen, Marina Golik, Judith Kraut-Cohen, Miao Wang, Xianlin Han, and Gad Asher. 2014. "Circadian Clocks and Feeding Time Regulate the Oscillations and Levels of Hepatic Triglycerides." *Cell Metabolism* 19 (2): 319–30. https://doi.org/10.1016/j.cmet.2013.12.016.

Adhvaryu, Keyur, Ghazaleh Firoozi, Kamyar Motavaze, and Patricia Lakin-Thomas. 2016. "PRD-1, a Component of the Circadian System of Neurospora Crassa, Is a Member of the DEAD-Box RNA Helicase Family." *Journal of Biological Rhythms* 31 (3): 258–71. https://doi.org/10.1177/0748730416639717.

Allada, Ravi, Neal E. White, W. Venus So, Jeffrey C. Hall, and Michael Rosbash. 1998. "A Mutant Drosophila Homolog of Mammalian Clock Disrupts Circadian Rhythms and Transcription of Period and Timeless." *Cell* 93 (5): 791–804. https://doi.org/10.1016/S0092-8674(00)81440-3.

Bass, Joseph. 2012. "Circadian Topology of Metabolism." *Nature* 491 (7424): 348–56. https://doi.org/10.1038/nature11704.

Bell-Pedersen, Deborah. 2000. "Understanding Circadian Rhythmicity in Neurospora Crassa: From Behavior to Genes and Back Again." *Fungal Genetics and Biology* 29 (1): 1–18. https://doi.org/10.1006/fgbi.2000.1185.

Beadle, G.W., Tatum, E. L.,1941. Genetic control of biochemical reactions in *Neurospora.* Genetics. 27, 499–506.

Binda, Matteo, Marie Pierre Péli-Gulli, Grégory Bonfils, Nicolas Panchaud, Jörg Urban, Thomas W. Sturgill, Robbie Loewith, and Claudio De Virgilio. 2009. "The Vam6 GEF Controls TORC1 by Activating the EGO Complex." *Molecular Cell* 35 (5): 563–73. https://doi.org/10.1016/j.molcel.2009.06.033.

Boutouja, Fahd, Rebecca Brinkmeier, Thomas Mastalski, Fouzi El Magraoui, and Harald W.

Platta. 2017. “Regulation of the Tumor-Suppressor Beclin 1 by Distinct Ubiquitination Cascades.” *International Journal of Molecular Sciences* 18 (12): 1–21. https://doi.org/10.3390/ijms18122541.

Boutouja, Fahd, Christian Stiehm, and Harald Platta. 2019. “MTOR: A Cellular Regulator Interface in Health and Disease.” *Cells* 8 (1): 18. https://doi.org/10.3390/cells8010018.

Burns, Jorge S., and Gina Manda. 2017. “Metabolic Pathways of Thewarburg Effect in Health and Disease: Perspectives of Choice, Chain or Chance.” *International Journal of Molecular Sciences* 18 (12): 1–28. https://doi.org/10.3390/ijms18122755.

Cao, Ruifeng. 2018. “MTOR Signaling, Translational Control, and the Circadian Clock.” *Frontiers in Genetics* 9 (SEP): 1–10. https://doi.org/10.3389/fgene.2018.00367.

Cogoni, Carlo, and Giuseppe Macino. 1999. “Gene Silencing in Neurospora Crassa Requires a Protein Homologous to RNA-Dependent RNA Polymerase.” *Nature* 399 (6732): 166–69. https://doi.org/10.1038/20215.

Darlington, Thomas K., Karen Wager-Smith, M. Fernanda Ceriani, David Staknis, Nicholas Gekakis, Thomas D.L. Steeves, Charles J. Weitz, Joseph S. Takahashi, and Steve A. Kay. 1998. “Closing the Circadian Loop: CLOCK-Induced Transcription of Its Own Inhibitors per and Tim.” *Science* 280 (5369): 1599–1603. https://doi.org/10.1126/science.280.5369.1599.

Diallinas, George, and George Thireos. 1994. “Genetic and Biochemical Evidence for Yeast GCN2 Protein Kinase Polymerization.” *Gene* 143 (1): 21–27. https://doi.org/10.1016/0378-1119(94)90599-1.

Dibner, C., and U. Schibler. 2015. “Circadian Timing of Metabolism in Animal Models and Humans.” *Journal of Internal Medicine* 277 (5): 513–27. https://doi.org/10.1111/joim.12347.

Diernfellner, Axel C. R., Linda Lauinger, Anton Shostak, and Michael Brunner. 2019. “A Pathway Linking Translation Stress to Checkpoint Kinase 2 Signaling in Neurospora Crassa.” *Proceedings of the National Academy of Sciences of the United States of America*

116: 17271–79. https://doi.org/10.1073/pnas.1815396116.

Doi, Ryosuke, Katsutaka Oishi, and Norio Ishida. 2010. "CLOCK Regulates Circadian Rhythms of Hepatic Glycogen Synthesis through Transcriptional Activation of Gys2." *Journal of Biological Chemistry* 285 (29): 22114–21. https://doi.org/10.1074/jbc.M110.110361.

Dong, Jinsheng, Hongfang Qiu, Minerva Garcia-Barrio, James Anderson, and Alan G. Hinnebusch. 2000. "Uncharged TRNA Activates GCN2 by Displacing the Protein Kinase Moiety from a Bipartite TRNA-Binding Domain." *Molecular Cell* 6 (2): 269–79. https://doi.org/10.1016/S1097-2765(00)00028-9.

Dunlap, J. C., C. Ringelberg, L. Litvinkova, H. V. Colot, G. E. Turner, G. Park, C. M. Crew, K. A. Borkovich, and R. L. Weiss. 2006. "A High-Throughput Gene Knockout Procedure for Neurospora Reveals Functions for Multiple Transcription Factors." *Proceedings of the National Academy of Sciences* 103 (27): 10352–57. https://doi.org/10.1073/pnas.0601456103.

Durán, Raúl V., and Michael N. Hall. 2012. "Regulation of TOR by Small GTPases." *EMBO Reports* 13 (2): 121–28. https://doi.org/10.1038/embor.2011.257.

Düvel, Katrin, Jessica L. Yecies, Suchithra Menon, Pichai Raman, Alex I. Lipovsky, Amanda L. Souza, Ellen Triantafellow, et al. 2010. "Activation of a Metabolic Gene Regulatory Network Downstream of MTOR Complex 1." *Molecular Cell* 39 (2): 171–83. https://doi.org/10.1016/j.molcel.2010.06.022.

Eskandari, Rosa, Lalanthi Ratnayake, and Patricia L. Lakin-Thomas. 2021. "Shared Components of the FRQ-Less Oscillator and TOR Pathway Maintain Rhythmicity in Neurospora." *Journal of Biological Rhythms* 36 (4): 329–45. https://doi.org/10.1177/0748730421999948.

Feeney, Kevin A., Louise L. Hansen, Marrit Putker, Consuelo Olivares-Yañez, Jason Day, Lorna J. Eades, Luis F. Larrondo, Nathaniel P. Hoyle, John S. O'Neill, and Gerben Van Ooijen. 2016. "Daily Magnesium Fluxes Regulate Cellular Timekeeping and Energy Balance." *Nature* 532 (7599): 375–79. https://doi.org/10.1038/nature17407.

Fleißner, André, Linda Petereit, Stefanie Pöggeler, Leila Rachid, Daniela Heine, Diana Patzelt,

Ulrike Brandt, Marcel R. Schumann, and Antonia Werner. 2016. " The Tetraspanin TSP3 of Neurospora Crassa Is a Vacuolar Membrane Protein and Shares Characteristics with IDI Proteins ." *Mycologia* 108 (3): 581–89. https://doi.org/10.3852/15-225.

Fontaine, Coralie, Guillaume Dubois, Yannick Duguay, Torben Helledie, Ngoc Vu-Dac, Philippe Gervois, Fabrice Soncin, et al. 2003. "The Orphan Nuclear Receptor Rev-Erbα Is a Peroxisome Proliferator-Activated Receptor (PPAR) γ Target Gene and Promotes PPARγ-Induced Adipocyte Differentiation." *Journal of Biological Chemistry* 278 (39): 37672–80. https://doi.org/10.1074/jbc.M304664200.

Fröhlich, Dominik, Alexandra K. Suchowerska, Carola Voss, Ruojie He, Ernst Wolvetang, Georg Von Jonquieres, Cas Simons, Thomas Fath, Gary D. Housley, and Matthias Klugmann. 2018. "Expression Pattern of the Aspartyl-TRNA Synthetase DARS in the Human Brain." *Frontiers in Molecular Neuroscience* 11 (March): 1–13. https://doi.org/10.3389/fnmol.2018.00081.

Gasch, Audrey P., and Margaret Werner-Washburne. 2002. "The Genomics of Yeast Responses to Environmental Stress and Starvation." *Functional and Integrative Genomics* 2 (4–5): 181–92. https://doi.org/10.1007/s10142-002-0058-2.

Gingras, Anne-claude, Steven P Gygi, Brian Raught, Roberto D Polakiewicz, Robert T Abraham, Merl F Hoekstra, Ruedi Aebersold, and Nahum Sonenberg. 1999. "Regulation of 4E-BP1 Phosphorylation : A Novel Two-Step Mechanism," 1422–37.

González, Asier, and Michael N Hall. 2017. " Nutrient Sensing and TOR Signaling in Yeast and Mammals ." *The EMBO Journal* 36 (4): 397–408. https://doi.org/10.15252/embj.201696010.

Guertin, David A., Deanna M. Stevens, Carson C. Thoreen, Aurora A. Burds, Nada Y. Kalaany, Jason Moffat, Michael Brown, Kevin J. Fitzgerald, and David M. Sabatini. 2006. "Ablation in Mice of the MTORC Components Raptor, Rictor, or MLST8 Reveals That MTORC2 Is Required for Signaling to Akt-FOXO and PKCα, but Not S6K1." *Developmental Cell* 11 (6): 859–71. https://doi.org/10.1016/j.devcel.2006.10.007.

Grobbelaar, N., Huang, T.C., Lin, H.Y., Chow, T.J., 1986. Dinitrogen-fixing endogenous rhythm in Synechococcus RF-1. FEMS Microbiol. Lett. 37, 173–177. https://doi.org/10.1111/j.1574-6968.1986.tb01788.x

Green M.R. and Sambrook J. 2012. Molecular Cloning: A Laboratory Manual. 4th ed. New York: Cold Spring Harbor Laboratory Press.

Haar, Emilie Vander, Seong il Lee, Sricharan Bandhakavi, Timothy J. Griffin, and Do Hyung Kim. 2007. "Insulin Signalling to MTOR Mediated by the Akt/PKB Substrate PRAS40." *Nature Cell Biology* 9 (3): 316–23. https://doi.org/10.1038/ncb1547.

Hara, Kenta, Yoshiko Maruki, Xiaomeng Long, Ken ichi Yoshino, Noriko Oshiro, Sujuti Hidayat, Chiharu Tokunaga, Joseph Avruch, and Kazuyoshi Yonezawa. 2002. "Raptor, a Binding Partner of Target of Rapamycin (TOR), Mediates TOR Action." *Cell* 110 (2): 177–89. https://doi.org/10.1016/S0092-8674(02)00833-4.

Hardin, Paul E. 2011. "Molecular Genetic Analysis of Circadian Timekeeping in Drosophila. Advances in Genetics". Vol. 74. https://doi.org/10.1016/B978-0-12-387690-4.00005-2.

Harmer, S.L., Kay, S.A., 2005. Positive and negative factors confer phase-specific circadian regulation of transcription in Arabidopsis. Plant Cell 17, 1926–1940. https://doi.org/10.1105/tpc.105.033035

Heitman, J., N. R. Movva, P. C. Hiestand, and M. N. Hall. 1991. "FK 506-Binding Protein Proline Rotamase Is a Target for the Immunosuppressive Agent FK 506 in Saccharomyces Cerevisiae." *Proceedings of the National Academy of Sciences of the United States of America* 88 (5): 1948–52. https://doi.org/10.1073/pnas.88.5.1948.

Hickey, Patrick C., David J. Jacobson, Nick D. Read, and N. Louise Glass. 2002. "Live-Cell Imaging of Vegetative Hyphal Fusion in Neurospora Crassa." *Fungal Genetics and Biology* 37 (1): 109–19. https://doi.org/10.1016/S1087-1845(02)00035-X.

Hickey, Patrick C., Samuel R. Swift, M. Gabriela Roca, and Nick D. Read. 2004. "Live-Cell Imaging of Filamentous Fungi Using Vital Fluorescent Dyes and Confocal Microscopy." *Methods in Microbiology* 34 (April 2018): 63–87. https://doi.org/10.1016/S0580-

9517(04)34003-1.

Hinnebusch, A. G. 1984. “Evidence for Translational Regulation of the Activator of General Amino Acid Control in Yeast.” *Proceedings of the National Academy of Sciences of the United States of America* 81 (20 I): 6442–46. https://doi.org/10.1073/pnas.81.20.6442.

Holz, Marina K., Bryan A. Ballif, Steven P. Gygi, and John Blenis. 2005. “MTOR and S6K1 Mediate Assembly of the Translation Preinitiation Complex through Dynamic Protein Interchange and Ordered Phosphorylation Events.” *Cell* 123 (4): 569–80. https://doi.org/10.1016/j.cell.2005.10.024.

Honda, Shinji, Ana Eusebio-Cope, Shuhei Miyashita, Ayumi Yokoyama, Annisa Aulia, Sabitree Shahi, Hideki Kondo, and Nobuhiro Suzuki. 2020. “Establishment of Neurospora Crassa as a Model Organism for Fungal Virology.” *Nature Communications* 11 (1): 1–13. https://doi.org/10.1038/s41467-020-19355-y.

Honda, Shinji, and Eric U. Selker. 2009. “Tools for Fungal Proteomics: Multifunctional Neurospora Vectors for Gene Replacement, Protein Expression and Protein Purification.” *Genetics* 182 (1): 11–23. https://doi.org/10.1534/genetics.108.098707.

Hughes Hallett, James E, Xiangxia Luo, and Andrew P Capaldi. 2015. “Snf1/AMPK Promotes the Formation of Kog1/Raptor-Bodies to Increase the Activation Threshold of TORC1 in Budding Yeast.” *ELife* 4: 1–19. https://doi.org/10.7554/elife.09181.

Hurley, Jennifer M., Arko Dasgupta, Jillian M. Emerson, Xiaoying Zhou, Carol S. Ringelberg, Nicole Knabe, Anna M. Lipzen, et al. 2014. “Analysis of Clock-Regulated Genes in Neurospora Reveals Widespread Posttranscriptional Control of Metabolic Potential.” *Proceedings of the National Academy of Sciences of the United States of America* 111 (48): 16995–2. https://doi.org/10.1073/pnas.1418963111.

Hurley, Jennifer M., Meaghan S. Jankowski, Hannah De los Santos, Alexander M. Crowell, Samuel B. Fordyce, Jeremy D. Zucker, Neeraj Kumar, et al. 2018. “Circadian Proteomic Analysis Uncovers Mechanisms of Post-Transcriptional Regulation in Metabolic Pathways.” *Cell Systems* 7 (6): 613-626.e5. https://doi.org/10.1016/j.cels.2018.10.014.

Imamura, Shintaro, Takeshi Yabu, and Michiaki Yamashita. 2012. “Protective Role of Cell Division Cycle 48 (CDC48) Protein against Neurodegeneration via Ubiquitin-Proteasome System Dysfunction during Zebrafish Development.” *Journal of Biological Chemistry* 287 (27): 23047–56. https://doi.org/10.1074/jbc.M111.332882.

Inoki, Ken, Tianqing Zhu, and Kun-Liang Guan. 2003. “TSC2 Mediates Cellular Energy Response to Control Cell Growth and Survival.” *Cell* 115 (5): 577–90.

Ishiura, M., Kutsuna, S., Aoki, S., Iwasaki, H., Carol, R., Tanabe, A., Golden, S.S., Johnson, C.H., Kondo, T., Ishiura, M., Kutsuna, S., Aoki, S., Iwasaki, H., Andersson, C.R., Tanabe, A., Golden, S.S., Johnson, C.H., Kondo, T., 2016. Expression of a Gene Cluster kaiABC as a Circadian Feedback Process in Cyanobacteria. *AAAS* 281, 1519–1523. http://www.jstor.org/stable/2895132 281.

Iwasaki, H., Nishiwaki, T., Kitayama, Y., Nakajima, M., Kondo, T., 2002. KaiA-stimulated KaiC phosphorylation in circadian timing loops in cyanobacteria. Proc. Natl. Acad. Sci. U. S. A. 99, 15788–15793. https://doi.org/10.1073/pnas.222467299

Jacinto, Estela, Robbie Loewith, Anja Schmidt, Shuo Lin, Markus A. Rüegg, Alan Hall, and Michael N. Hall. 2004. “Mammalian TOR Complex 2 Controls the Actin Cytoskeleton and Is Rapamycin Insensitive.” *Nature Cell Biology* 6 (11): 1122–28. https://doi.org/10.1038/ncb1183.

Janji, Bassam, Elodie Viry, Etienne Moussay, Jérôme Paggetti, Tsolère Arakelian, Takouhie Mgrditchian, Yosra Messai, et al. 2016. “The Multifaceted Role of Autophagy in Tumor Evasion from Immune Surveillance.” *Oncotarget* 7 (14): 17591–607. https://doi.org/10.18632/oncotarget.7540.

Jewell, Jenna L, Ryan C Russell, and Kun-liang Guan. 2013. “Amino Acid Signalling Upstream of MTOR - Nrm3522.Pdf.” *Nature Reviews Molecular Cell Biology* 14 (3): 133–39. https://doi.org/10.1038/nrm3522.Amino.

Kamada, Yoshiaki, Ken-ichi Yoshino, Chika Kondo, Tomoko Kawamata, Noriko Oshiro, Kazuyoshi Yonezawa, and Yoshinori Ohsumi. 2010. “Tor Directly Controls the Atg1

Kinase Complex To Regulate Autophagy." *Molecular and Cellular Biology* 30 (4): 1049–58. https://doi.org/10.1128/mcb.01344-09.

Kim, Hyung J., Mi Young Jeong, Un Na, and Dennis R. Winge. 2012. "Flavinylation and Assembly of Succinate Dehydrogenase Are Dependent on the C-Terminal Tail of the Flavoprotein Subunit." *Journal of Biological Chemistry* 287 (48): 40670–79. https://doi.org/10.1074/jbc.M112.405704.

Koltin, Y, L Faucette, D J Bergsma, M A Levy, R Cafferkey, P L Koser, R K Johnson, and G P Livi. 1991. "Rapamycin Sensitivity in Saccharomyces Cerevisiae Is Mediated by a Peptidyl-Prolyl Cis-Trans Isomerase Related to Human FK506-Binding Protein." *Molecular and Cellular Biology* 11 (3): 1718–23. https://doi.org/10.1128/mcb.11.3.1718.

Kumar Jha, Pawan, Etienne Challet, and Andries Kalsbeek. 2015. "Circadian Rhythms in Glucose and Lipid Metabolism in Nocturnal and Diurnal Mammals." *Molecular and Cellular Endocrinology* 418: 74–88. https://doi.org/10.1016/j.mce.2015.01.024.

Lakin-Thomas, P. L. 2006. "Circadian Clock Genes Frequency and White Collar-1 Are Not Essential for Entrainment to Temperature Cycles in Neurospora Crassa." *Proceedings of the National Academy of Sciences* 103 (12): 4469–74. https://doi.org/10.1073/pnas.0510404103.

Lakin-Thomas, Patricia L., Deborah Bell-Pedersen, and Stuart Brody. 2011. "The Genetics of Circadian Rhythms in Neurospora." In *Advances in Genetics*, 74:55–103. Academic Press. https://doi.org/10.1016/B978-0-12-387690-4.00003-9.

Lakin-Thomas, Patricia L. 2019. "Circadian Rhythms, Metabolic Oscillators, and the Target of Rapamycin (TOR) Pathway: The Neurospora Connection." *Current Genetics* 65 (2): 339–49. https://doi.org/10.1007/s00294-018-0897-6.

Lakin-Thomas PL and Brody S, 2000. Circadian rhythms in Neurospora crassa: Lipid deficiencies restore robust rhythmicity to null frequency and white-collar mutants. Proc. Natl. Acad. Sci. U. S. A. 97, 256–261. https://doi.org/10.1073/pnas.97.1.256

Laplante, M., and D. M. Sabatini. 2009. "MTOR Signaling at a Glance." *Journal of Cell Science*

122 (20): 3589–94. https://doi.org/10.1242/jcs.051011.

Lee, Jeongkyung, Mousumi Moulik, Zhe Fang, Pradip Saha, Fang Zou, Yong Xu, David L. Nelson, Ke Ma, David D. Moore, and Vijay K. Yechoor. 2013. "Bmal1 and β-Cell Clock Are Required for Adaptation to Circadian Disruption, and Their Loss of Function Leads to Oxidative Stress-Induced β-Cell Failure in Mice." *Molecular and Cellular Biology* 33 (11): 2327–38. https://doi.org/10.1128/mcb.01421-12.

Li, Sanshu, Kamyar Motavaze, Elizabeth Kafes, Sujiththa Suntharalingam, and Patricia L Lakin-Thomas. 2011. "A New Mutation Affecting Frq-Less Rhythms in the Circadian System of Neurospora Crassa." *PLoS Genetics* 7 (6): 1002151. https://doi.org/10.1371/journal.pgen.1002151.

Lipton, Jonathan O., Lara M. Boyle, Elizabeth D. Yuan, Kevin J. Hochstrasser, Fortunate F. Chifamba, Ashwin Nathan, Peter T. Tsai, Fred Davis, and Mustafa Sahin. 2017. "Aberrant Proteostasis of BMAL1 Underlies Circadian Abnormalities in a Paradigmatic MTOR-Opathy." *Cell Reports* 20 (4): 868–80. https://doi.org/10.1016/j.celrep.2017.07.008.

Liu, Guangwei, Yujing Bi, Bo Shen, Hui Yang, Yan Zhang, Xiao Wang, Huanrong Liu, et al. 2014. "SIRT1 Limits the Function and Fate of Myeloid-Derived Suppressor Cells in Tumors by Orchestrating HIF-1α-Dependent Glycolysis." *Cancer Research* 74 (3): 727–37. https://doi.org/10.1158/0008-5472.CAN-13-2584.

Liu, Pengda, Wenjian Gan, Y. Rebecca Chin, Kohei Ogura, Jianping Guo, Jinfang Zhang, Bin Wang, et al. 2015. "Ptdins(3,4,5) P3 -Dependent Activation of the MTORC2 Kinase Complex." *Cancer Discovery* 5 (11): 1194–11209. https://doi.org/10.1158/2159-8290.CD-15-0460.

Locke, J.C.W., Kozma-Bognár, L., Gould, P.D., Fehér, B., Kevei, É., Nagy, F., Turner, M.S., Hall, A., Millar, A.J., 2006. Experimental validation of a predicted feedback loop in the multi-oscillator clock of Arabidopsis thaliana. Mol. Syst. Biol. 2, 1–6. https://doi.org/10.1038/msb4100102

Loewith, Robbie, and Michael N. Hall. 2011. "Target of Rapamycin (TOR) in Nutrient Signaling

and Growth Control." *Genetics* 189 (4): 1177–1201. https://doi.org/10.1534/genetics.111.133363.

Loewith, Robbie, Estela Jacinto, Stephan Wullschleger, Anja Lorberg, José L. Crespo, Débora Bonenfant, Wolfgang Oppliger, Paul Jenoe, and Michael N. Hall. 2002. "Two TOR Complexes, Only One of Which Is Rapamycin Sensitive, Have Distinct Roles in Cell Growth Control." *Molecular Cell* 10 (3): 457–68. https://doi.org/10.1016/S1097-2765(02)00636-6.

Long, Xiaomeng, Yenshou Lin, Sara Ortiz-Vega, Kazuyoshi Yonezawa, and Joseph Avruch. 2005. "Rheb Binds and Regulates the MTOR Kinase." *Current Biology* 15 (8): 702–13. https://doi.org/10.1016/j.cub.2005.02.053.

Loros, Jennifer J, and Jay C Dunlap. 2001. "Genetic and Molecular Analysis Of Circadian Rhythms in *Neurospora*." *Annual Review of Physiology* 63 (2): 757–94.

Madden, T., 2013. The BLAST Sequence Analysis Tool. Available from: https://www.ncbi.nlm.nih.gov/books/NBK153387/#BLAST.

Marcheva, Biliana, Kathryn Moynihan Ramsey, Ethan D. Buhr, Yumiko Kobayashi, Hong Su, Caroline H. Ko, Ganka Ivanova, et al. 2010. "Disruption of the Clock Components CLOCK and BMAL1 Leads to Hypoinsulinaemia and Diabetes." *Nature* 466 (7306): 627–31. https://doi.org/10.1038/nature09253.

Martina, Jose A., Yong Chen, Marjan Gucek, and Rosa Puertollano. 2012. "MTORC1 Functions as a Transcriptional Regulator of Autophagy by Preventing Nuclear Transport of TFEB." *Autophagy* 8 (6): 903–14. https://doi.org/10.4161/auto.19653.

Martı, Paula. 2005. "Divergence of Stp1 and Stp2 Transcription Factors In *Candida albicans* Places Virulence Factors Required for Proper Nutrient Acquisition under Amino Acid Control." *Microbiology* 25 (21): 9435–46. https://doi.org/10.1128/MCB.25.21.9435.

Mauthe, M., Orhon, I., Rocchi, C., Zhou, X., Luhr, M., Hijlkema, K.J., Coppes, R.P., Engedal, N., Mari, M., Reggiori, F., 2018. Chloroquine inhibits autophagic flux by decreasing autophagosome-lysosome fusion. Autophagy 14, 1435–1455.

https://doi.org/10.1080/15548627.2018.1474314

Marchler-Bauer A., Bo Y., Han L., He J., Lanczycki C.J., Lu, S., et al., 2017. CDD/SPARCLE: Functional classification of proteins via subfamily domain architectures. Nucleic. Acids. Res. 45: D200-D203.

O' Neill, Ooijen, G. Van, Dixon, L.E., Troein, C., Bouget, F., Reddy, A.B., Millar, A.J., 2011. Circadian rhythms persist without transcription in a eukaryote. Nature 469, 554–558. https://doi.org/10.1038/nature09654.

Napolioni, Valerio, and Paolo Curatolo. 2008. "Genetics and Molecular Biology of Tuberous Sclerosis Complex." *Current Genomics* 9 (7): 475–87. https://doi.org/10.2174/138920208786241243.

Park, Gyungsoon, Jacqueline A. Servin, Gloria E. Turner, Lorena Altamirano, Hildur V. Colot, Patrick Collopy, Liubov Litvinkova, et al. 2011. "Global Analysis of Serine-Threonine Protein Kinase Genes in Neurospora Crassa." *Eukaryotic Cell* 10 (11): 1553–64. https://doi.org/10.1128/EC.05140-11.

Peterson, Timothy R., Shomit S. Sengupta, Thurl E. Harris, Anne E. Carmack, Seong A. Kang, Eric Balderas, David A. Guertin, et al. 2011. "MTOR Complex 1 Regulates Lipin 1 Localization to Control the Srebp Pathway." *Cell* 146 (3): 408–20. https://doi.org/10.1016/j.cell.2011.06.034.

Pilorz, Violetta, Charlotte Helfrich-Förster, and Henrik Oster. 2018. "The Role of the Circadian Clock System in Physiology." *Pflugers Archiv European Journal of Physiology* 470 (2): 227–39. https://doi.org/10.1007/s00424-017-2103-y.

Pinto, Débora, Margarida Duarte, Susana Soares, Maximilian Tropschug, and Arnaldo Videira. 2008. "Identification of All FK506-Binding Proteins from Neurospora Crassa." *Fungal Genetics and Biology* 45 (12): 1600–1607. https://doi.org/10.1016/j.fgb.2008.09.011.

Pittendrigh, C. S. 1960. "Circadian Rhythms and the Circadian Organization of Living Systems." *Cold Spring Harbor Symposia on Quantitative Biology* 25: 159–84. https://doi.org/10.1101/SQB.1960.025.01.015.

Powis, Katie, Tianlong Zhang, Nicolas Panchaud, Rong Wang, Claudio De Virgilio, and Jianping Ding. 2015. “Crystal Structure of the Ego1-Ego2-Ego3 Complex and Its Role in Promoting Rag GTPase-Dependent TORC1 Signaling.” *Cell Research* 25 (9): 1043–59. https://doi.org/10.1038/cr.2015.86.

Preitner, Nicolas, Francesca Damiola, Luis-Lopez-Molina, Joszef Zakany, Denis Duboule, Urs Albrecht, and Ueli Schibler. 2002. “The Orphan Nuclear Receptor REV-ERBα Controls Circadian Transcription within the Positive Limb of the Mammalian Circadian Oscillator.” *Cell* 110 (2): 251–60. https://doi.org/10.1016/S0092-8674(02)00825-5.

Ramos-García, Silvia L., Robert W. Roberson, Michael Freitage, Salomón Bartnicki-García, and Rosa R. Mouriño-Pérez. 2009. “Cytoplasmic Bulk Flow Propels Nuclei in Mature Hyphae of Neurospora Crassa.” *Eukaryotic Cell* 8 (12): 1880–90. https://doi.org/10.1128/EC.00062-09.

Ratnayake, Lalanthi, Keyur K. Adhvaryu, Elizabeth Kafes, Kamyar Motavaze, and Patricia Lakin-Thomas. 2018. “A Component of the TOR (Target Of Rapamycin) Nutrient-Sensing Pathway Plays a Role in Circadian Rhythmicity in Neurospora Crassa.” *PLoS Genetics* 14 (6): 1–29. https://doi.org/10.1371/journal.pgen.1007457.

Resco, V., Hartwell, J., Hall, A., 2009. Ecological implications of plants’ ability to tell the time. Ecol. Lett. 12, 583–592. https://doi.org/10.1111/j.1461-0248.2009.01295.x

Robitaille, Aaron M., Stefan Christen, Mitsugu Shimobayashi, Marion Cornu, Luca L. Fava, Suzette Moes, Cristina Prescianotto-Baschong, Uwe Sauer, Paul Jenoe, and Michael N. Hall. 2013. “Quantitative Phosphoproteomics Reveal MTORC1 Activates de Novo Pyrimidine Synthesis.” *Science* 339 (6125): 1320–23. https://doi.org/10.1126/science.1228771.

Rohringer, Roland, and David W. Holden. 1985. “Protein Blotting: Detection of Proteins with Colloidal Gold, and of Glycoproteins and Lectins with Biotin-Conjugated and Enzyme Probes.” *Analytical Biochemistry* 144 (1): 118–27. https://doi.org/10.1016/0003-2697(85)90092-2.

Rudic, R. Daniel, Peter McNamara, Anne Maria Curtis, Raymond C. Boston, Satchidananda Panda, John B. Hogenesch, and Garret A. FitzGerald. 2004. "BMAL1 and CLOCK, Two Essential Components of the Circadian Clock, Are Involved in Glucose Homeostasis." *PLoS Biology* 2 (11). https://doi.org/10.1371/journal.pbio.0020377.

Rutila, Joan E., Vipin Suri, Myai Le, W. Venus So, Michael Rosbash, and Jeffrey C. Hall. 1998. "Cycle Is a Second BHLH-PAS Clock Protein Essential for Circadian Rhythmicity and Transcription of Drosophila Period and Timeless." *Cell* 93 (5): 805–14. https://doi.org/10.1016/S0092-8674(00)81441-5.

Sadacca, L. A., K. A. Lamia, A. S. DeLemos, B. Blum, and C. J. Weitz. 2011. "An Intrinsic Circadian Clock of the Pancreas Is Required for Normal Insulin Release and Glucose Homeostasis in Mice." *Diabetologia* 54 (1): 120–24. https://doi.org/10.1007/s00125-010-1920-8.

Salgado-Delgado, Roberto C., Nadia Saderi, María del Carmen Basualdo, Natali N. Guerrero-Vargas, Carolina Escobar, and Ruud M. Buijs. 2013. "Shift Work or Food Intake during the Rest Phase Promotes Metabolic Disruption and Desynchrony of Liver Genes in Male Rats." *PLoS ONE* 8 (4). https://doi.org/10.1371/journal.pone.0060052.

Salomé, P.A., McClung, C.R., 2005. What makes the Arabidopsis clock tick on time? A review on entrainment. Plant, Cell Environ. 28, 21–38. https://doi.org/10.1111/j.1365-3040.2004.01261.x

Sancak, Yasemin, Liron Bar-Peled, Roberto Zoncu, Andrew L. Markhard, Shigeyuki Nada, and David M. Sabatini. 2010. "Ragulator-Rag Complex Targets MTORC1 to the Lysosomal Surface and Is Necessary for Its Activation by Amino Acids." *Cell* 141 (2): 290–303. https://doi.org/10.1016/j.cell.2010.02.024.

Sancak, Yasemin, Timothy R Peterson, Yoav D Shaul, Robert A Lindquist, Carson C Thoreen, Liron Bar-peled, and David M Sabatini. 2008. "The Rag GTPases Bind Raptor and Mediate Amino Acid Signalin to mTORC1." 320 (5882): 1496–1501. https://doi.org/10.1126/science.1157535.

Sancak, Yasemin, Carson C. Thoreen, Timothy R. Peterson, Robert A. Lindquist, Seong A. Kang, Eric Spooner, Steven A. Carr, and David M. Sabatini. 2007. "PRAS40 Is an Insulin-Regulated Inhibitor of the MTORC1 Protein Kinase." *Molecular Cell* 25 (6): 903–15. https://doi.org/10.1016/j.molcel.2007.03.003.

Saxton, Robert A., and David M. Sabatini. 2017. "MTOR Signaling in Growth, Metabolism, and Disease." *Cell* 168 (6): 960–76. https://doi.org/10.1016/j.cell.2017.02.004.

Schmelzle, Tobias, Stephen B. Helliwell, and Michael N. Hall. 2002. "Yeast Protein Kinases and the RHO1 Exchange Factor TUS1 Are Novel Components of the Cell Integrity Pathway in Yeast." *Molecular and Cellular Biology* 22 (5): 1329–39. https://doi.org/10.1128/mcb.22.5.1329-1339.2002.

Schmutz, Isabelle, Jürgen A. Ripperger, Stéphanie Baeriswyl-Aebischer, and Urs Albrecht. 2010. "The Mammalian Clock Component PERIOD2 Coordinates Circadian Output by Interaction with Nuclear Receptors." *Genes and Development* 24 (4): 345–57. https://doi.org/10.1101/gad.564110.

Scott, E. M., A. M. Carter, and P. J. Grant. 2008. "Association between Polymorphisms in the Clock Gene, Obesity and the Metabolic Syndrome in Man." *International Journal of Obesity* 32 (4): 658–62. https://doi.org/10.1038/sj.ijo.0803778.

Settembre, Carmine, Roberto Zoncu, Diego L. Medina, Francesco Vetrini, Serkan Erdin, Serpiluckac Erdin, Tuong Huynh, et al. 2012. "A Lysosome-to-Nucleus Signalling Mechanism Senses and Regulates the Lysosome via MTOR and TFEB." *EMBO Journal* 31 (5): 1095–1108. https://doi.org/10.1038/emboj.2012.32.

Shertz, Cecelia A., Robert J. Bastidas, Wenjun Li, Joseph Heitman, and Maria E. Cardenas. 2010. "Conservation, Duplication, and Loss of the Tor Signaling Pathway in the Fungal Kingdom." *BMC Genomics* 11 (1): 1–14. https://doi.org/10.1186/1471-2164-11-510.

Srivastava, D., Shamim, M., Kumar, M., Mishra, A., Maurya, R., Sharma, D., Pandey, P., Singh, K.N., 2019. Role of circadian rhythm in plant system: An update from development to stress response. Environ. Exp. Bot. 162, 256–271.

https://doi.org/10.1016/j.envexpbot.2019.02.025

Stajich J.E., Harris T., Brunk B.P., Brestelli J., Fischer S., Harb O.S., Kissinger J.C., Li W., Nayak V., Pinney D.F., 2012 FungiDB: An integrated functional genomics database for fungi. Nucleic. Acids. Res. 40: D675-681.

Sookoian, S., C. Gemma, T. Fernández Gianotti, A. Burgueño, A. Alvarez, C. D. González, and C. J. Pirola. 2007. "Effects of Rotating Shift Work on Biomarkers of Metabolic Syndrome and Inflammation." *Journal of Internal Medicine* 261 (3): 285–92. https://doi.org/10.1111/j.1365-2796.2007.01766.x.

Sturgill, Thomas W., Adiel Cohen, Melanie Diefenbacher, Mark Trautwein, Dietmar E. Martin, and Michael N. Hall. 2008. "TOR1 and TOR2 Have Distinct Locations in Live Cells." *Eukaryotic Cell* 7 (10): 1819–30. https://doi.org/10.1128/EC.00088-08.

Tanigawa, Mirai, Katsuyoshi Yamamoto, Satoru Nagatoishi, Koji Nagata, Daisuke Noshiro, Nobuo N. Noda, Kouhei Tsumoto, and Tatsuya Maeda. 2021. "A Glutamine Sensor That Directly Activates TORC1." *Communications Biology* 4 (1): 1–12. https://doi.org/10.1038/s42003-021-02625-w.

Tataroglu, Ozgur, and Patrick Emery. 2014. "Studying Circadian Rhythms in Drosophila Melanogaster." *Methods* 68 (1): 140–50. https://doi.org/10.1016/j.ymeth.2014.01.001.

Tomita, J., Nakajima, M., Kondo, T., Iwasaki, H., Science, S., Series, N., Jan, N., Tomita, J., Nakajima, M., Kondo, T., Iwasaki, H., 2005. "No Transcription-Translation Feedback in Circadian Rhythm of KaiC Phosphorylation. "*Science* 307(5707): 251–254. https://www.jstor.org/stable/3840110

Teboul, Michèle, Fabienne Guillaumond, Aline Gréchez-Cassiau, and Franck Delaunay. 2008. "The Nuclear Hormone Receptor Family Round the Clock." *Molecular Endocrinology* 22 (12): 2573–82. https://doi.org/10.1210/me.2007-0521.

Trent, Jonathan D., Elmar Nimmesgern, Joseph S. Wall, F. Ulrich Hartl, and Arthur L. Horwich. 1991. "A Molecular Chaperone from a Thermophilic Archaebacterium Is Related to the Eukaryotic Protein T-Complex Polypeptide-1." *Nature* 354 (6353): 490–93.

https://doi.org/10.1038/354490a0.

Tsang, Adrian. 2014. “Fungal Genomics.” *Briefings in Functional Genomics* 13 (6): 421–23. https://doi.org/10.1093/bfgp/elu041.

Tseng, Roger, Nicolette F Goularte, Archana Chavan, Jansen Luu, Susan E Cohen, Yong-gang Chang, Joel Heisler, et al. 2017. “Structural Basis of the Day-Night Transition in a Bacterial Circadian Clock” 355 (6330): 1174–80. https://doi.org/10.1126/science.aag2516.Structural.

Urban, Jörg, Alexandre Soulard, Alexandre Huber, Soyeon Lippman, Debdyuti Mukhopadhyay, Olivier Deloche, Valeria Wanke, et al. 2007. “Sch9 Is a Major Target of TORC1 in Saccharomyces Cerevisiae.” *Molecular Cell* 26 (5): 663–74. https://doi.org/10.1016/j.molcel.2007.04.020.

Ursic, D, and M R Culbertson. 1991. “The Yeast Homolog to Mouse Tcp-1 Affects Microtubule-Mediated Processes.” *Molecular and Cellular Biology* 11 (5): 2629–40. https://doi.org/10.1128/mcb.11.5.2629-2640.1991.

Vaidya, Anand T., Deniz Top, Craig C. Manahan, Joshua M. Tokuda, Sheng Zhang, Lois Pollack, Michael W. Young, and Brian R. Crane. 2013. “Flavin Reduction Activates Drosophila Cryptochrome.” *Proceedings of the National Academy of Sciences of the United States of America* 110 (51): 20455–60. https://doi.org/10.1073/pnas.1313336110.

Vellai, Tibor, Kriztina Takacs-Vellai, Yue Zhang, Attila L. Kovacs, László Orosz, and Fritz Müller. 2003. “Influence of TOR Kinase on Lifespan in C. Elegans.” *Nature* 426 (6967): 620. https://doi.org/10.1038/426620a.

Verma, Sumit Kumar, Rajeev Ranjan, Vikash Kumar, Mohammad Imran Siddiqi, and Shakil Ahmed. 2014. “Wat1/Pop3, a Conserved WD Repeat Containing Protein Acts Synergistically with Checkpoint Kinase Chk1 to Maintain Genome Ploidy in Fission Yeast S. Pombe.” *PLoS ONE* 9 (2). https://doi.org/10.1371/journal.pone.0089587.

Virgilio, Claudio de. 2012. “The Essence of Yeast Quiescence.” *FEMS Microbiology Reviews* 36 (2): 306–39. https://doi.org/10.1111/j.1574-6976.2011.00287.x.

Walton, Zandra E., Chirag H. Patel, Rebekah C. Brooks, Yongjun Yu, Arig Ibrahim-Hashim, Malini Riddle, Alessandra Porcu, et al. 2018. "Acid Suspends the Circadian Clock in Hypoxia through Inhibition of MTOR." *Cell* 174 (1): 72-87.e32. https://doi.org/10.1016/j.cell.2018.05.009.

Wang, Yan, Yumei Qin, Bin Li, Yuanyuan Zhang, and Lei Wang. 2020. "Attenuated TOR Signaling Lengthens Circadian Period in Arabidopsis." *Plant Signaling and Behavior* 15 (2). https://doi.org/10.1080/15592324.2019.1710935.

Wanke, Valeria, Elisabetta Cameroni, Aino Uotila, Manuele Piccolis, Jörg Urban, Robbie Loewith, and Claudio De Virgilio. 2008. "Caffeine Extends Yeast Lifespan by Targeting TORC1." *Molecular Microbiology* 69 (1): 277–85. https://doi.org/10.1111/j.1365-2958.2008.06292.x.

Wek, R. C., B. M. Jackson, and A. G. Hinnebusch. 1989. "Juxtaposition of Domains Homologous to Protein Kinase and Histidyl-TRNA Synthetases in GCN2 Protein Suggests a Mechanism for Coupling GCN4 Expression to Amino Acid Availability." *Proceedings of the National Academy of Sciences of the United States of America* 86 (12): 4579–83. https://doi.org/10.1073/pnas.86.12.4579.

Wiederrecht, G., L. Brizuela, K. Elliston, N. H. Sigal, and J. J. Siekierka. 1991. "FKB1 Encodes a Nonessential FK 506-Binding Protein in Saccharomyces Cerevisiae and Contains Regions Suggesting Homology to the Cyclophilins." *Proceedings of the National Academy of Sciences of the United States of America* 88 (3): 1029–33. https://doi.org/10.1073/pnas.88.3.1029.

Woon, Peng Y., Pamela J. Kaisaki, José Bragança, Marie Thérèse Bihoreau, Jonathan C. Levy, Martin Farrall, and Dominique Gauguier. 2007. "Aryl Hydrocarbon Receptor Nuclear Translocator-like (BMAL1) Is Associated with Susceptibility to Hypertension and Type 2 Diabetes." *Proceedings of the National Academy of Sciences of the United States of America* 104 (36): 14412–17. https://doi.org/10.1073/pnas.0703247104.

Xu, Y., Mori, T., Johnson, C.H., 2000. Circadian clock-protein expression in cyanobacteria: Rhythms and phase setting. EMBO J. 19, 3349–3357.

https://doi.org/10.1093/emboj/19.13.3349

Yadav, Rahul B., Pierre Burgos, Anthony W. Parker, Valentina Iadevaia, Christopher G. Proud, Rodger A. Allen, James P. O'Connell, Ananya Jeshtadi, Christopher D. Stubbs, and Stanley W. Botchway. 2013. "MTOR Direct Interactions with Rheb-GTPase and Raptor: Sub-Cellular Localization Using Fluorescence Lifetime Imaging." *BMC Cell Biology* 14 (1): 1. https://doi.org/10.1186/1471-2121-14-3.

Yakir, E., Hilman, D., Harir, Y., Green, R.M., 2007. Regulation of output from the plant circadian clock. FEBS J. 274, 335–345. https://doi.org/10.1111/j.1742-4658.2006.05616.x

Yang, Guang, Danielle S. Murashige, Sean J. Humphrey, and David E. James. 2015. "A Positive Feedback Loop between Akt and MTORC2 via SIN1 Phosphorylation." *Cell Reports* 12 (6): 937–43. https://doi.org/10.1016/j.celrep.2015.07.016.

Yonehara, Ryo, Shigeyuki Nada, Tomokazu Nakai, Masahiro Nakai, Ayaka Kitamura, Akira Ogawa, Hirokazu Nakatsumi, et al. 2017. "Structural Basis for the Assembly of the Ragulator-Rag GTPase Complex." *Nature Communications* 8 (1): 1–10. https://doi.org/10.1038/s41467-017-01762-3.

Yorimitsu, Tomohiro, Congcong He, Ke Wang, and Daniel J. Klionsky. 2009. "Tap42-Associated Protein Phosphatase Type 2A Negatively Regulates Induction of Autophagy." *Autophagy* 5 (5): 616–24. https://doi.org/10.4161/auto.5.5.8091.

Yu, Wangjie, Hao Zheng, Jeffrey L. Price, and Paul E. Hardin. 2009. " DOUBLETIME Plays a Noncatalytic Role To Mediate CLOCK Phosphorylation and Repress CLOCK-Dependent Transcription within the Drosophila Circadian Clock ." *Molecular and Cellular Biology* 29 (6): 1452–58. https://doi.org/10.1128/mcb.01777-08.

Zani, Fabio, Ludovic Breasson, Barbara Becattini, Ana Vukolic, Jean Pierre Montani, Urs Albrecht, Alessandro Provenzani, Juergen A. Ripperger, and Giovanni Solinas. 2013. "PER2 Promotes Glucose Storage to Liver Glycogen during Feeding and Acute Fasting by Inducing Gys2 PTG and GL Expression." *Molecular Metabolism* 2 (3): 292–305. https://doi.org/10.1016/j.molmet.2013.06.006.

Zeilinger, M.N., Farré, E.M., Taylor, S.R., Kay, S.A., Doyle, F.J., 2006. A novel computational model of the circadian clock in Arabidopsis that incorporates PRR7 and PRR9. Mol. Syst. Biol. 2. https://doi.org/10.1038/msb4100101

Zeng, Hongkui, Zuwei Qian, Michael P. Myers, and Michael Rosbash. 1996. "A Light-Entrainment Mechanism for the Drosophila Circadian Clock." *Nature* 380 (6570): 129–35. https://doi.org/10.1038/380129a0.

Zhang, Nan, Yanyan Meng, Xu Li, Yu Zhou, Liuyin Ma, Liwen Fu, Markus Schwarzländer, Hongtao Liu, and Yan Xiong. 2019. "Metabolite-Mediated TOR Signaling Regulates the Circadian Clock in Arabidopsis." *Proceedings of the National Academy of Sciences of the United States of America* 116 (51): 25395–97. https://doi.org/10.1073/pnas.1913095116.

Zhao, Yue, Ying Zhang, Mengyi Zhou, Shiming Wang, Zichun Hua, and Jianfa Zhang. 2012. "Loss of MPer2 Increases Plasma Insulin Levels by Enhanced Glucose-Stimulated Insulin Secretion and Impaired Insulin Clearance in Mice." *FEBS Letters* 586 (9): 1306–11. https://doi.org/10.1016/j.febslet.2012.03.034.

Zheng, Xiangzhong, and Amita Sehgal. 2010. "AKT and TOR Signaling Set the Pace of the Circadian Pacemaker." *Current Biology* 20 (13): 1203–8. https://doi.org/10.1016/j.cub.2010.05.027.

Ziv, Carmit, Galia Kra-Oz, Rena Gorovits, Sabine März, Stephan Seiler, and Oded Yarden. 2009. "Cell Elongation and Branching Are Regulated by Differential Phosphorylation States of the Nuclear Dbf2-Related Kinase COT1 in Neurospora Crassa." *Molecular Microbiology* 74 (4): 974–89. https://doi.org/10.1111/j.1365-2958.2009.06911.x.

APPENDIX I

6x loading dye (6 mL total volume) based on NEB protocol

- 0.015% Bromophenol blue: 5.4 mg
- 2.5 % Ficol : 0.9 grams.
- 11mM EDTA: 800 µl (what stock concentration?) EDTA
- 3.3 mM Tris-HCL: 119 µl (what stock concentration?)
- 0.017 % SDS: 6.1 mg
- Add distilled water up to 6 ml.
- Vortex to dissolve
- Centrifuge for 30 Sec.
- Dispense 1 mL in small microfuge tubes and store in 4 °C

Vogel's 50x stock:

Add successively to 250 mL flask, stirring continuously:

- 188 mL DI water stir and heat
- 32.8 g Na_3-citrate.$2H_2O$, let dissolve
- 62.5 g KH_2PO_4 anhydrous, let dissolve
- 25.0 g NH4NO3 anhydrous, let dissolve
- Turn off heat and add water to 250 mL.
- Add the following while stirring:
- 2.5 g $MgSO_4.7H_2O$, let dissolve
- 1.25 g $CaCl_2.2H_2O$ dissolved in 5 mL water *
- 1.25 mL trace elements solution
- 0.625 mL biotin solution (Make fresh)
- Allow to cool, add about 2 mL chloroform, cap tightly.

*Add calcium very slowly and carefully to avoid precipitation, using pasture pipette submerged below the surface of stirring solution to avoid precipitation.

Allow solution to cool completely, add 2 mL chloroform and cap tightly. Store at room temperature.

Fresh biotin solution:

- 1 mg per 10 mL of 50/50 ethanol/water

Trace Elements:

Add successively to 9.5 mL water (ddH_2O), while stirring:

- 0.5 g citric acid. H_2O
- 0.5 g $ZnSO_4.7H_2O$
- g Fe $(NH_4)_2(SO_4)_2.6H_2O$
- 0.025 g $CuSO_4.5H_2O$
- 0.066 g $MnSO_4.4H_2O$ (Or: 0.050 g $MnSO_4.H_2O$)
- 0.005 g H_3BO_3 anhydrous
- 0.0037 g $(NH_4)_6Mo_7O_{24}.4H_2O$

Store in the refrigerator and wrapped in foil to keep dark.

2x Synthetic crossing medium (SCM) stock:

Add successively to 250 mL water, with stirring:

- 0.46 g $K_2HPO_4.3H_2O$ (Or: 0.35 g K_2HPO_4 anhydrous)
- 0.25 g KH_2PO_4
- 0.5 g KNO_3
- 0.05 g NaCl
- 0.25 g $MgSO_4.7H_20$
- 0.05 g $CaCl_2.2H_2O$ dissolved in 1 mL water
- 1.25 mL fresh biotin
- 0.05 mL trace elements

Store in refrigerator with chloroform.

Liquid minimal medium:

(For micro-titer wells or shaker flasks)

- 2 mL - Vogel's 50x stock
- 2 g - D-Glucose

- 100 mL - Water

Minimal agar medium:

(For stock tubes and baby tubes; allow 3 mL per stock tube and 1 mL per baby tube)

- 2 mL -Vogel's 50x stock
- 2 g -D-Glucose
- 2 g -Agar
- 100 mL-Water

Maltose-arginine (MA) medium:

(MA medium for race tubes; allow 6 mL per short race tube, 8.5 mL per long race tube and 17 mL per square tube)

- 2 mL - Vogel's 50x stock
- 0.5 mL - L-arginine (20 mg/mL)
- 0.5 g - Maltose
- 2 g - Agar
- 100 mL - Water

Synthetic crossing medium (SCM):

(Allow 3 mL per tube)

- 50 mL - 2x Synthetic crossing medium (SCM) stock
- 2 g - Sucrose
- 2 g - Agar
- 50 mL - Water

Growth supplements:

- **Choline** for stock tubes: approximately 2 mg/mL, weighed out from wet choline. Add 1.5 mL per 100 mL = 215 ⌈M.

Choline for exact concentrations: stocks must be weighed out of dried choline. 1.0 M= 139.6 mg/mL. Make sterile stock and dilute in sterile Eppendorf tubes for working stocks.

Add 1 mL of 10 mM stock per 100 mL = 100 μM.

Choline 10 mM stock – 139.6 mg in 100 mL water.

- **Histidine**: 25 mg/mL L-His HCl. Use 2mL per 100 mL = 500 ⌈g/mL final concentration.
- **Leucine**: 4 mg / mL stock. Use 4 mL per 100 mL medium.
- **Hygromycin:** Final concentration 200 ⌈g/mL. Use 0.4 mL per 100 mL media from 50 mg/mL stock.

Sorbose Plating Media:

A:

- 0.1 g - Fructose (0.1%)
- 0.1 g - Glucose (0.1%)
- 2 g - Sorbose (2%)
- 50 mL - Water

B:

- 2 mL - Vogel's 50x stock
- 2 g - Agar (2%)
- 1.5 mL - Choline (if required) from 2 mg/mL stock (215 μM)
- 50 mL - Water
- • Autoclave both media in two separate containers and allow to cool down and mix before plating.

Race tubes

Maltose-arginine for race tubes: Mix all ingredients together. Sterilize media separately from race tubes sealed with cotton plugs at both ends. Allow 6 mL per short race tube (30 cm), and 8.5 mL per long race tube (40 cm).

1 M sorbitol:

- 9.1 g - Sorbitol
- Dissolved in about 30 mL water, then top up volume to 50 mL.

Recovery medium:

- 0.2 mL - Vogel's 50x stock

- 1.82 g - Sorbitol
- 9 mL - ddH_2O
- Choline (150 µL of 2 mg/ mL) or any other supplement as needed (No histidine)
- Autoclave, allow to cool, add 1 mL FIGS.

Top Agar (Plating media):

- 91 g - Sorbitol (Dissolved in about 350 mL water, then add water to 450 mL total)
- 10 mL - Vogel's 50x stock
- 14 g - Agar
- Choline (7.5 mL of 2 mg/ mL) or other supplement as needed (No histidine)

Autoclave, cool in oven to 50-60^oC, add 50 mL FIGS. After mixing top agar and FIGS, keep at 55^oC in oven or water bath until needed. Measure out 20 mL into sterile 50 mL conical tube, add spores, mix thoroughly and pour into 10 cm petri plates. Allow solidifying the media.

FIGS:

- 10 g - Sorbose
- 0.25 g - Fructose
- 0.25 g - Glucose
- 50 mL - ddH_2O
- Autoclave, cool to 50-60^oC and mix with top agar plating medium.

DNA Extraction Buffer:

- 1.21 g - Tris (final concentration 100 mM)
- 1.86 g - EDTA (final concentration 50 mM)
- 1 mL - 10% SDS

Dissolve Tris and EDTA with stirring in 80 mL dd H2O. Adjust pH to 8.0. Add water (ddH_2O) for a total volume of 100 mL. Store at room temperature.

To make DNA extraction buffer with 1% SDS, mix 1 mL 10% SDS with 9 mL DNA extraction buffer.

Tris-EDTA (TE) Buffer:

- 0.121 g -Tris (final concentration 10 mM)
- 0.0372 g -EDTA (final concentration 1 mM)

Dissolve Tris and EDTA with stirring in 80 mL dd H2O. Adjust pH to 8.0. Add water (ddH_2O) for a final volume of 100 mL.

10X TAE Buffer:

- 48.4 g -Tris (40 mM)
- 3.72 g -EDTA disodium salt, dehydrate (1mM)
- 11.4 mL-Acetic Acid (20mM)
- ~ 600 mL- ddH_2O

Measure out approximately 600 ml water in a beaker. Add one at a time of Tris, EDTA and Acetic Acid, stirring to dissolve completely after each. Adjust pH to 8.0. Pour into a graduated cylinder and add water to up to 1 L total.

60% Glycerol:

- 60 mL -Glycerol
- 40 mL -ddH_2O

Make sure mixture is very homogeneous by mixing by pipetting, shaking, vortexing. Autoclave on liquid cycle and store in the refrigerator.

10% APS

- 10mg - Ammonium persulfate
- 100µl - Water

10% SDS

- 10 g - SDS
- 100 mL - Water

0.1% SDS

- 100 µl - 10% SDS
- 9.9 mL - Water

0.5 M Tris – HCl

- 6.06 g - Tris-HCl
- Up to 100 ml - Water

  pH to 6.8

0.4% Bromphenol Blue stock

- 4 mg - Bromphenol Blue
- 1 mL - Water

  Store at 4°C.

0.1M PMSF

- 17 mg/ml dissolved in 100% ethanol.
- Store few months at 4°C.

SDS-Protein Extraction Buffer

To make 10 ml of extraction buffer:

- 50 mM tris pH 6.8 - 1 ml of 0.5 M tris pH 6.8 (stored at 4°C)
- 2% SDS - 2 ml of 10% SDS (stored at RT)
- 10% Glycerol - 1 ml glycerol (add by weight = 1.25 g)
- 5 mM EDTA-Na_2 - 100 µl of 0.5 M EDTA
- Water - 5.9 ml

Divide into 10 x 1 ml before use. Freeze extra at -20°C.

Add to 1 ml extraction buffer just before use:

- 1 mM PMSF - 10 µl of 0.1 M PMSF (or 30 µl of 5 mg/ml stock)

15 % acrylamide separating gel

- Final acrylamide % : - 15% acrylamide for 2 * 15% gels
- Total volume - 5.0 ml 10 ml

- Water - 1.79 ml 3.58 ml
- 1.5M Tris pH 8.8 - 1.25 ml 2.50 ml
- 10% SDS - 0.05 ml 0.10 ml
- 40% acrylamide - 1.88 ml 3.76 ml
- Add just before pouring:
- 10% APS - 25 µl 50 µl
- TEMED - 2.5 µl 5 µl

7.5% acrylamide separating gel

- Final acrylamide % : - 7.5% acrylamide for 2 * 7.5% gels
- Total - 5 ml 10 ml
- 1.5M Tris pH 8.8 - 1.25 ml 2.5 ml
- Water - 2.958 ml 5.917 ml
- 10% SDS - 0.05 ml 0.10 ml
- 40% acrylamide - 0.9375 ml 1.875 ml
- De-gas under vacuum to get rid of oxygen. Add:
- 10% APS - 25 µl 50 µl
- TEMED - 2.5 µl 5 µl

Pour the gel into the apparatus, add 0.1% SDS on the top of the gel (0.1 ml 10% SDS +10 ml water) to make a level top.

After 30 minutes, pour off the 0.1% SDS, rinse with water.

Stacking gel

Before preparing the stacking gel, immerse the comb into 0.1%SDS to avoid bubbles.

One gel Two gels

- Total - 2.5 ml 5.0 ml
- Water - 1.55 ml 3.11 ml
- 0.5 M Tris pH 6.8 - 0.647 ml 1.29 ml
- 10% SDS - 25.9 µl 51.8 µl
- 40% acrylamide - 259 µl 518 µl

Then before pouring:

- 10% APS - 12.9 µl 25.9 µl
- TEMED - 2.59 µl 5.18 µl

Wet comb in 0.1%S DS. Pour some of the stacking gel on top of the separating gel, put the comb in. Fill up space with stacking gel and insert comb to full depth. Allow at least 30 min to polymerize.

Running buffer (Tris-glycine-SDS buffer)

- Total volume - 2 L
- Glycine - 28.8 g
- Tris base - 6.0 g
- SDS - 2.0 g
- Water - up to 2 L

Anode buffer I

- 34.3 g - Tris base (0.3 M)
- 100 ml - Methanol (10%)
- Up to 1000 ml - Water

  pH 10.4 (check pH on meter, adjust if necessary)

Anode buffer II

- 3.03 g - Tris base (25 mM)
- 100 ml - Methanol (10%)

  Up to 1000 ml - Water

  pH 10.4 (check pH on meter, adjust if necessary)

Cathode buffer

- 3.03 g - Tris base (25mM)
- 3.00 g - Glycine (40mM)
- 100 ml - Methanol (10%)
- Up to 1000 ml - Water

  pH 9.4

To prepare: measure Tris base and glycine into a 1 l beaker, add water to 800 ml, adjust pH using pH meter, then add 100 ml methanol, and finally transfer to 1 l graduated cylinder and add water to 1000 ml.

1X TBS

- 1.21g - Tris
- 8.5g - NaCl
- Up to 1000 ml - Water
  pH 7.5 with HCl.

1X TBST

- To 1L of 1X TBS add 500 µl Tween-20.
  Store in fridge.

10X Blocking buffer (5% BSA+5% skimmed milk powder)

Into a 50mL falcon tube weigh out 2.5g BSA+2.5g skimmed milk powder. Add 1xTBST up to 50mL.Dissolve on rotating wheel at RT for 1hr. Centrifuge for 5 min at 4000rpm to remove un-dissolved particles. Filter the supernatant through filter paper in funnel. Store in fridge for up to one month. Dilute this 1 in 10 with TBST to make 1xBlocking buffer

100 mM Na_2EDTA

- 3.7224 g - Na_2EDTA
- 100 mL - ddH_2O
- pH adjusted to 7.5with Tris base

100 mM HEPES

- 2.383 g - HEPES
- 100 mL -ddH_2O

PBS

- 10 mM - phosphate

- 137 mM - NaCl
- 2.7 mM - KCl

  pH adjusted to 7.4.

IP lysis buffer

- 50 mL - HEPES from 100 mM stock at pH 7.5 (50 mM)
- 15 mL - NaCl from 1 M stock (150 mM)
- 10 mL - Glycerol (10% v/v)
- 20 µL - NP40 (0.02% v/v)
- 1 mL - Na_2EDTA 100 mM stock (1 mM)
- 100 µL - Leupeptin from 1 mg/mL stock (1 µg /mL)
- 100 µL - Pepstatin A from 1 mg/mL stock (1 µg /mL)
- 1000 µL - PMSF from 100 mM stock (1 mM)
- Up to 100 mL - ddH_2O
- Stored at 4°C.

- **1 mg/mL Leupeptin**
- 1 mg of Leupeptin in 1 mL of ddH_2O.

- **1 mg/mL Pepstatin A**
- 1 mg of Pepstatin A in 1 mL of methanol.

- **FLAG-rinsing buffer**
- 5 mL - NH_4HCO_3 from 0.5 M stock at pH 8 (50 mM)
- 3.75 mL - KCl from 1 M stock (75 mM)
- 500 µL - Na_2EDTA from 200 mM stock (2 mM)
- Up to 50 mL - ddH_2O
- Stored at 4°C.

YPD: for 600ml (or 20 plates):

- 6 g yeast extract
- 12 g peptone

  12 g dextrose
- (10 g Agar)
- 600 ml water

Luria-Bertani (LB) Broth

Make 1 L, autoclave and use as required

- 10 g - NaCl (1%)
- 5 g - Yeast Extract (0.5%)
- 10 g - Tryptone/peptone (1%)
- 1 L - ddH2O

Luria-Bertani (LB) agar plates

Make 1 L:

- 10 g - NaCl (1%)
- 5 g - Yeast Extract (0.5%)
- 10 g - Tryptone/peptone (1%)
- 15 g - Agar (1.5%)
- 1 L - ddH2O

Dissolve first three ingredients in ddH2O and add agar. Autoclave and cool it to 60oC in oven then add any antibiotics (if require). Add 1 mL ampicillin (100mg/mL) for 1000 ml LB agar.

SC-Ura: for a liter of liquid medium:

- 26.7 g of the drop-out base with glucose
- g drop-out mix minus Ura
- autoclave (or filter sterilize)

sheared salmon sperm DNA:

- dilute to 2 mg/ml in water

- boil it for 5 min and put on ice
  (doesn't need to be reboiled each time you thaw it)

FGS plate + hyg, 2% yeast extract, 100 µg/ml His for plating transformations per liter:

- 50x Vogel's 20ml
- yeast extract 20g
- Agar 10g
- H2O 880ml
- autoclave 20 min
  add 100 ml 10x FGS, 2ml 500x L-histidine, and hygromycin (to 300 µg/ml)

10x FGS additive per 1 liter:

- sorbose 200g
- fructose 5g
- glucose 5g
- filter-sterilize

Regeneration agar with 2% yeast extract, 100 µg/ml His

per 600 ml:

- 50x Vogel's 12ml
- sorbitol 109.2g
- yeast extract 12g
- Agar 6g
- H2O 504ml

autoclave 20 min and then add 60 ml of 10x FGS additive and 1.2ml of 500X L- histidine

Recovery solution with 2% yeast extract, 100 µg/ml His per 600 ml:

- 50x vogel's 12ml
- yeast extract 12g
- H2O to 600 ml
- autoclave 20 min and then add 1.2 ml of 500X L-histidine

1 M lithium acetate (LiOAc)

- Lithium acetate dihydrate 10.2g
- ddH2O 100mL
- Autoclave and adjust PH to 7.5

50% PEG 3350:

- 50 g PEG 3350 (Sigma P 3640)
- add 35 ml water and stir till dissolved (will take maybe 30 min)
- bring to 100 ml with water
- filters sterilize (or autoclave)

  keep tightly capped; increasing concentration will lower efficiencies

8% Paraformaldehyde

Make 1 L:

- Prepare 800 mL of distilled water in a suitable container.
- Add 80 g of paraformaldehyde to the solution.
- Heat to 60°C and add 2-3 drops of 1 M NaOH.
- Add distilled water until the volume is 1 L.
- Store this stock solution at -20 freezer.

APPENDIX II

Constructed plasmids and strains

Plasmid Name	Neurospora Transformant Genotype	SG Numbers
Gtr2-FLAG	Gtr2-FLAG *bd- csp-1 chol-1* Gtr2-Flag *bd-csp-1-chol-1-vta ko*	SG # 657 (*bd- csp-1 chol-1)* SG# 658 (*bd-csp-1-chol-1-vta ^{ko})*
Gtr2-RFP	Gtr2-RFP *bd csp-1* Gtr2-RFP *bd csp-1 chol-1* Gtr2-RFP *Mus 51-his-3 bar+* Gtr2-RFP *bd-csp-1-chol-1-vta ko*	SG # 698 (*Mus 51-his-3 bar+)* 699 (*Mus 51-his-3 bar+)* 708 *(bd csp-1 chol-1)* 710 (*bd-csp-1-chol-1-vta ^{ko})* 711 (*bd-csp-1-chol-1-vta ^{ko})* 714(*bd-csp-1-chol-1-vta ^{ko})* 715(*bd-csp-1-chol-1-vta ^{ko})* 725 *(bd csp-1)* 726*(bd csp-1 chol-1)*
KOG1-GFP	KOG1-GFP *bd- csp-1 chol-1* KOG1-GFP *bd-csp-1-chol-1-vta ko* KOG1-GFP *Mus 51-his-3 bar+* KOG1-GFP *bd csp-1*	700 *(Mus 51-his-3 bar+)* 709 *(bd-csp-1-chol-1-vta ^{ko})* 712 *(bd-csp-1-chol-1-vta ^{ko})* 713 *(bd-csp-1-chol-1-vta ^{ko})* 716, *(bd-csp-1-chol-1-vta ^{ko})* 719(*bd csp-1)* 720 *(bd- csp-1 chol-1)* 727 *(bd- csp-1 chol-1)*
KOG1-FLAG	KOG1-FLAG *Mus 51-his-3 bar+*	722 (*Mus 51-his-3 bar+)*
KOG-1-RFP	Bacterial plasmids stored in the -80 Freezer	
GTR2-GFP	Gtr2-GFP-*Mus 51-his-3 bar+*	696 (*Mus 51-his-3 bar+)*

		697 *(Mus 51-his-3 bar+)* 698 *(Mus 51-his-3 bar+)* 721 *(Mus 51-his-3 bar+)*
TOR-GFP	TOR-GFP-*Mus 51-his-3 bar+*	681 *(Mus 51-his-3 bar+)*
TOR-FLAG	Bacterial plasmids stored in the -80 Freezer	
Atg8-RFP	Atg8-RFP *bd- csp-1 chol-1* Atg8-RFP *bd- csp-1 chol-1 VTA KO*	659 (*bd- csp-1 chol-1 vta ^{ko})* 701 (*bd- csp-1 chol-1 vta^{ko})* 717 (*bd- csp-1 chol-1 vta^{ko})* 718 (*bd- csp-1 chol-1)* 723 *(bd- csp-1 chol-1)* 724 (*bd- csp-1 chol-1 vta^{ko})* 728 (*bd- csp-1 chol-1 vta^{ko})* 729 (*bd- csp-1 chol-1)* 730(*bd- csp-1 chol-1)* 731 *(bd- csp-1 chol-1)* 732 *(bd- csp-1 chol-1)* 733 *(bd- csp-1 chol-1 vta^{ko})* 734 (*bd- csp-1 chol-1)*